NASA TECHNICAL NOTE

STATIC STABILITY INVESTIGATION OF A SOUNDING-ROCKET VEHICLE AT MACH NUMBERS FROM 1.50 TO 4.63

by C. Donald Babb and Dennis E. Fuller

Langley Research Center
Langley Station, Hampton, Va.

NATIONAL AERONAUTICS AND SPACE ADMINISTRATION • WASHINGTON, D. C. • JUNE 1967

NASA TN D-4014

STATIC STABILITY INVESTIGATION OF A SOUNDING-ROCKET VEHICLE AT MACH NUMBERS FROM 1.50 TO 4.63

By C. Donald Babb and Dennis E. Fuller

Langley Research Center
Langley Station, Hampton, Va.

NATIONAL AERONAUTICS AND SPACE ADMINISTRATION

For sale by the Clearinghouse for Federal Scientific and Technical Information
Springfield, Virginia 22151 – CFSTI price $3.00

STATIC STABILITY INVESTIGATION OF A SOUNDING-ROCKET VEHICLE AT MACH NUMBERS FROM 1.50 TO 4.63

By C. Donald Babb and Dennis E. Fuller
Langley Research Center

SUMMARY

Tests were conducted in the Langley Unitary Plan wind tunnel on a single-stage sounding-rocket vehicle to determine the effect of body length and fin cant. Tests were performed through an angle-of-attack range from about -4° to 20° and for angles of sideslip from about -4° to 8°. The Mach number was varied from 1.50 to 4.63 and all tests were made at a Reynolds number per foot of 3.0×10^6 (9.84×10^6 per meter). Tests were made for two vehicles with length-to-diameter ratios of 18.20 and 23.77. Results were obtained with tail fins off and with fins on at cant angles of 0° and 2°.

The results indicate that the configuration with either a short or a long body had a rather severe pitch-up at moderately low angles of attack. The center of pressure moved forward with increasing Mach number for the vehicle with either a short or a long body with the variation being somewhat greater for the longer vehicle. Each configuration indicated large values of rolling moment due to sideslip particularly at the lower Mach numbers and higher angles of attack. Each configuration indicated a progressive decrease in directional stability with increasing angle of attack and Mach number with the decrease being somewhat greater for the long configuration than for the short configuration. The canted fins were effective in producing roll throughout the Mach number and angle-of-attack ranges.

INTRODUCTION

The National Aeronautics and Space Administration has been conducting high altitude research with a number of different vehicles. One of the vehicles in use is the Arcas, which is a small single-stage tube-launched sounding rocket. Flights conducted with this vehicle have become more varied and exacting and entail modifications to the original configuration. In order to meet the requirements for the several versions of the vehicle, it was considered necessary to conduct a wind-tunnel investigation to determine the static stability characteristics as affected by body length and fin cant.

One model tested (configuration 1) was representative of the Arcas Robin meteorological rocket vehicle, whereas the other (configuration 2) represented the Arcas vehicle modified by NASA to accommodate a bioscience payload. Results from a subsonic and transonic wind-tunnel investigation of these two configurations may be found in reference 1.

Tests were conducted in the Langley Unitary Plan wind tunnel at Mach numbers from 1.50 to 4.63 for angles of attack from about -4° to 20° and for angles of sideslip from -4° to 8°. The Reynolds number per foot was about 3.0×10^6 (9.84×10^6 per meter).

SYMBOLS

The aerodynamic force and moment data are referred to the body axis system with the moment center located at 63.37 and 66.36 percent body length for configurations 1 and 2, respectively (fig. 1). These moment centers are more rearward than the flight centers of gravity.

C_A axial-force coefficient, $\frac{\text{Axial force}}{qA}$

$C_{A,c}$ chamber-axial-force coefficient, $\frac{\text{Chamber axial force}}{qA}$

x_{cp} center of pressure, percent body length

C_l rolling-moment coefficient, $\frac{\text{Rolling moment}}{qAd}$

$C_{l_\beta} = \frac{\partial C_l}{\partial \beta}$, per degree

C_{l_δ} roll effectiveness, per degree of fin cant

C_m pitching-moment coefficient, $\frac{\text{Pitching moment}}{qAd}$

C_N normal-force coefficient, $\frac{\text{Normal force}}{qA}$

C_n yawing-moment coefficient, $\frac{\text{Yawing moment}}{qAd}$

$C_{n_\beta} = \frac{\partial C_n}{\partial \beta}$, per degree

C_Y side-force coefficient, $\frac{\text{Side force}}{qA}$

$C_{Y_\beta} = \frac{\partial C_Y}{\partial \beta}$, per degree

d body diameter

M free-stream Mach number

q free-stream dynamic pressure, pounds per foot^2 (newtons per meter^2)

A maximum cross-sectional area of body, feet^2 (centimeter^2)

α angle of attack of model center line, degree

β angle of sideslip of model center line, degree

δ_F angle of fin cant, degree

x longitudinal distance, inches (centimeters)

r radius, inches (centimeters)

APPARATUS AND TESTS

Tests were conducted in both the low and high Mach number test sections of the Langley Unitary Plan wind tunnel which is a variable-pressure continuous-flow tunnel. The test sections are approximately 4 ft (1.2192 m) square and 7 ft (2.1336 m) long. The nozzles leading to the test sections are of the asymmetric sliding-block type, which permits a continuous variation in Mach number from about 1.4 to 2.9 in the low Mach number test section and from about 2.3 to 4.7 in the high Mach number test section.

Model

One model tested (configuration 1) was representative of the Arcas Robin meteorological rocket vehicle, whereas the other (configuration 2) represented the Arcas vehicle as modified by NASA to accommodate a bioscience payload. Results from a subsonic and transonic wind-tunnel investigation of these two configurations may be found in reference 1.

Dimensional details of the half-scale models are presented in figure 1 and photographs of the models are presented as figure 2. The model had an ogive nose, a

cylindrical centerbody, a boattailed afterbody, and trapezoidal double-wedge fins. The afterbody boattail ended with a reflexed lip. Two models differing in the length of the cylindrical centerbody were tested. These models had length-to-diameter ratios of 18.20 (configuration 1) and 23.77 (configuration 2).

Fin cant angles of 0° and 2° were provided. The cant angle of 2° for each fin was in such a direction as to produce a positive rolling moment.

Test Conditions

The test conditions for the investigation were as follows:

Mach number	Stagnation temperature		Stagnation pressure		Reynolds number	
	$^{\circ}$F	$^{\circ}$K	lb/in^2 abs	N/m^2	per ft	per m
1.50	150	339	11.58	79 841.29	3.0×10^6	9.84×10^6
1.80	150	339	12.72	87 701.31		
2.30	150	339	15.93	109 833.48		
2.96	150	339	22.50	155 132.03		
3.96	175	352	40.11	276 548.71		
4.63	175	352	54.74	377 419.00		

Tests were made through an angle-of-attack range from about -4° to 20° and for angles of sideslip from about -4° to 8°. The stagnation dewpoint was maintained near -30° F (239° K) in order to assure negligible condensation effects. In order to obtain turbulent flow over the model a 1/16-in-wide (0.159 cm) strip of No. 60 carborundum grains were affixed around the model 3/4 in. (1.91 cm) rearward of the nose and 1/2 in. (1.27 cm) rearward of the leading edge of each fin.

Measurements

Aerodynamic forces and moments were measured by means of a six-component electrical strain-gage balance housed within the model. The balance, in turn, was rigidly fastened to a sting support and, thence, to the tunnel support system. The balance chamber pressure was measured for each model and test condition. Typical schlieren photographs are presented as figure 3.

CORRECTIONS

Angles of attack were corrected for tunnel flow angularity and angles of attack and sideslip were corrected for deflection of the balance and sting support as a result of aerodynamic loads. Axial-force data were not corrected to free-stream conditions at the model base; however, values of chamber-axial-force coefficient are presented in figure 4.

ACCURACY

The accuracy of α and β is estimated to be within $\pm 0.1^{\circ}$, and the accuracy of the Mach number ranges M = 1.5 to 2.96 and M = 3.96 to 4.63 is estimated to be ±0.015 and ±0.050, respectively.

The accuracy of the individual measured quantities, based on calibrations and repeatability of data, is estimated to be within the following limits:

C_A	±0.004
C_l	±0.01
C_m	±0.05
C_n	±0.05
C_N	±0.03
C_Y	±0.03

PRESENTATION OF RESULTS

The results are presented in the following figures:

RESULTS AND DISCUSSION

The chamber-axial-force coefficients $C_{A,c}$ for configuration 1 (fig. 4(a)) indicate low values at $M = 1.50$ and 1.80 with respect to the other Mach numbers near $\alpha = 0^{\circ}$, particularly for the fin-off condition. This is believed to be because of the reflex lip at the model base; when separation occurs over the afterbody boattail at the higher Mach numbers or the boundary layer is thickened by the addition of the fins, the effect of the reflex lip is masked. This phenomenon at the lower test Mach numbers does not occur for configuration 2 probably because of the thicker boundary layer at the model base due to the increase in length of body.

The results shown in figures 5 and 6 indicate that, in general, the slope of the normal-force curve for each configuration increases considerably with increasing angle of attack. This trend is characteristic of slender bodies and may be noted for both the long and short bodies, with and without fins. Although the addition of the fins provides a stabilizing increment of C_m, it appears that the effectiveness of the fins is considerably reduced by the wake and downwash which are caused by vortices shedding from the forebody (fig. 3), and a severe pitch-up tendency occurs near $\alpha = 8^{\circ}$ for both configurations 1 and 2. To improve the stability characteristics would require the use of higher aspect ratio fins in order to get more of the fin out of the influence of the adverse wake and downwash regions.

The variation of the center-of-pressure location in percent body length with Mach number is summarized in figure 7. In this form the margin of stability at low angles can be readily determined for a given center-of-gravity variation. The center of pressure progressively moves forward with increasing Mach number for both configurations with the variation being somewhat greater for the longer vehicle.

The rolling-moment and yawing-moment coefficients are generally nonlinear with change in sideslip angle for either test configuration (figs. 8, 9, 11, and 12). The summary of sideslip parameters shown in figures 10 and 13 for configurations 1 and 2, respectively, show that both configurations generally display large values of rolling moment due to sideslip particularly at the higher angles of attack. These values are reduced with increasing Mach number, however. For the reference model center used, configuration 1 becomes directionally unstable at angles of attack above about 10° for $M = 1.50$ and at progressively lower angles with increasing Mach number. Directional instability occurs for configuration 2 at lower angles of attack than for configuration 1.

The fins are effective in producing roll throughout the angle-of-attack and Mach number ranges and the effectiveness is about the same for either vehicle (fig. 14).

However, there is a loss in C_{l_δ} with increasing Mach number particularly at the lower angles of attack.

CONCLUSIONS

Static stability tests at Mach numbers from 1.50 to 4.63 of a sounding-rocket vehicle with variations in body length and fin cant lead to the following conclusions:

1. The configuration with either a short or a long body indicated a rather severe pitch-up at moderately low angles of attack.

2. The center of pressure moved forward with increasing Mach number for the vehicle with either a short or a long body, with the variation being somewhat greater for the longer vehicle.

3. Each configuration indicated large values of rolling moment due to sideslip particularly at the lower Mach numbers and higher angles of attack.

4. Each configuration indicated a progressive decrease in directional stability with increasing angle of attack and Mach number with the decrease being somewhat greater for the long body than for the short body.

5. The canted fins were effective in producing roll throughout the Mach number and angle-of-attack ranges.

Langley Research Center,
National Aeronautics and Space Administration,
Langley Station, Hampton, Va., November 22, 1966,
607-06-00-01-23.

REFERENCE

1. Ferris, James C.: Static Stability Investigation of a Single-Stage Sounding Rocket at Mach Numbers From 0.60 to 1.20. NASA TN D-4013, 1967.

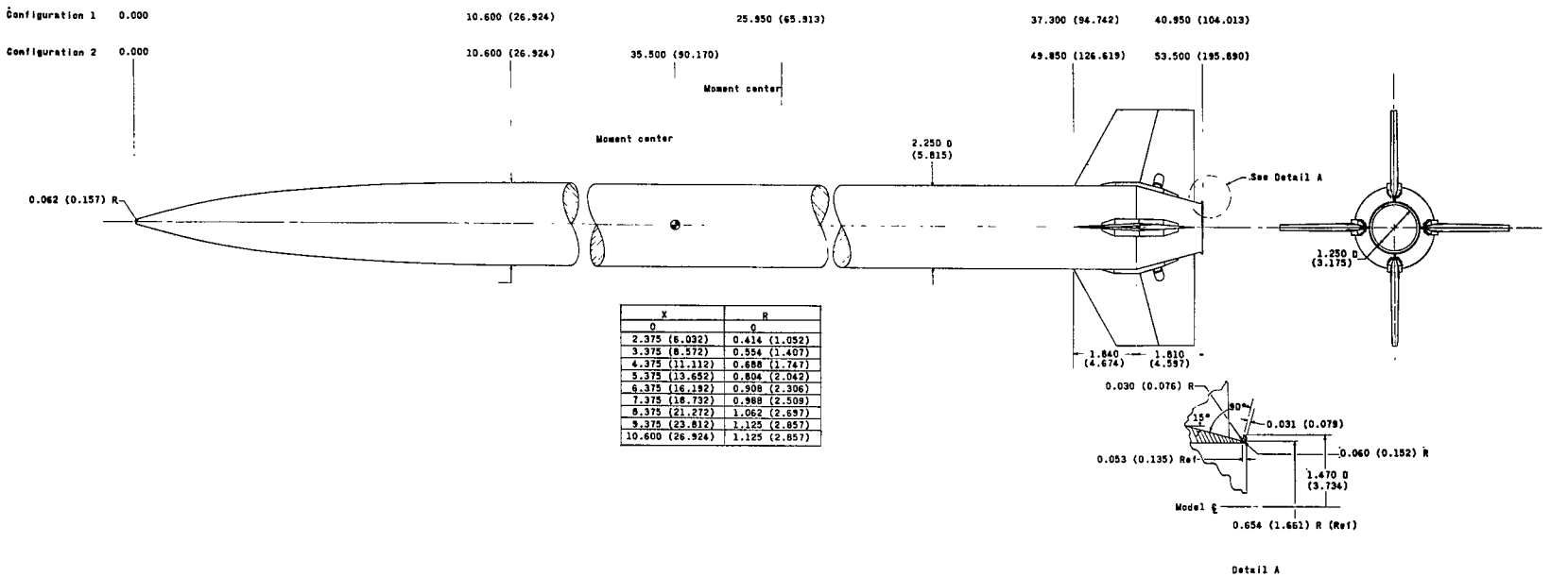

X	R
0	0
2.375 (6.032)	0.414 (1.052)
3.375 (8.572)	0.554 (1.407)
4.375 (11.112)	0.688 (1.747)
5.375 (13.652)	0.804 (2.042)
6.375 (16.192)	0.908 (2.306)
7.375 (18.732)	0.988 (2.509)
8.375 (21.272)	1.062 (2.697)
9.375 (23.812)	1.125 (2.857)
10.600 (26.924)	1.125 (2.857)

(a) Complete model.

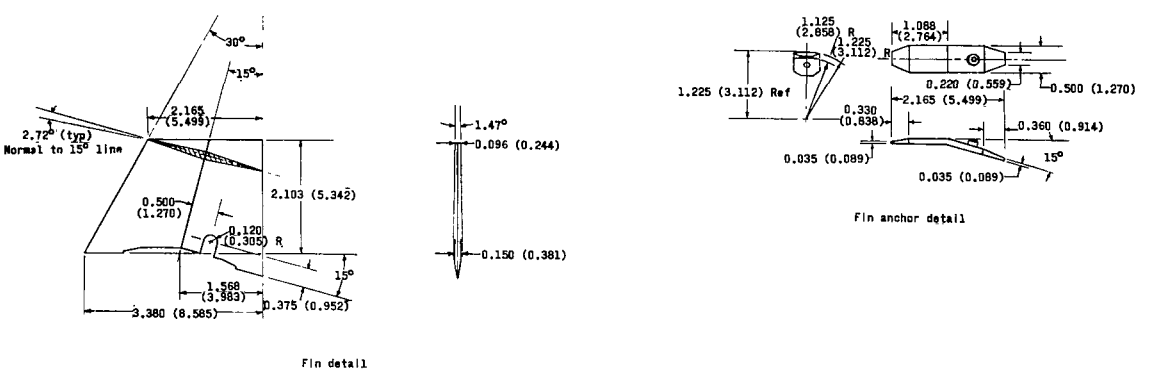

(b) Fin details.

Figure 1.- Model details. All dimensions are in in. (cm).

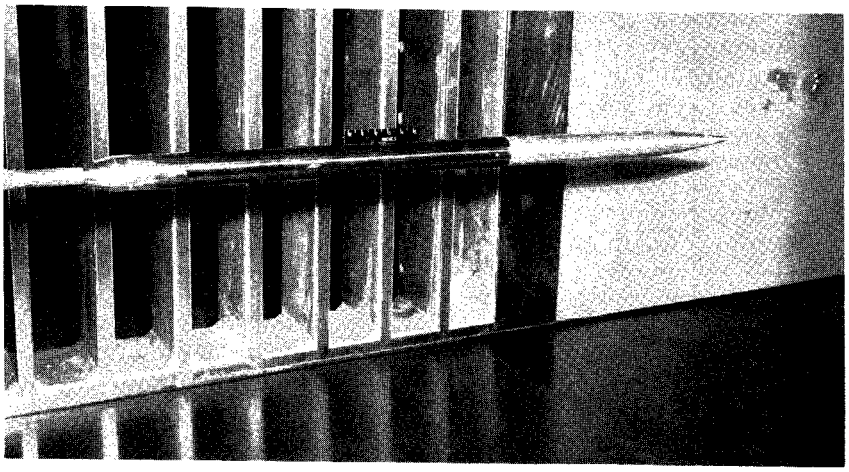

Configuration 2, fins off

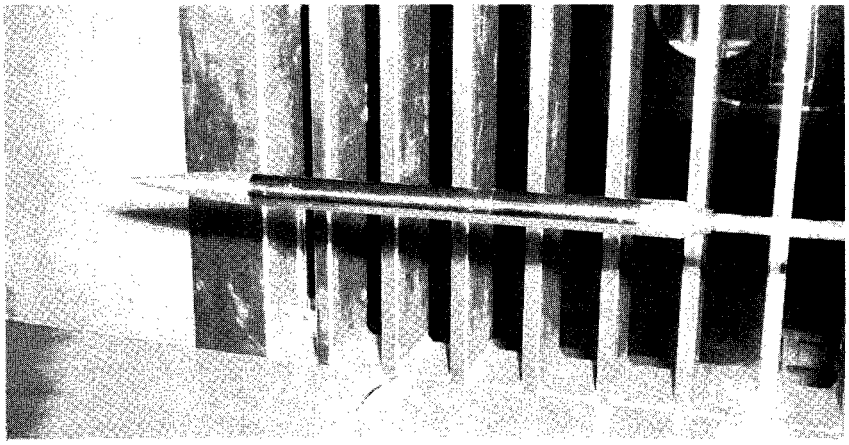

Configuration 1, fins off

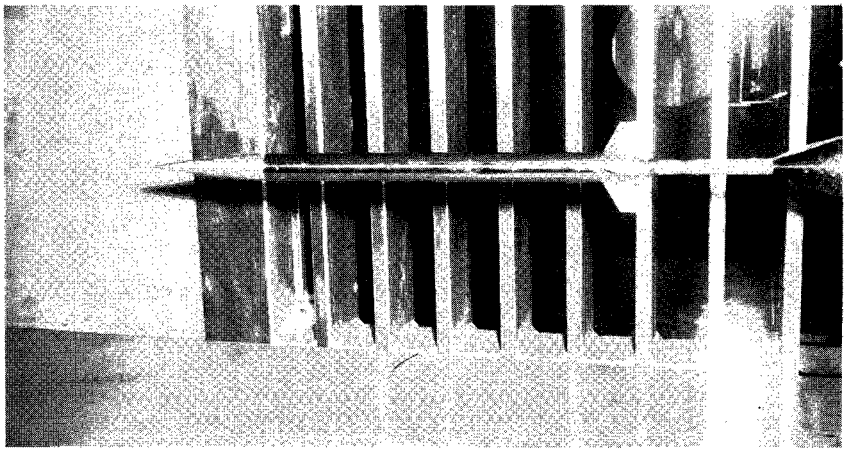

Configuration 1, fins on

Figure 2.- Model.

L-66-7656

α = -0.2°

α = 8.0°

α = 16.5°

α = 21.1°

M = 1.50

(a) Configuration 1.

L-66-7657

Figure 3.- Schlieren photographs through angle-of-attack range.

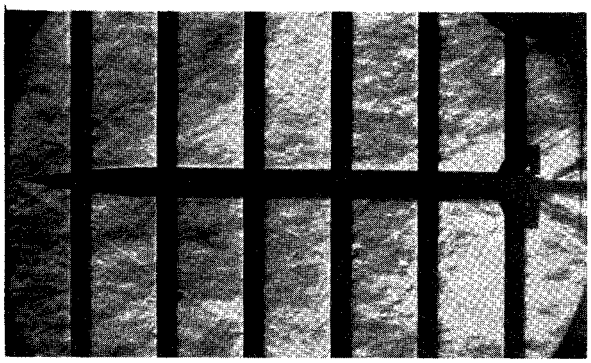

α = -0.1°

α = 8.2°

α = 12.4°

α = 16.9°

α = 21.5°
M = 1.80

(a) Continued.

Figure 3.- Continued.

L-66-7658

α = -0.4°

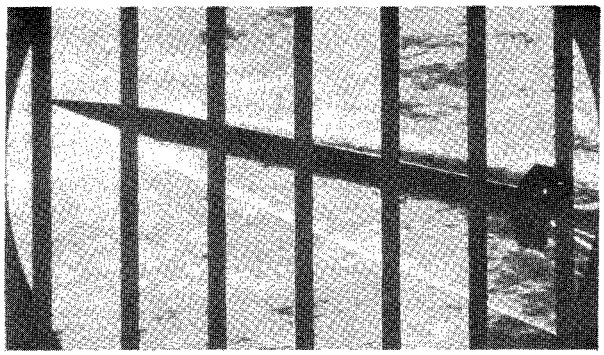

α = 12.2°

α = 16.4°

α = 20.5°

M = 2.96

(a) Continued.

Figure 3.- Continued.

L-66-7659

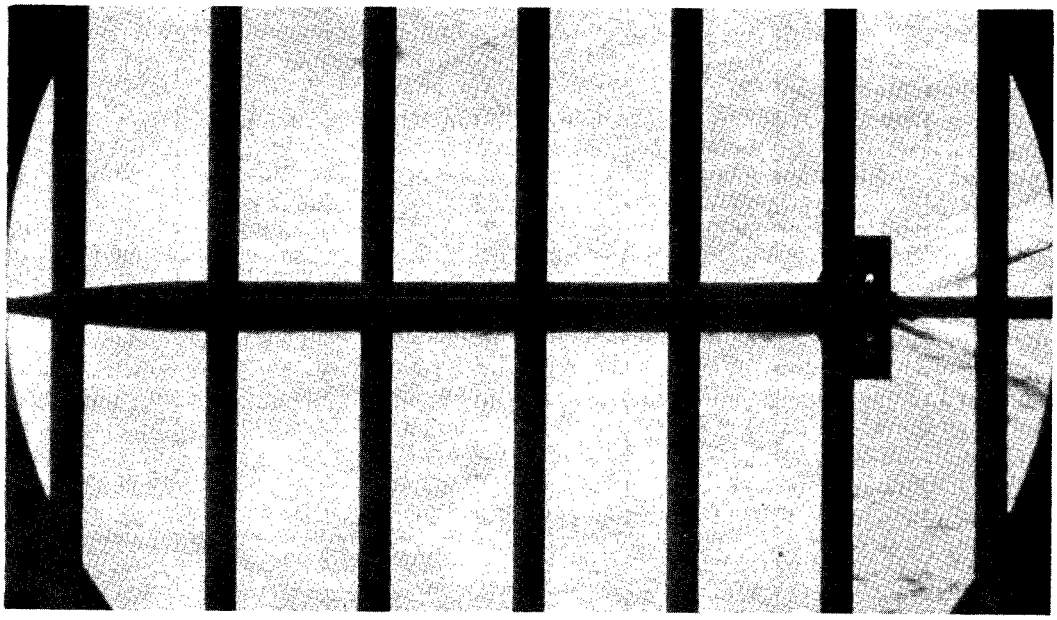

$\alpha = -0.3°$

$\alpha = 8.0°$

$M = 2.30$

(a) Continued.

Figure 3.- Continued.

L-66-7660

$\alpha = 16.4°$

$M = 3.96$

(a) Continued.

Figure 3.- Continued.

L-66-7661

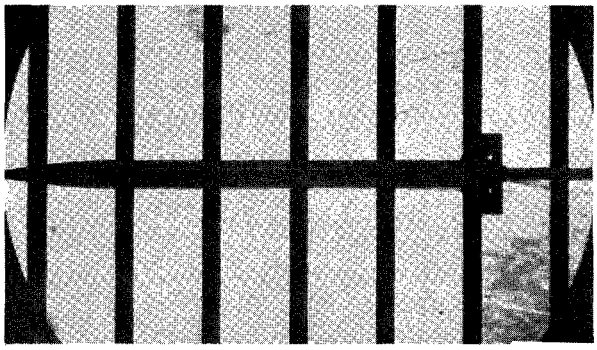

α = -0.3°

α = 7.9°

α = 12.1°

α = 16.2°

α = 20.2°

M = 4.63

(a) Concluded.

Figure 3.- Continued.

L-66-7662

α = 8.2°

α = 12.5°

α = 17.3°

α = 22.4°

M = 1.80

(b) Configuration 2.

Figure 3.- Continued.

L-66-7663

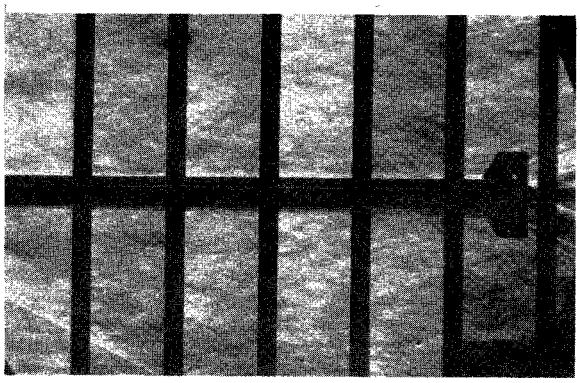

α = -0.2°

α = 8.2°

α = 12.6°

α = 17.3°

α = 21.6°

M = 2.30

(b) Continued.

Figure 3.- Continued.

L-66-7664

α = -0.6°

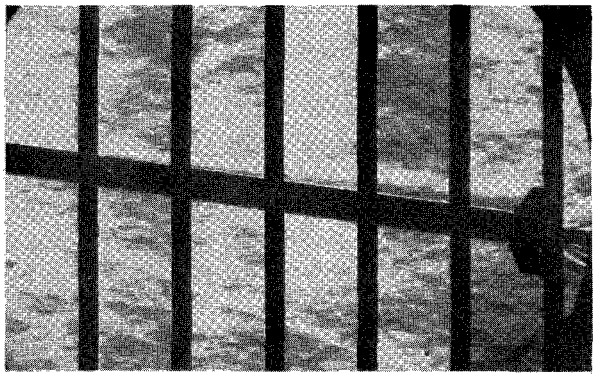

α = 7.8°

α = 12.2°

α = 16.7°

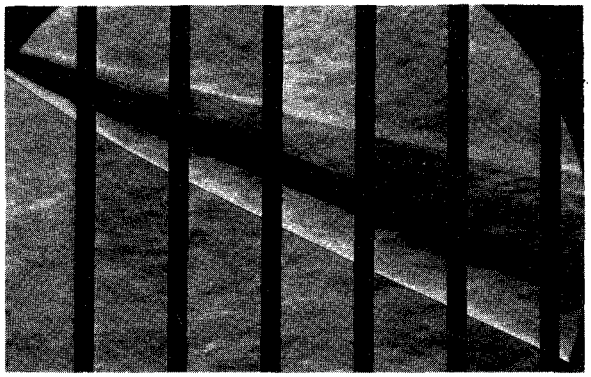

α = 21.1°

M = 2.96

(b) Continued.

L-66-7665

Figure 3.- Continued.

α = -0.2°

α = 8.1°

α = 12.5°

α = 16.8°

α = 20.9°
M = 3.96

(b) Continued.

Figure 3.- Continued.

L-66-7666

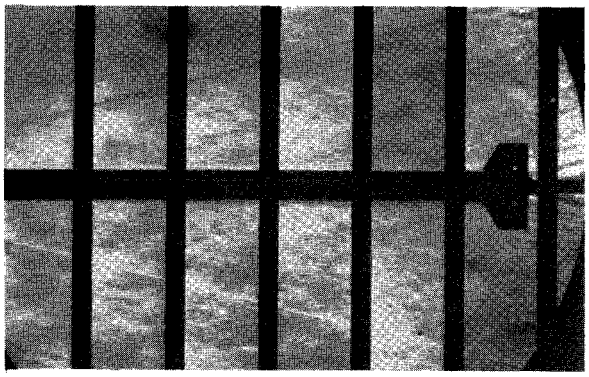

α = 0.4°

α = 8.6°

α = 12.9°

α = 17.1°

α = 21.2°
M = 4.63

(b) Concluded.

L-66-7667

Figure 3.- Concluded.

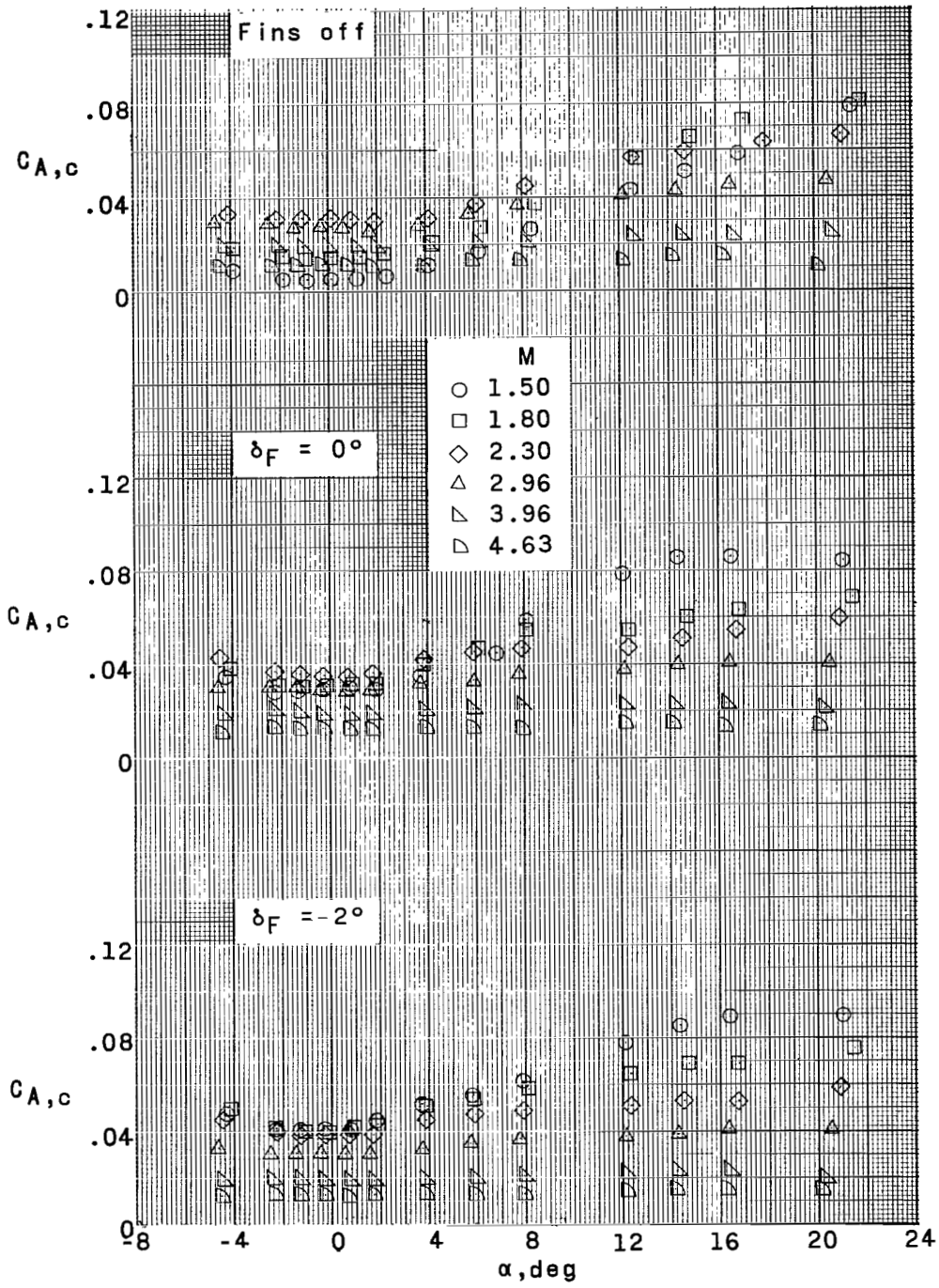

(a) Configuration 1.

Figure 4.- Values of chamber-axial-force coefficient.

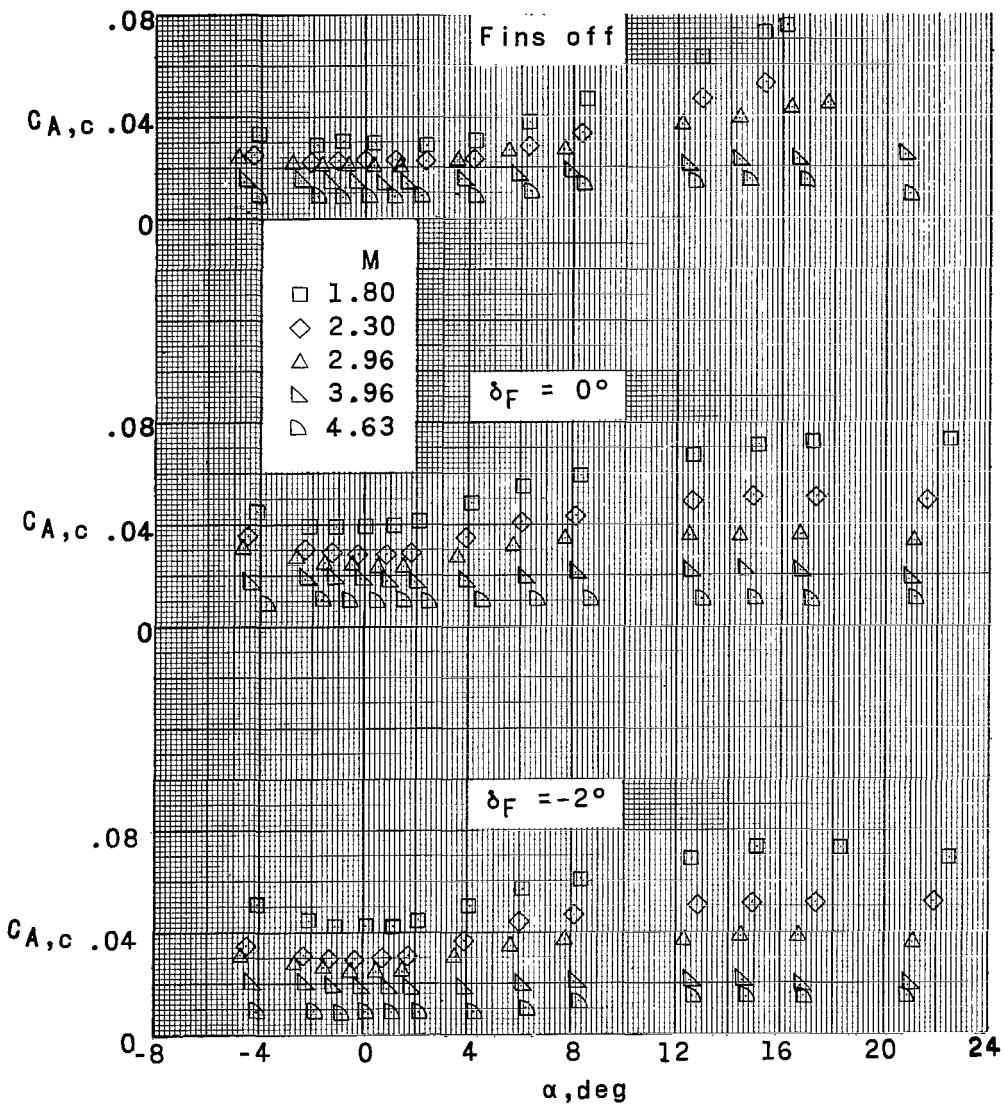

(b) Configuration 2.

Figure 4.- Concluded.

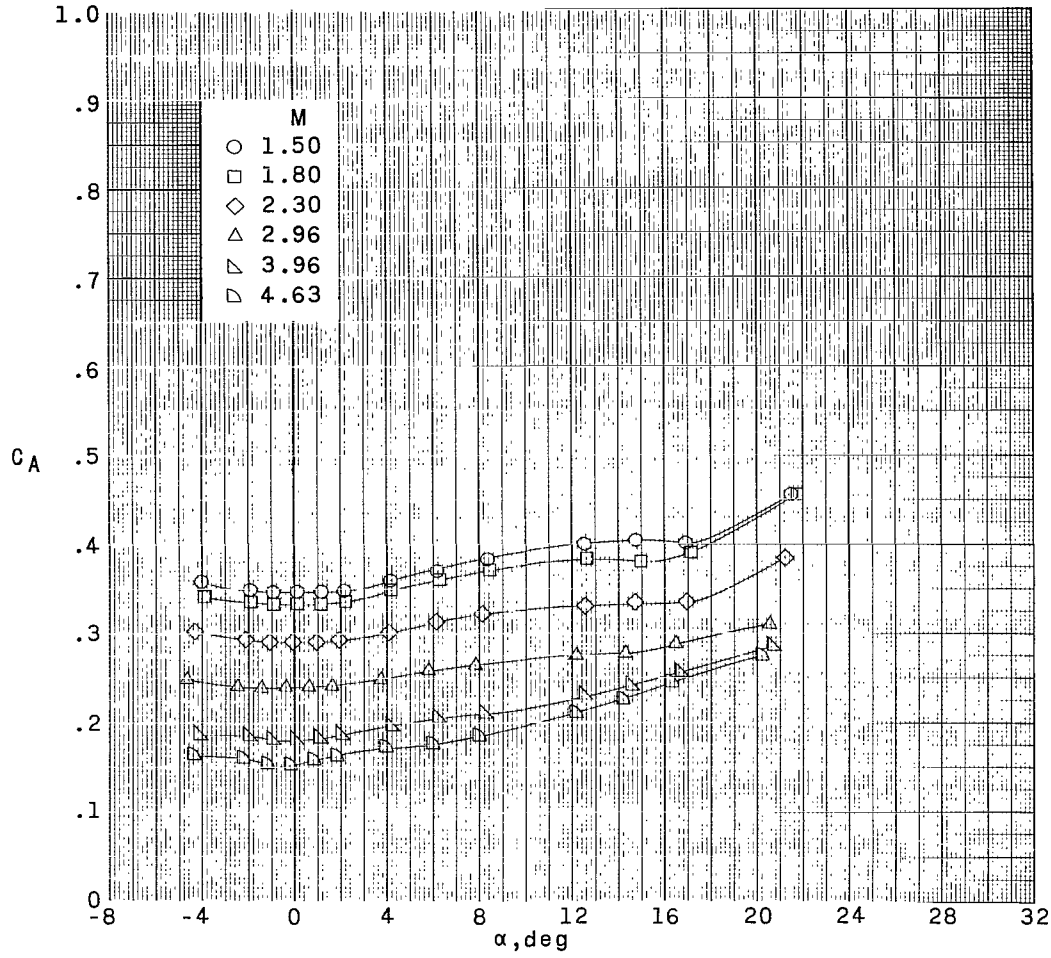

(a) Fins off.

Figure 5.- Aerodynamic characteristics in pitch for configuration 1.

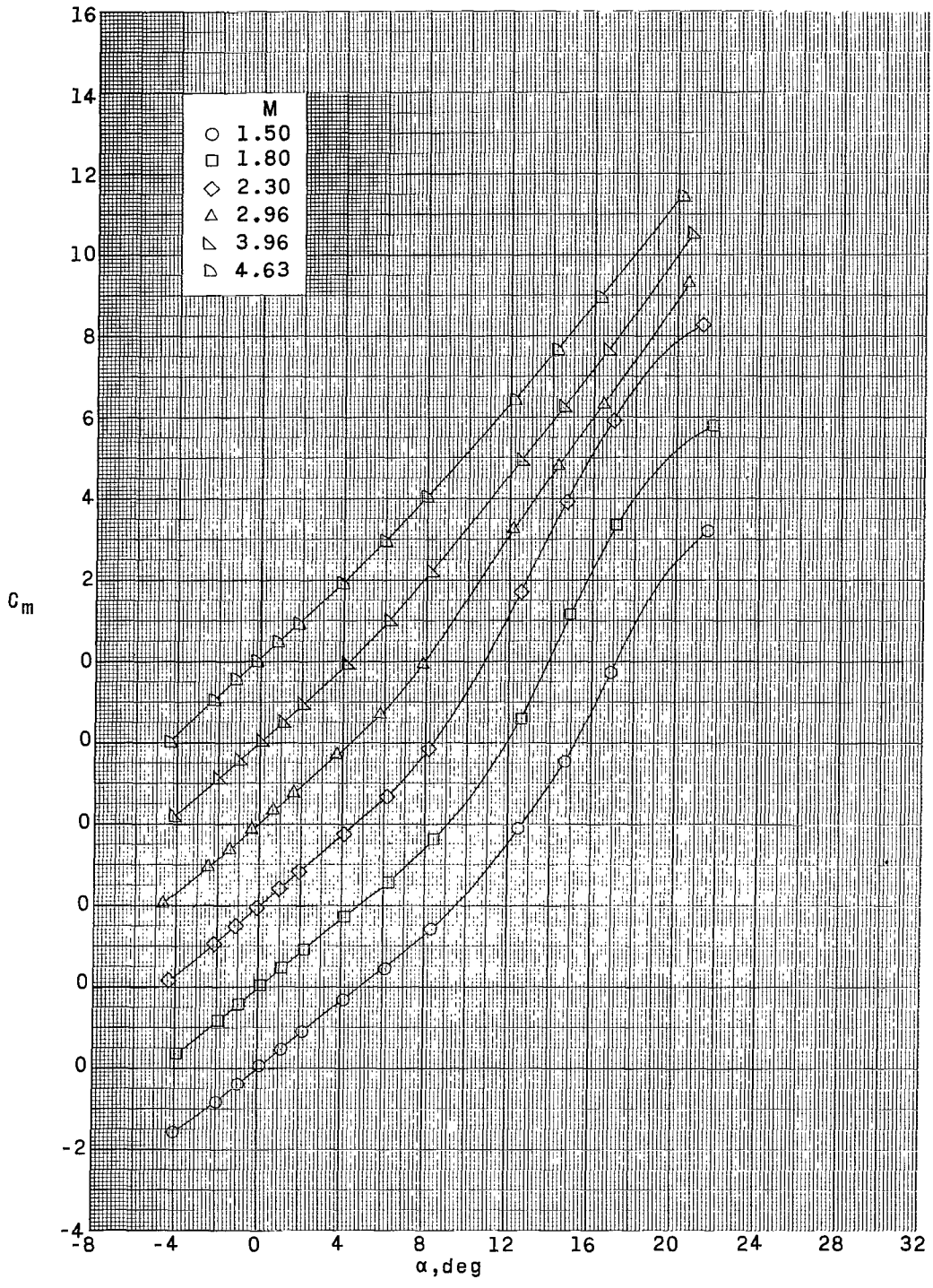

(a) Continued.

Figure 5.- Continued.

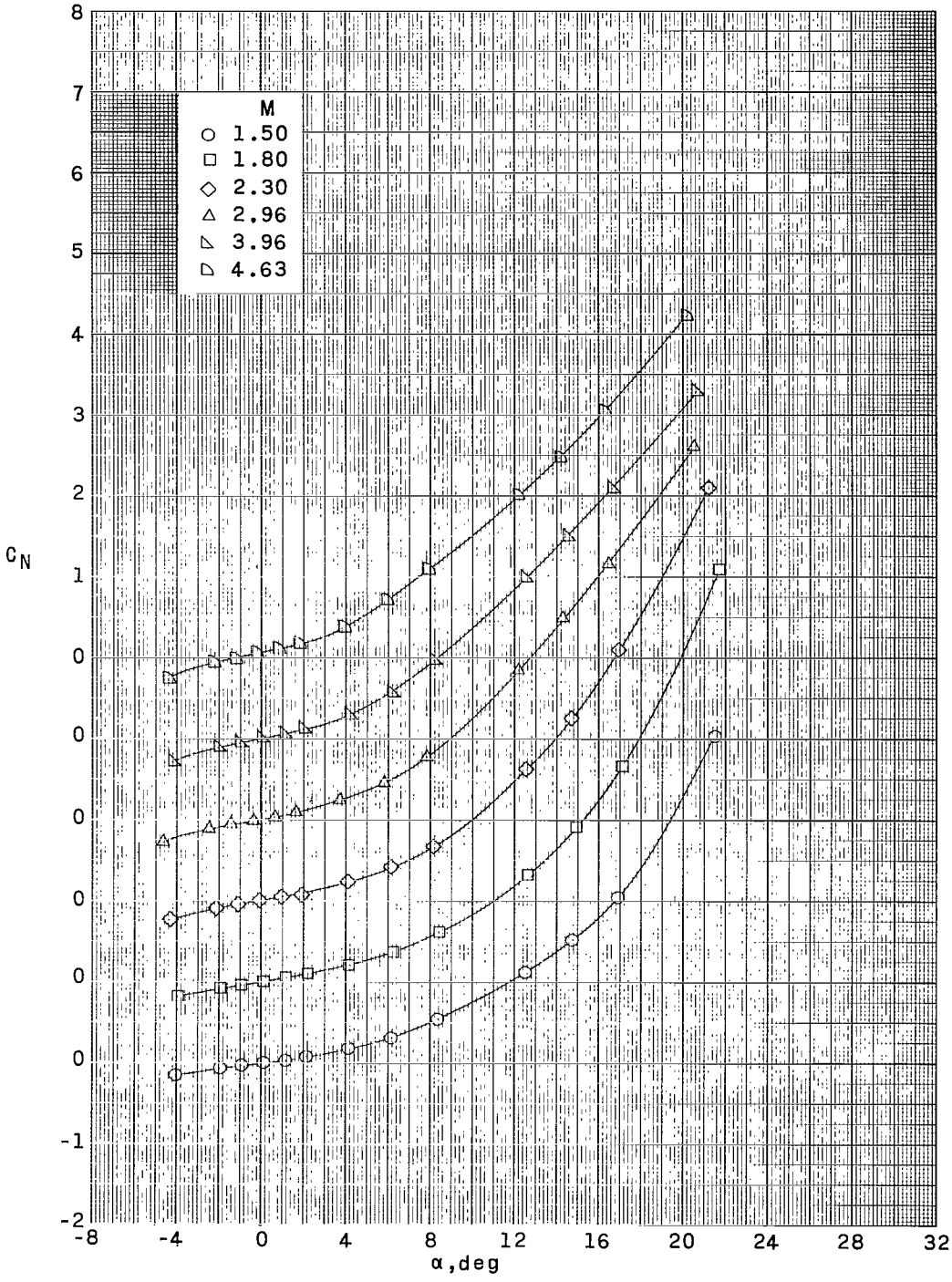

(a) Concluded.

Figure 5.- Continued.

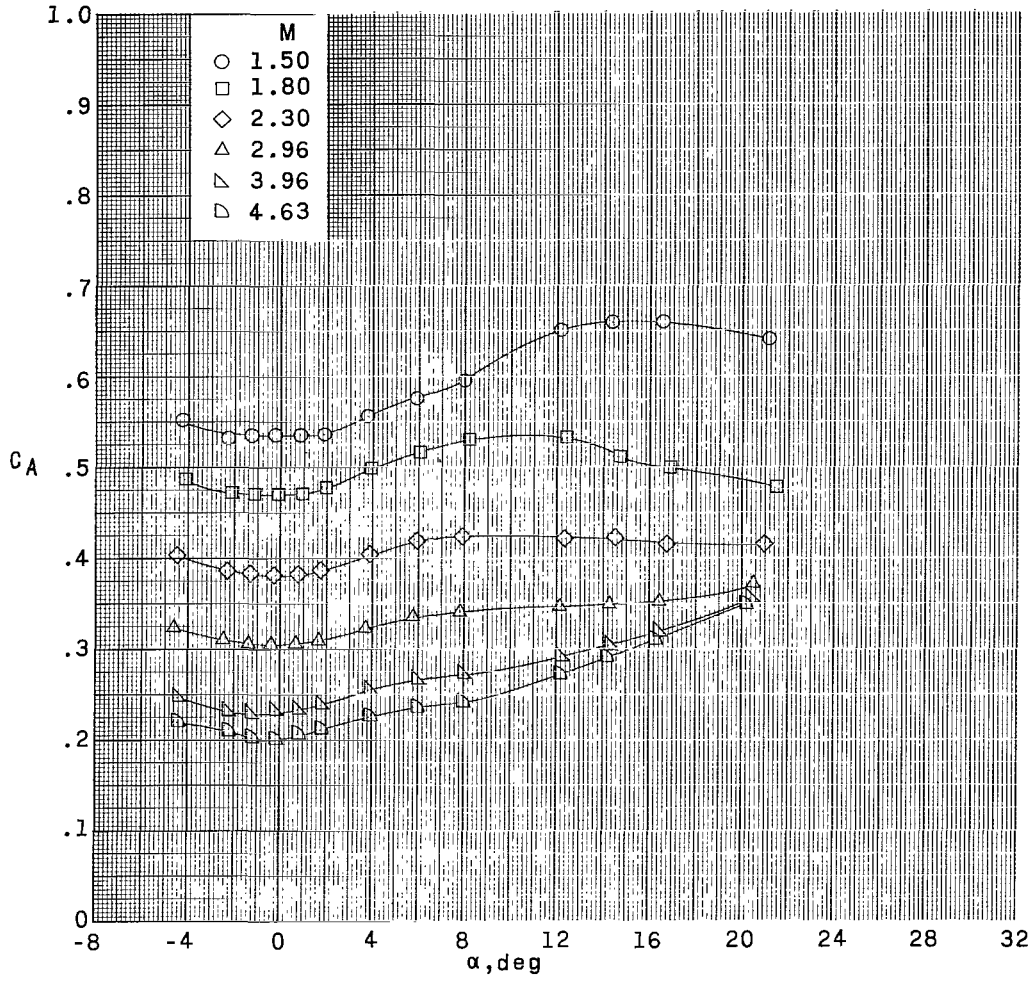

(b) $\delta_F = 0^0$.

Figure 5.- Continued.

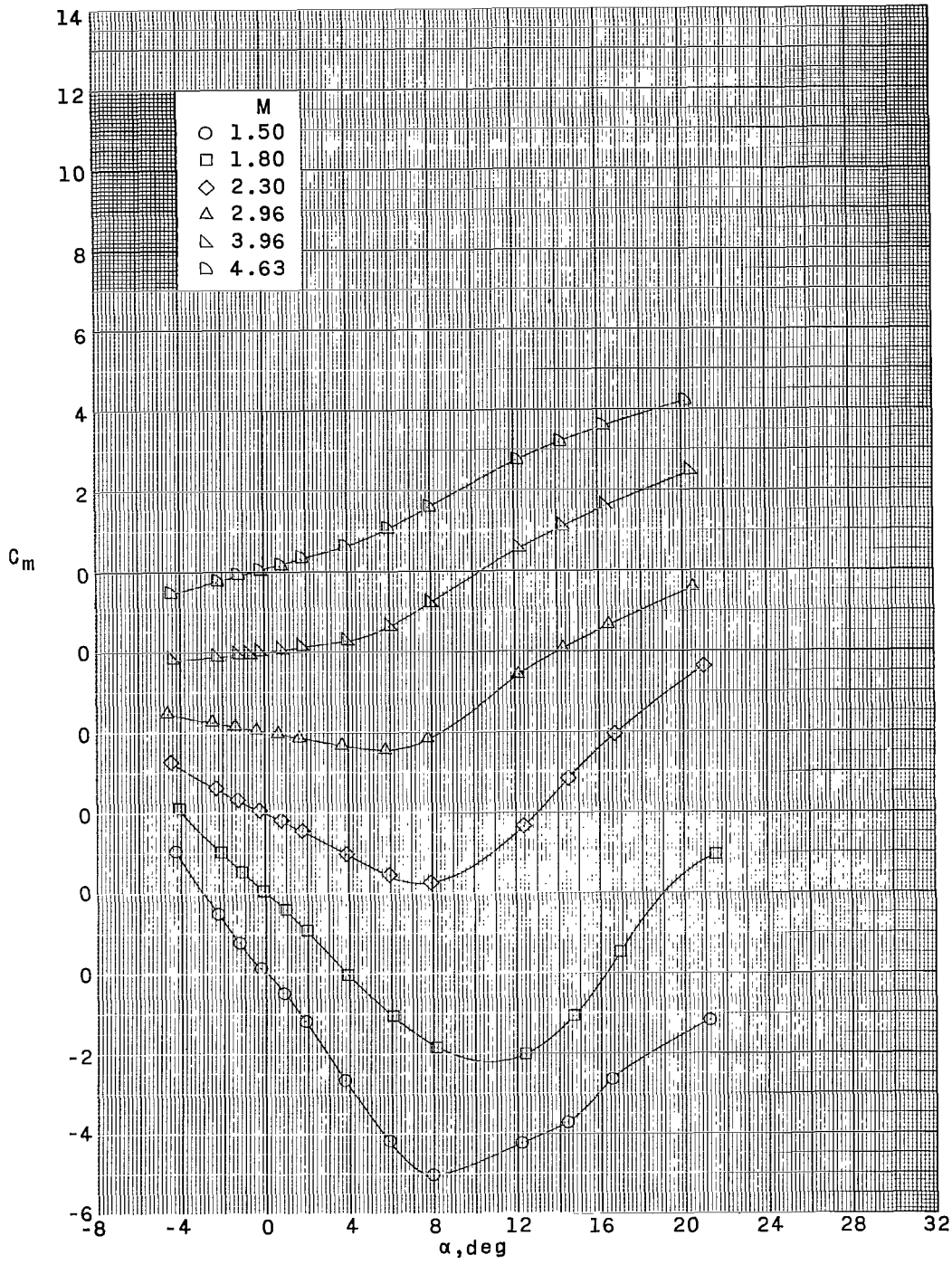

(b) Continued.

Figure 5.- Continued.

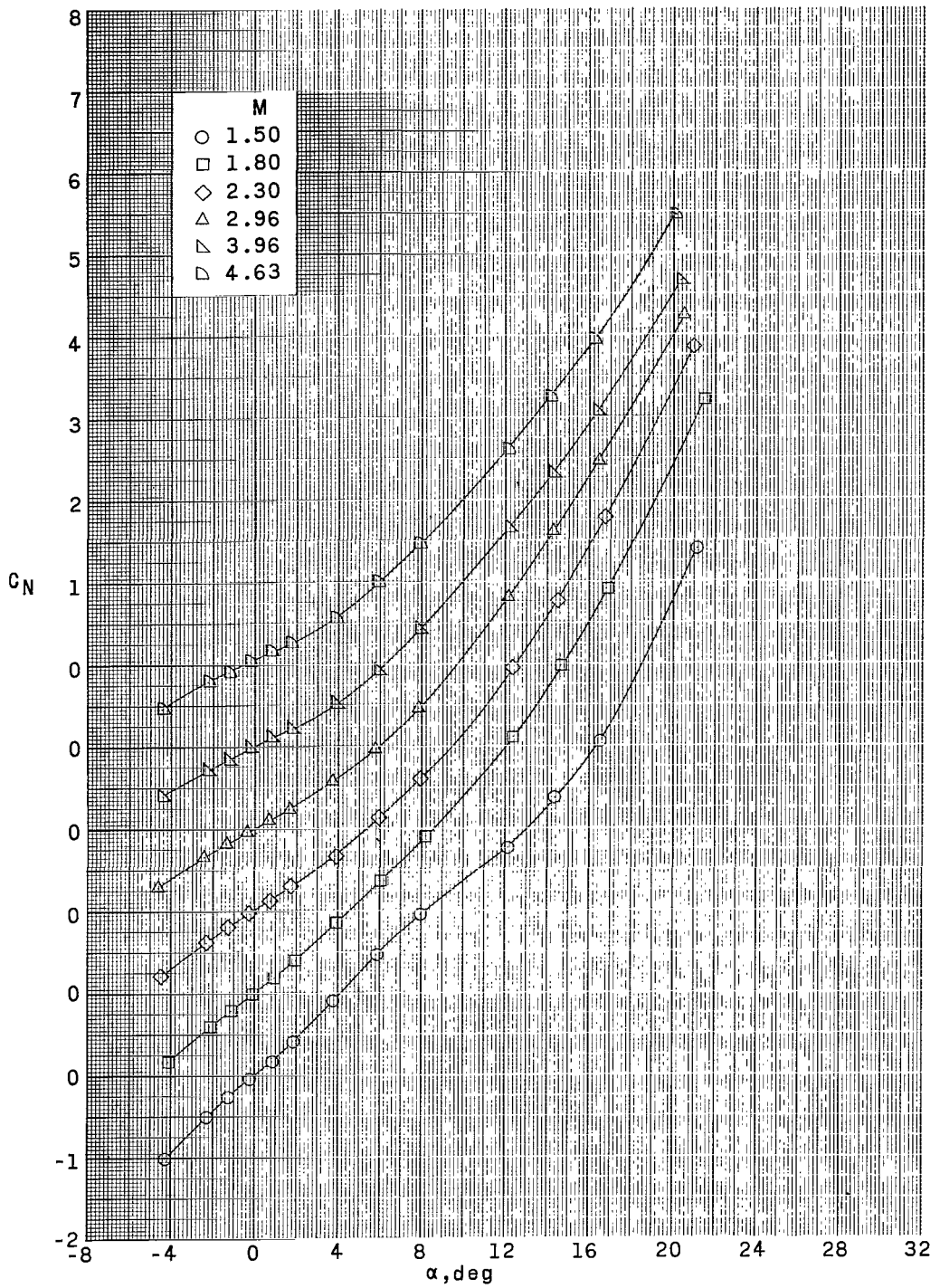

(b) Concluded.

Figure 5.- Continued.

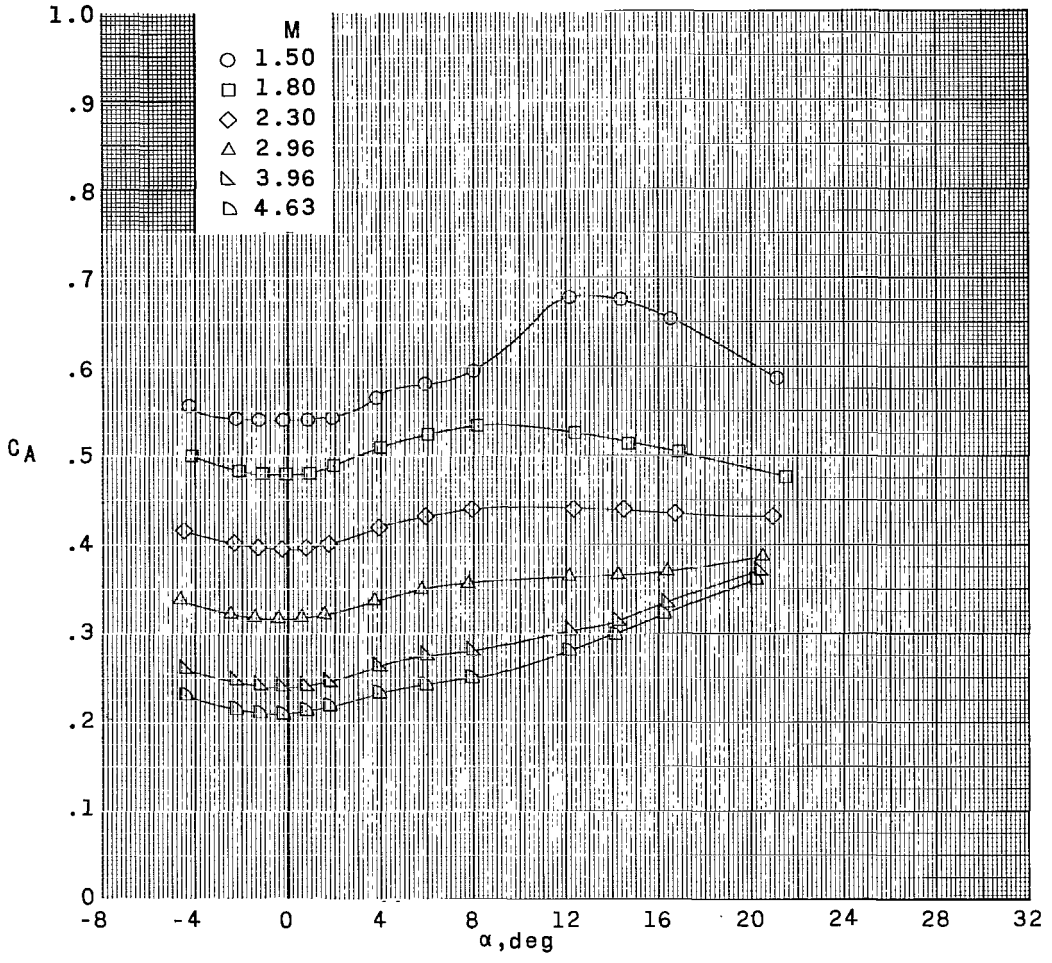

(c) $\delta_F = 2^0$.

Figure 5.- Continued.

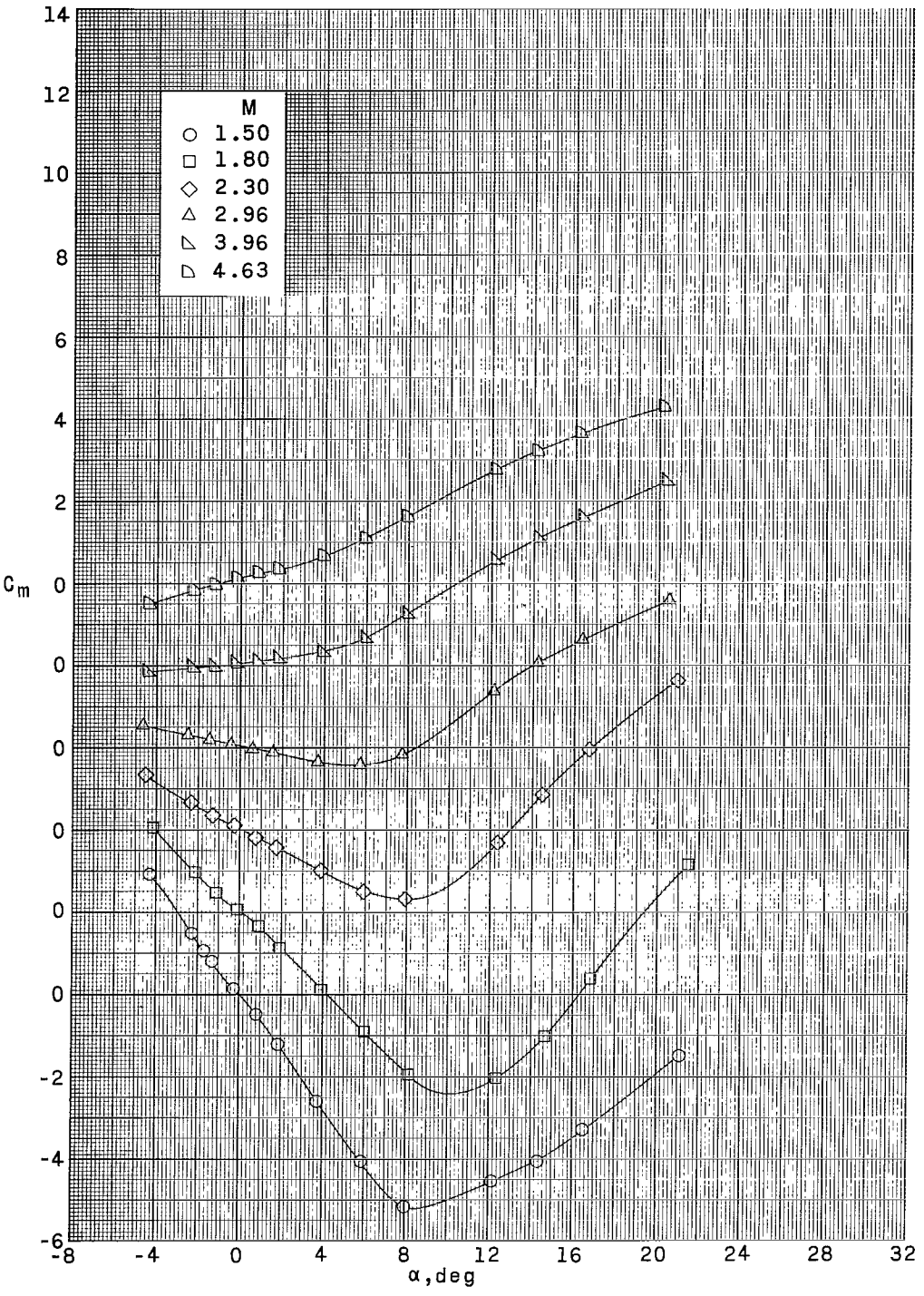

(c) Continued.

Figure 5.- Continued.

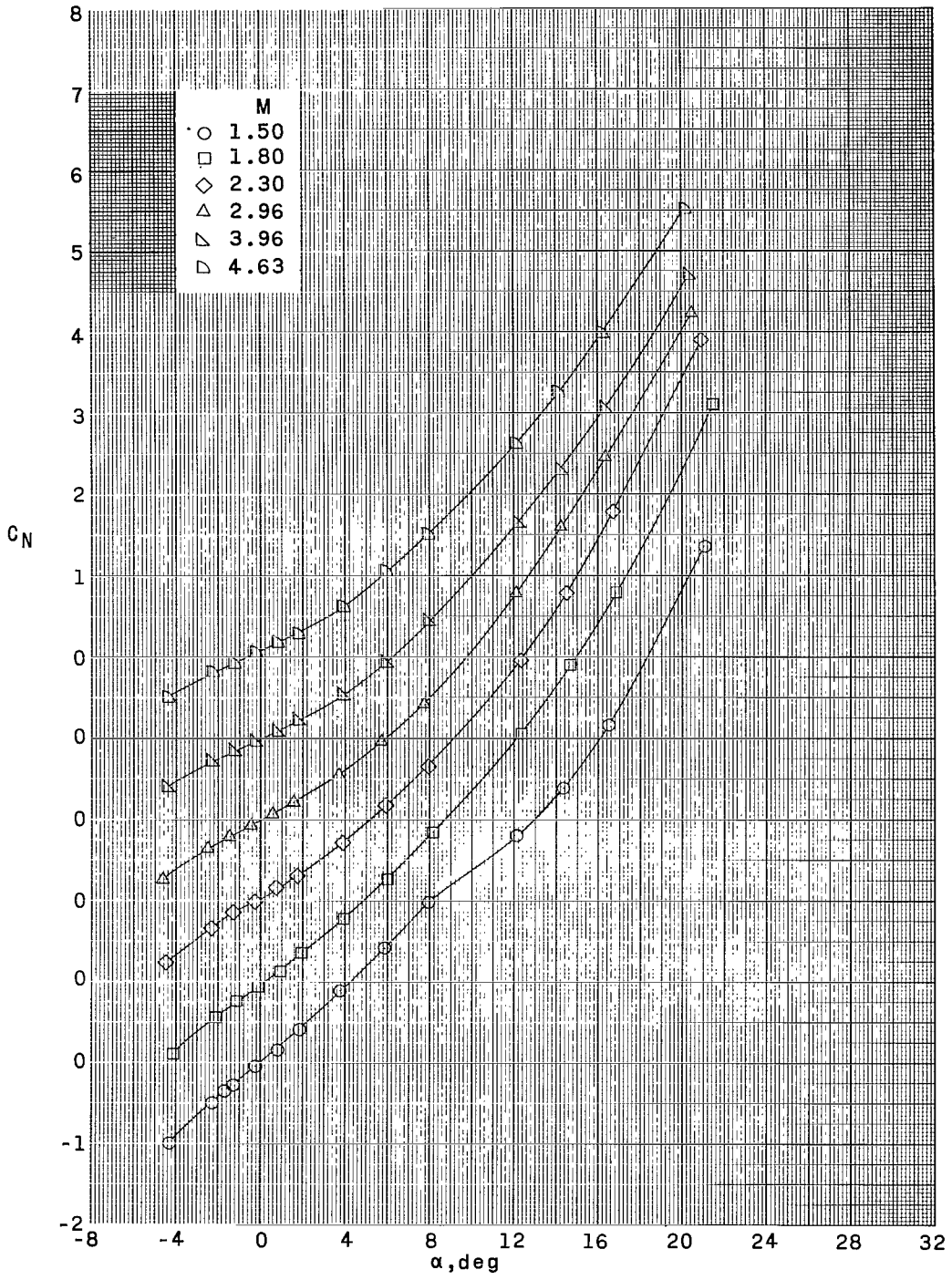

(c) Concluded.

Figure 5.- Concluded.

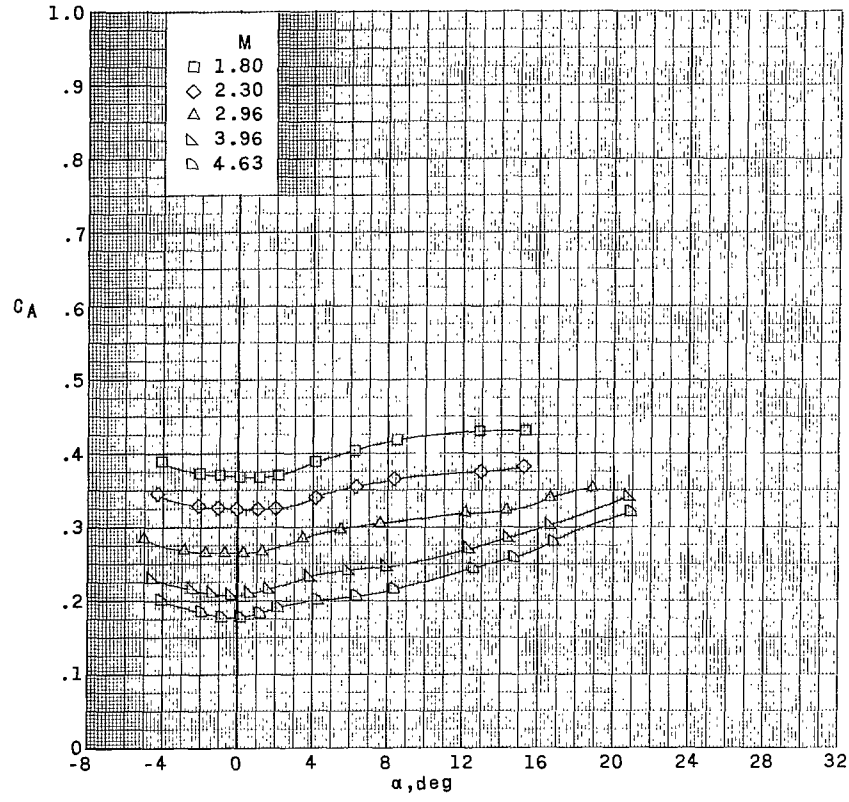

(a) Fins off.

Figure 6.- Aerodynamic characteristics in pitch for configuration 2.

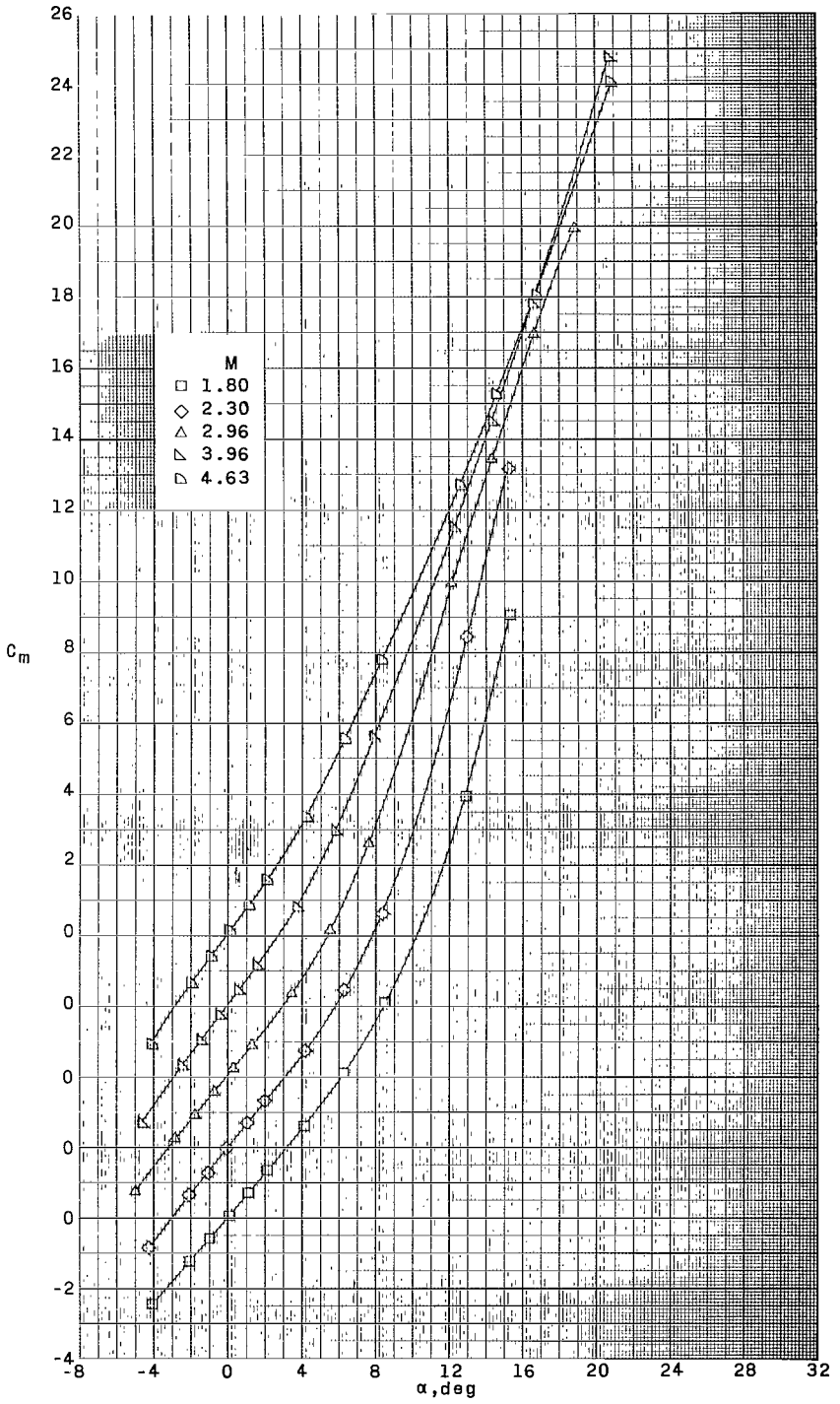

(a) Continued.

Figure 6.- Continued.

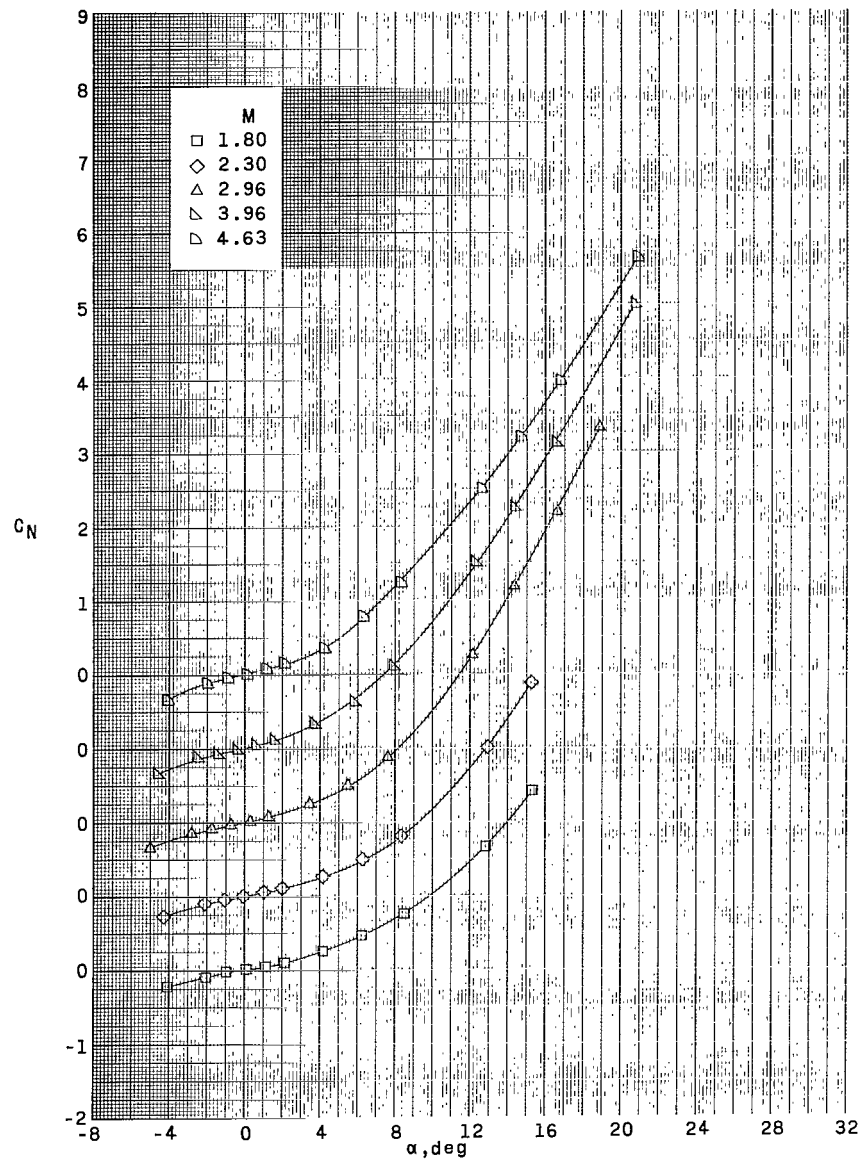

(a) Concluded.

Figure 6.- Continued.

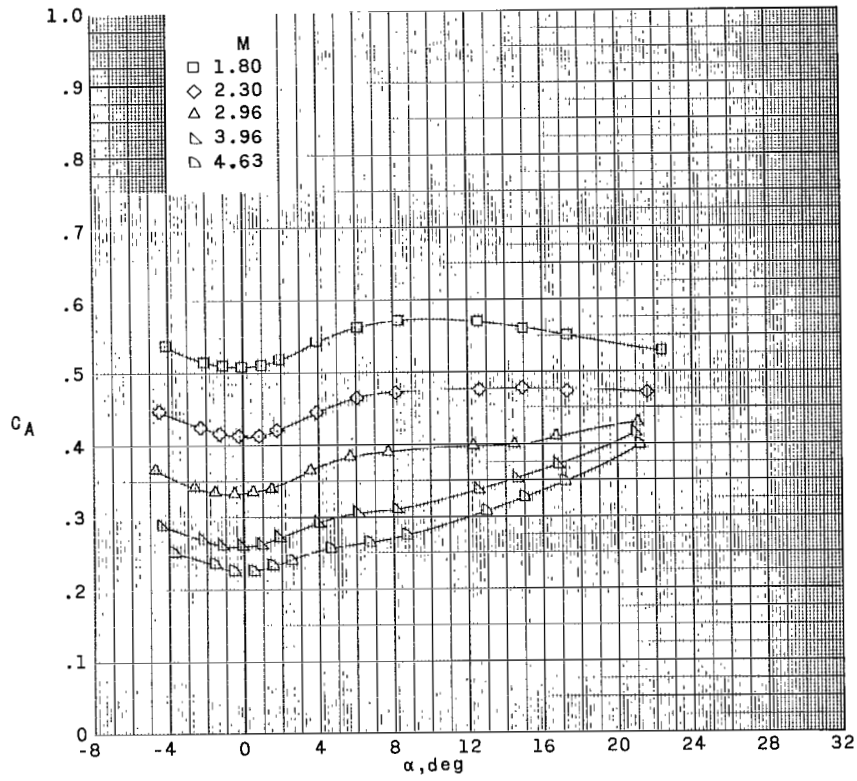

(b) $\delta_F = 0^o$.

Figure 6.- Continued.

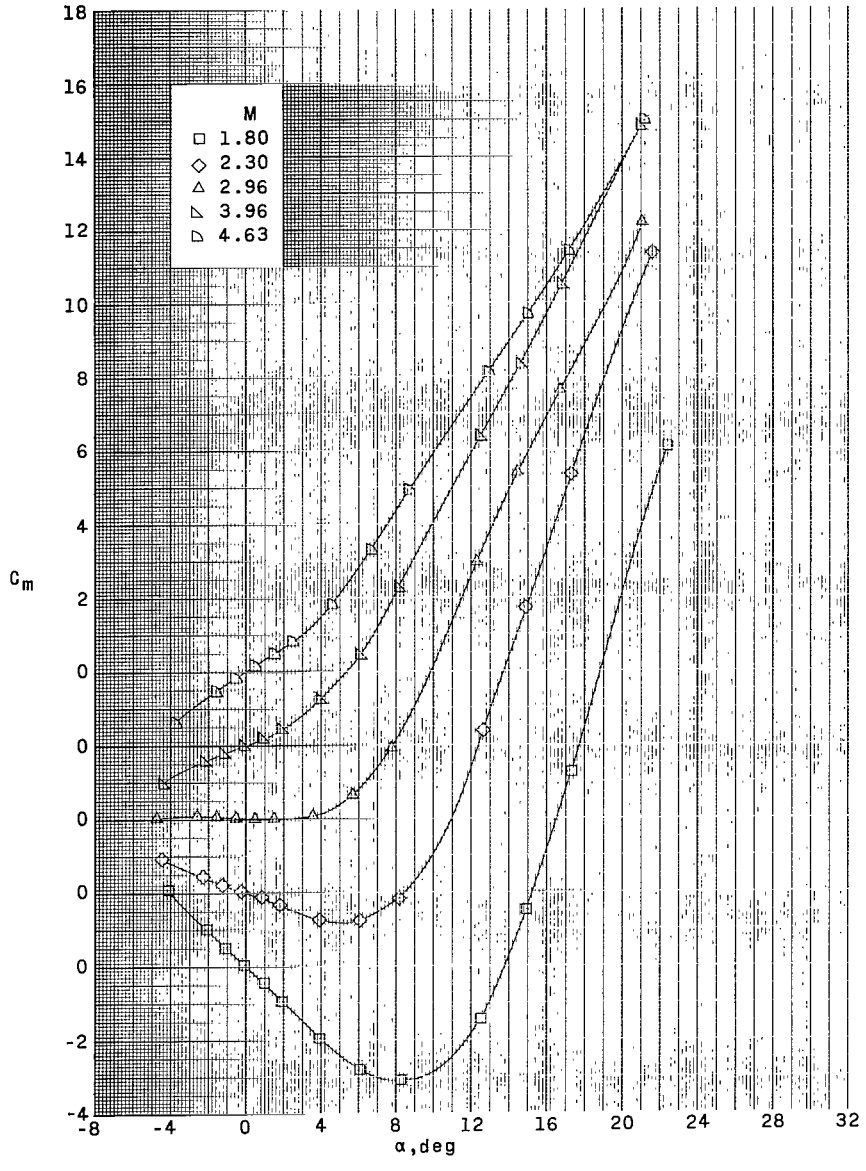

(b) Continued.

Figure 6.- Continued.

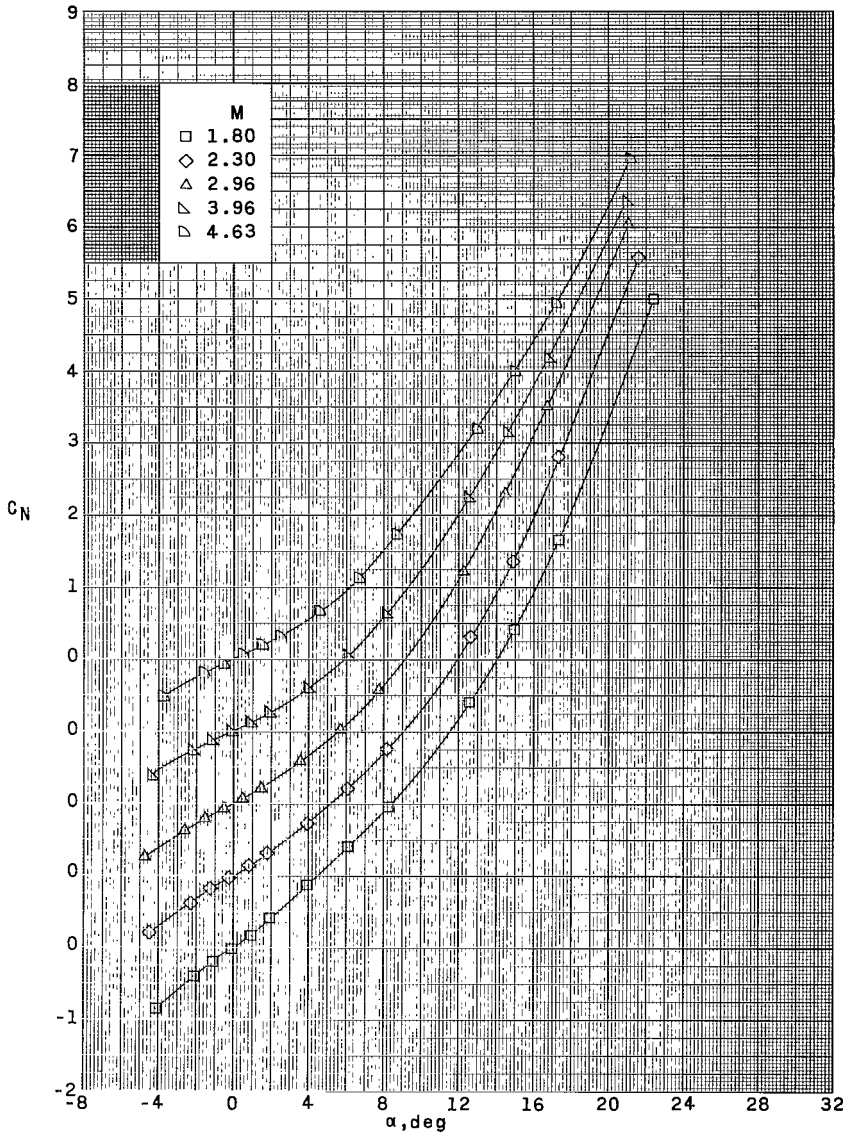

(b) Concluded.

Figure 6.- Continued.

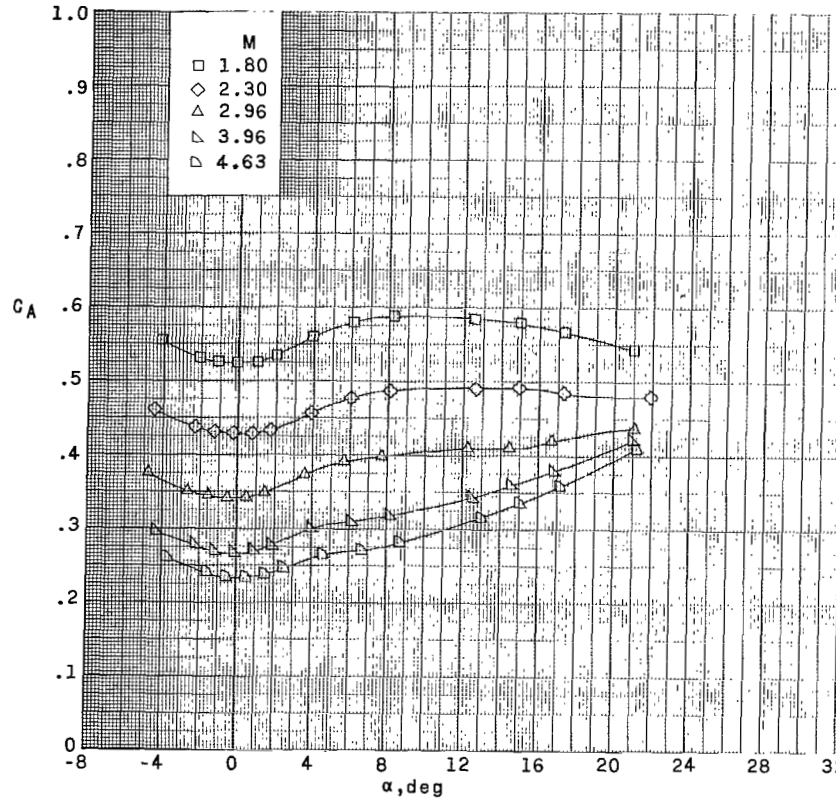

(c) $\delta_F = -2^0$.

Figure 6.- Continued.

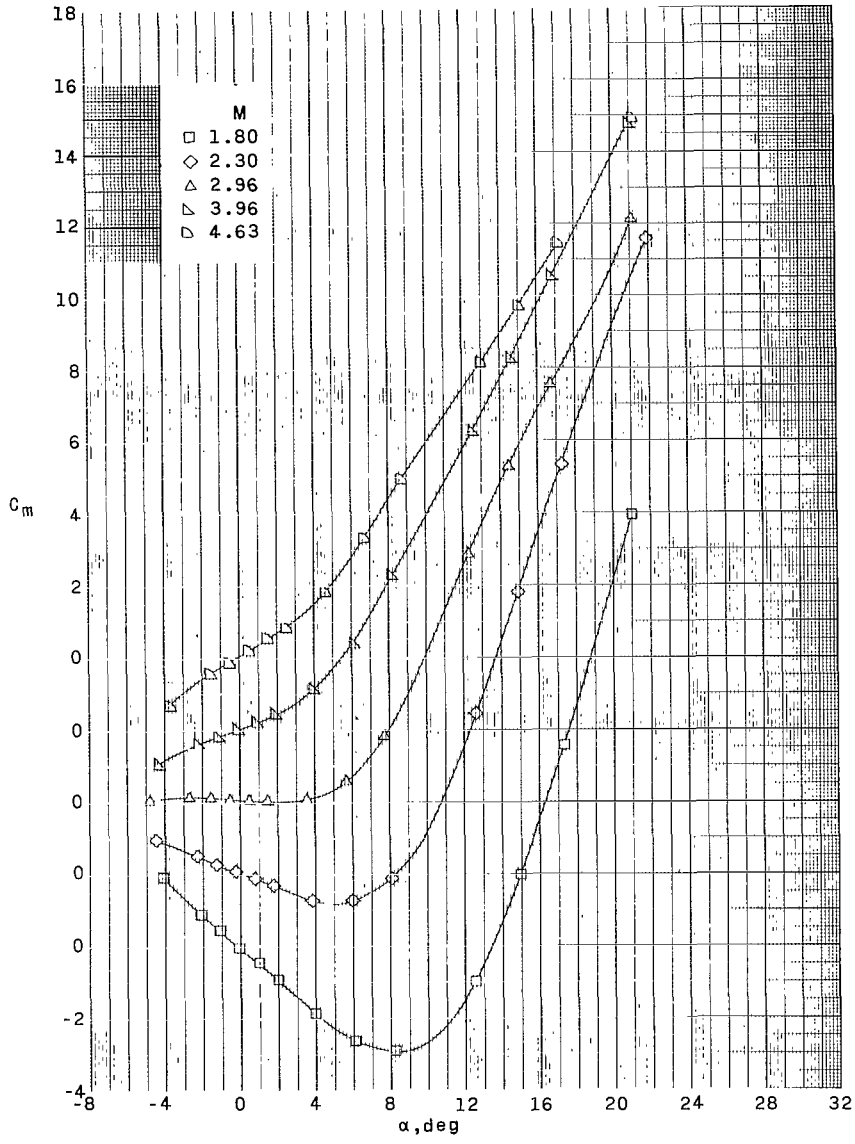

(c) Continued.

Figure 6.- Continued.

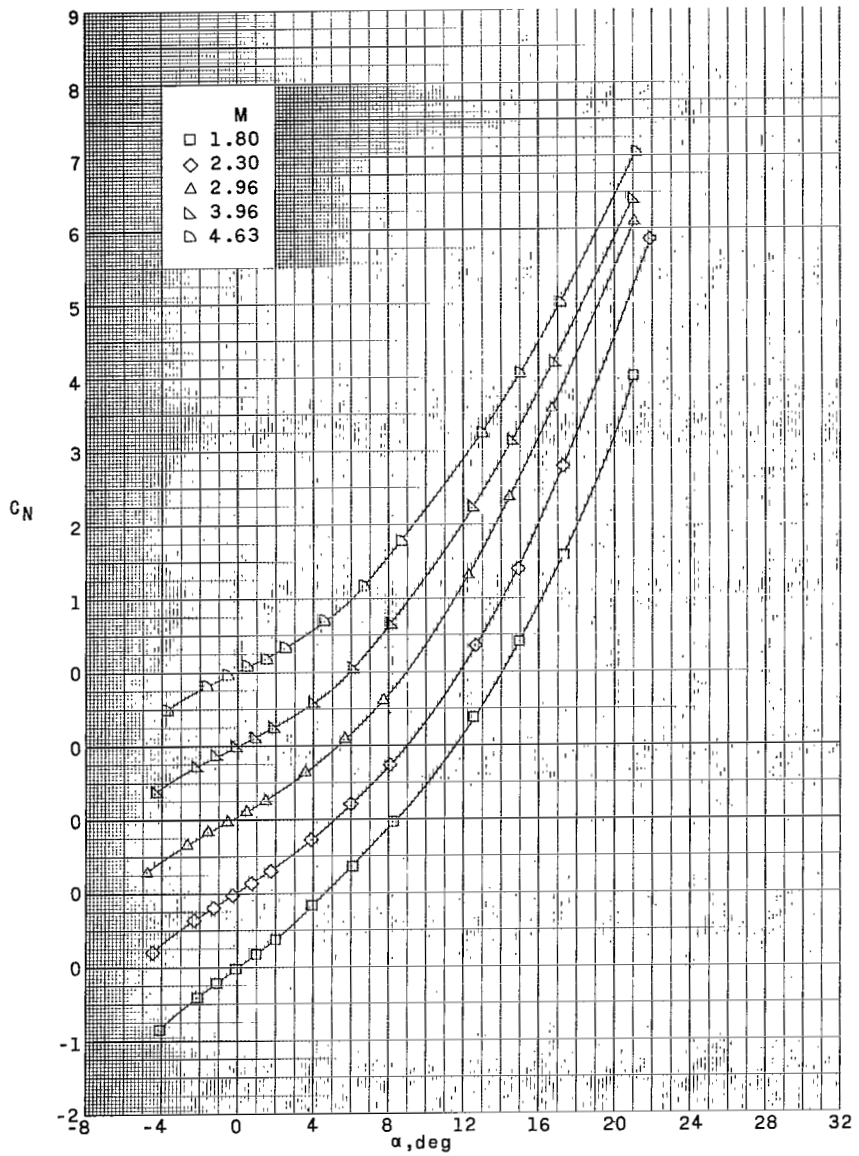

(c) Concluded.

Figure 6.- Concluded.

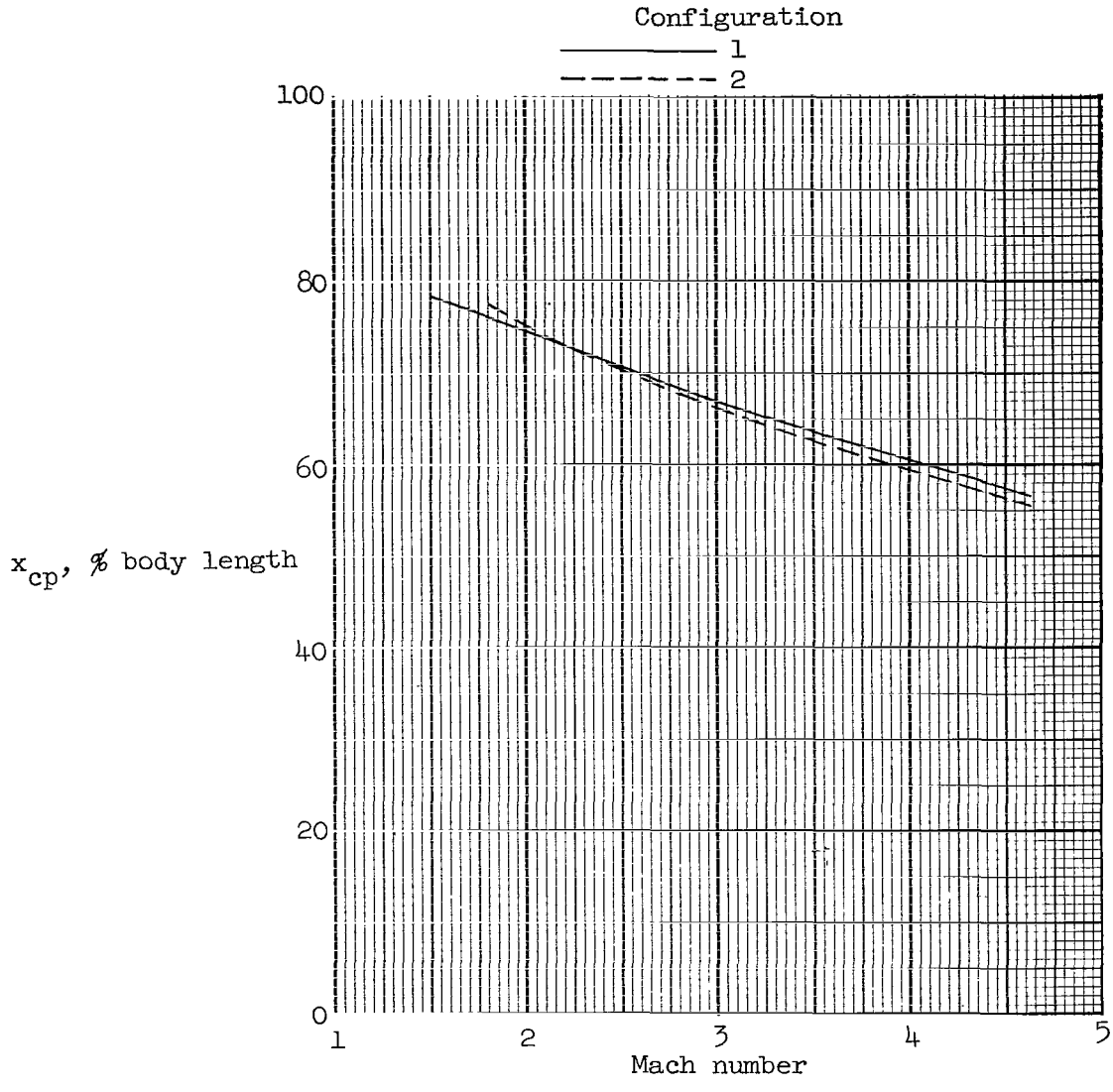

Figure 7.- Variation of center of pressure with Mach number at low angles of attack.

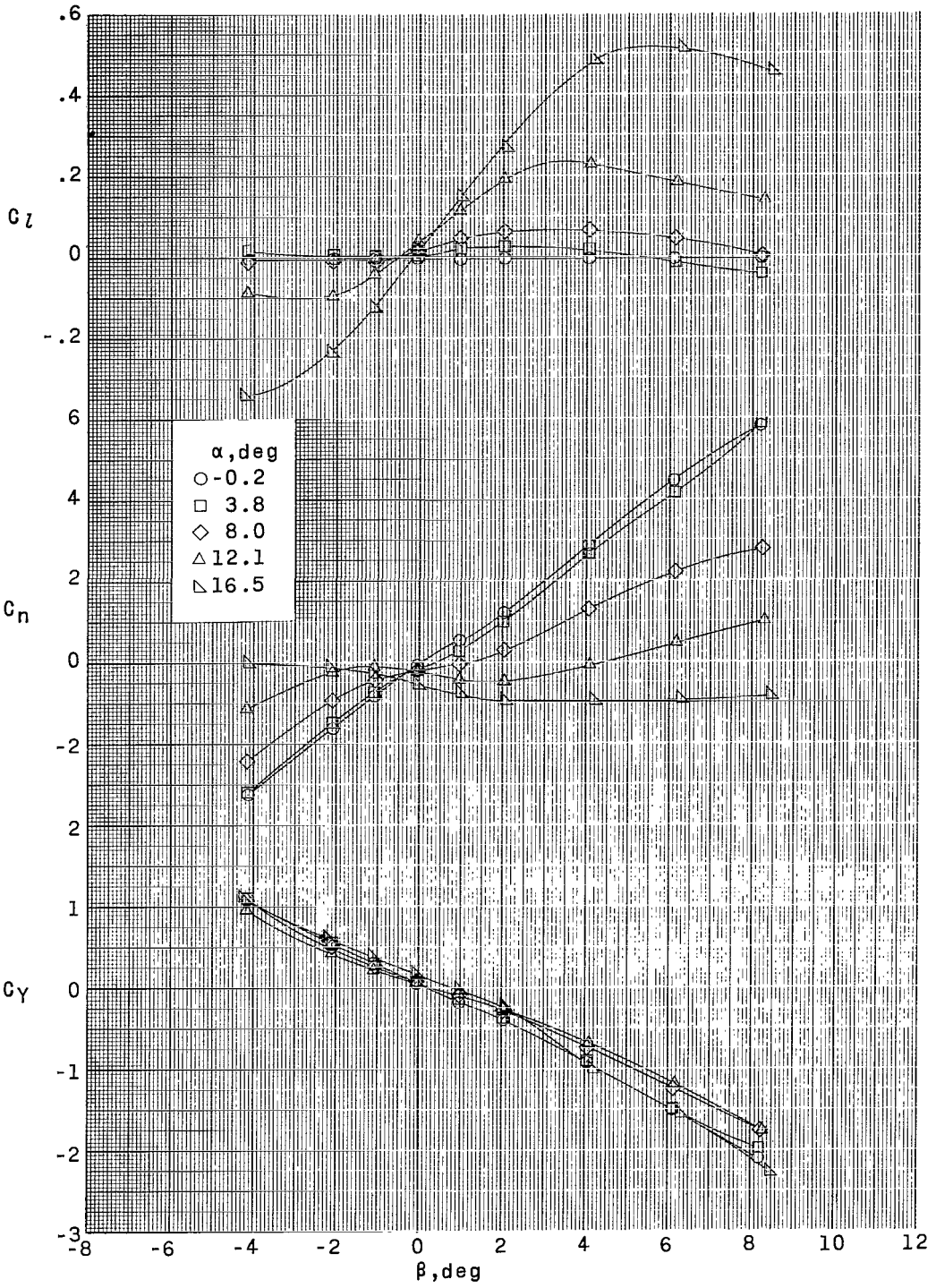

(a) M = 1.50.

Figure 8.- Aerodynamic characteristics in sideslip for configuration 1. $\delta_F = 0^0$.

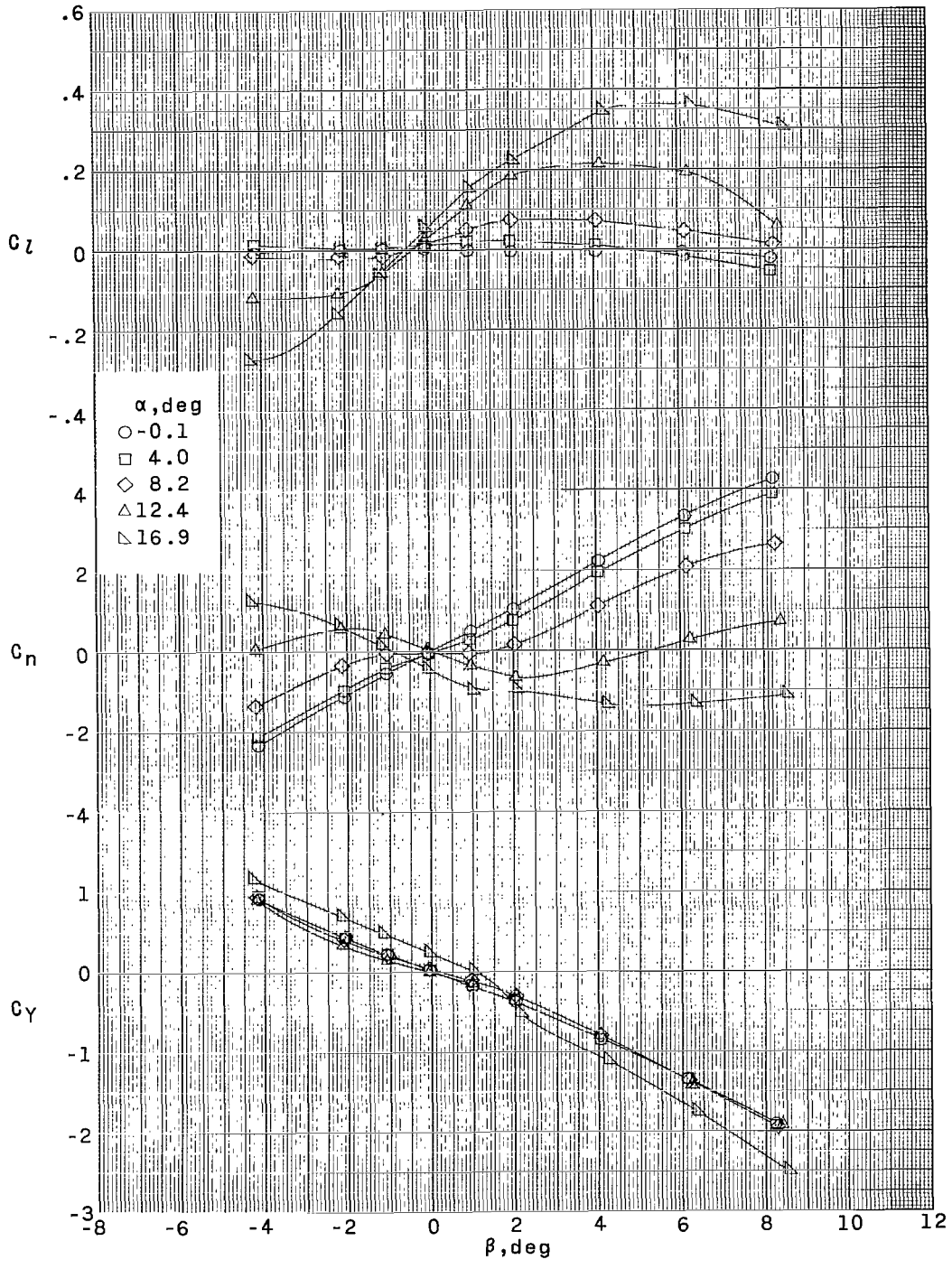

(b) M = 1.80.

Figure 8.- Continued.

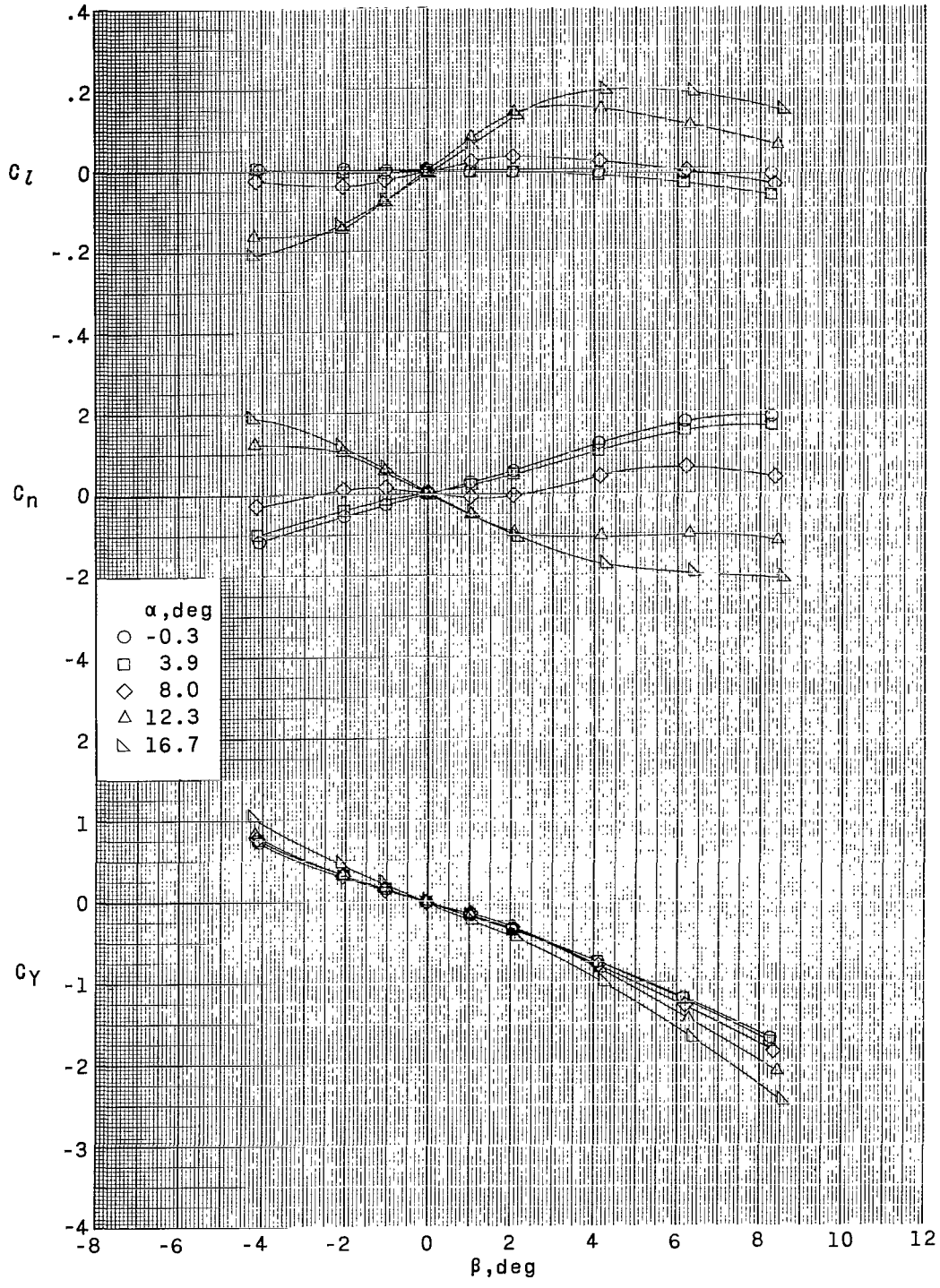

(c) M = 2.30.

Figure 8.- Continued.

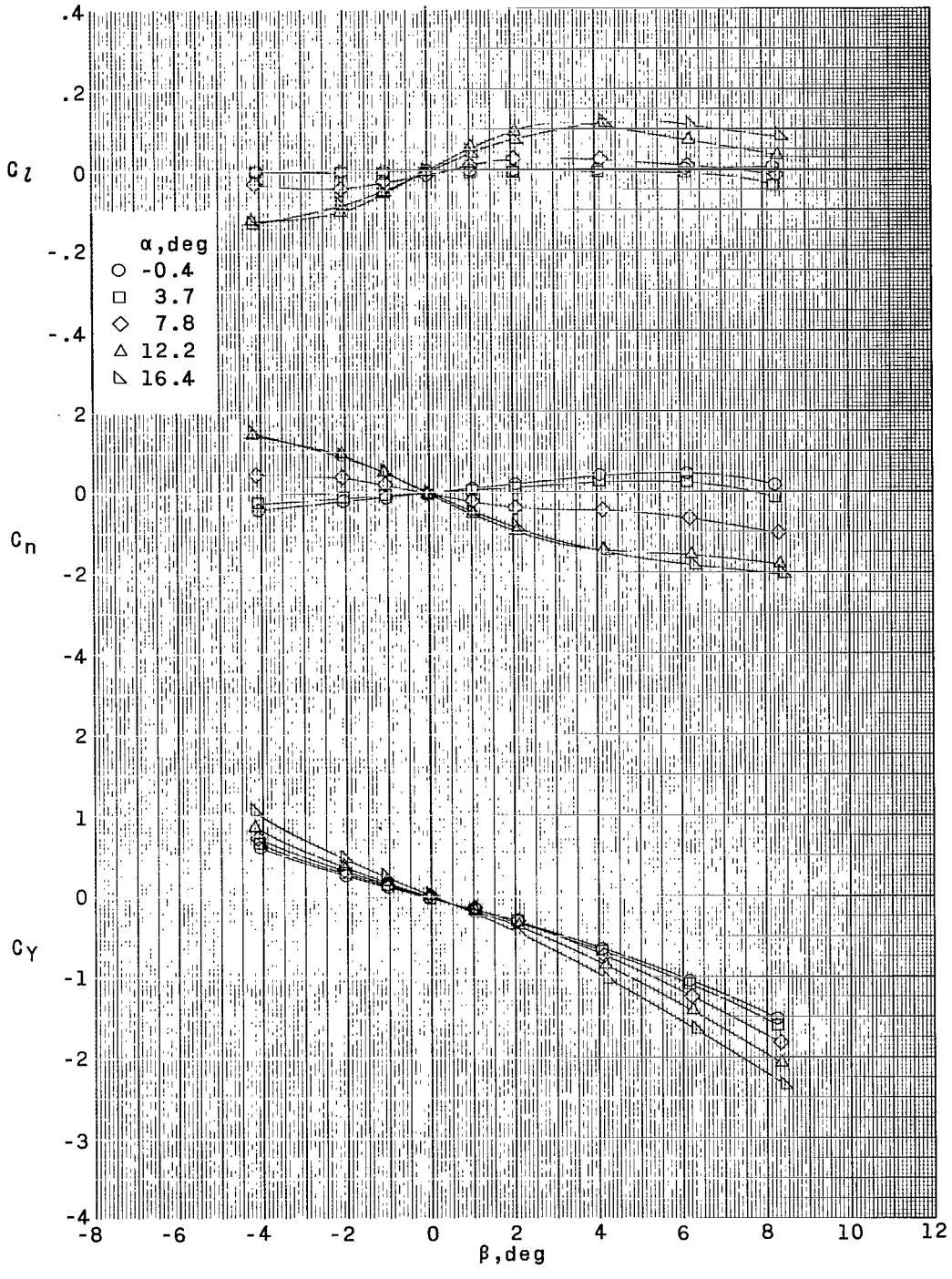

(d) M = 2.96.

Figure 8.- Continued.

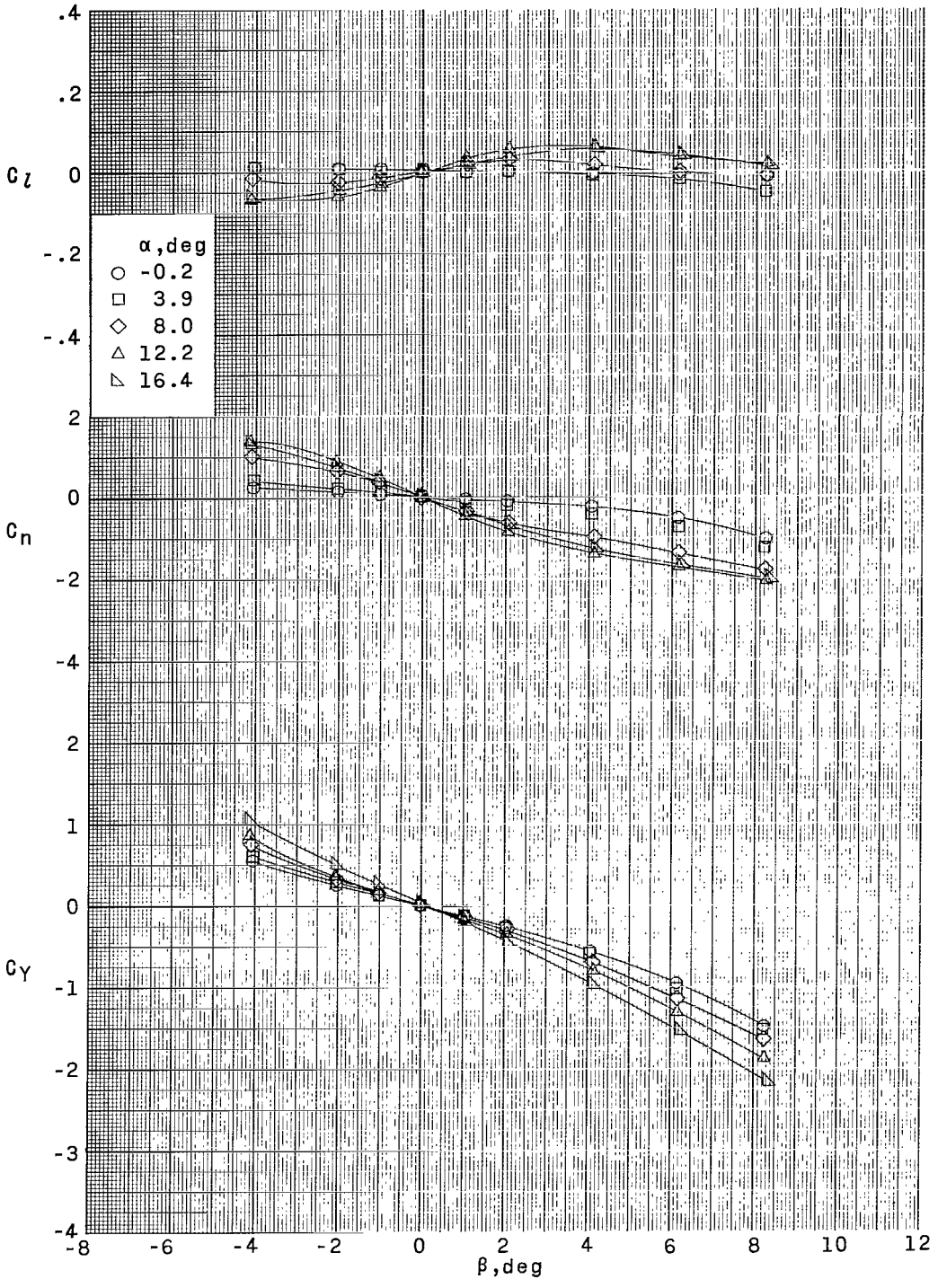

(e) M = 3.96.

Figure 8.- Continued.

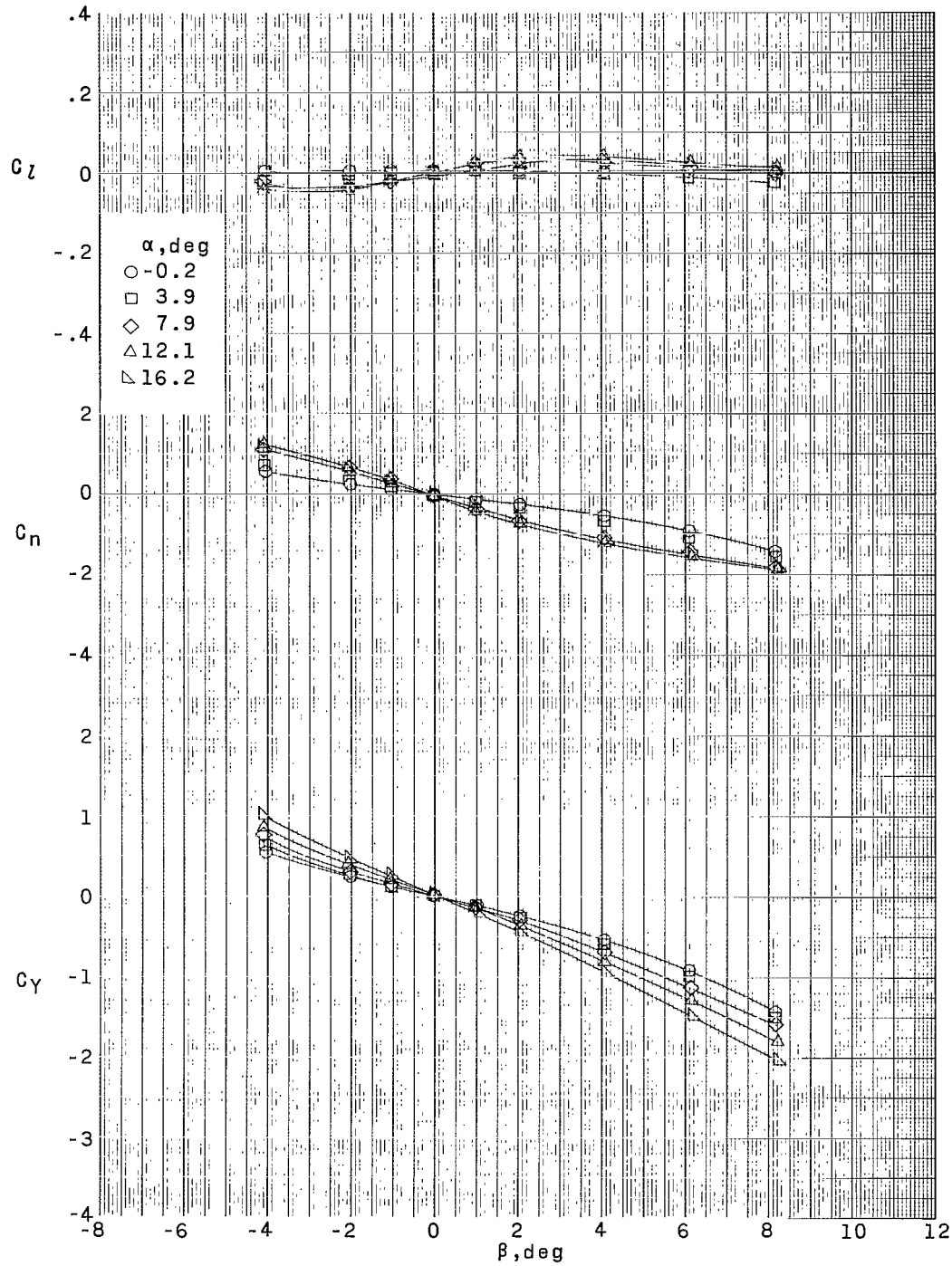

(f) M = 4.63.

Figure 8.- Concluded.

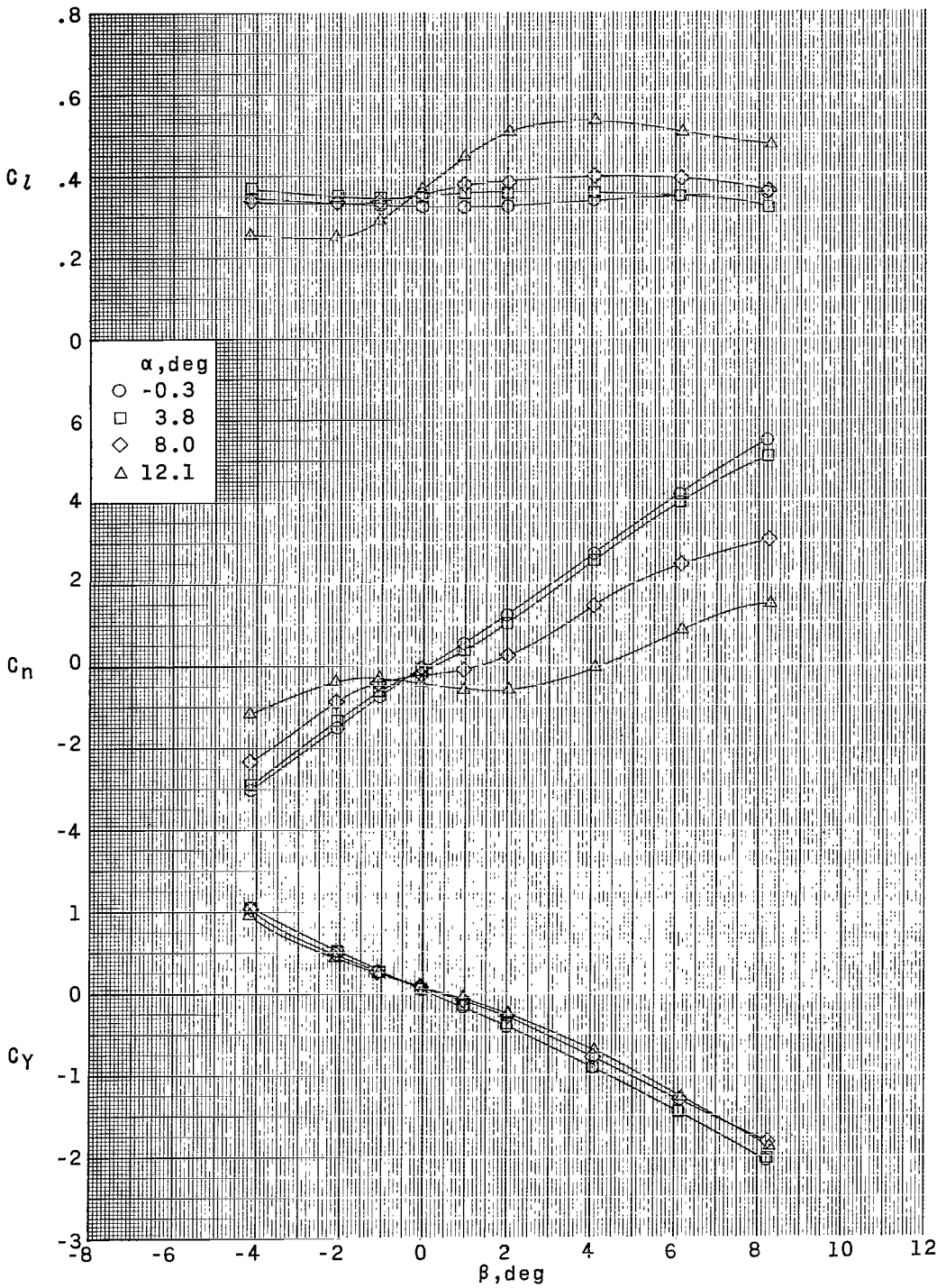

(a) M = 1.50.

Figure 9.- Aerodynamic characteristics in sideslip for configuration 1. $\delta_F = -2^0$.

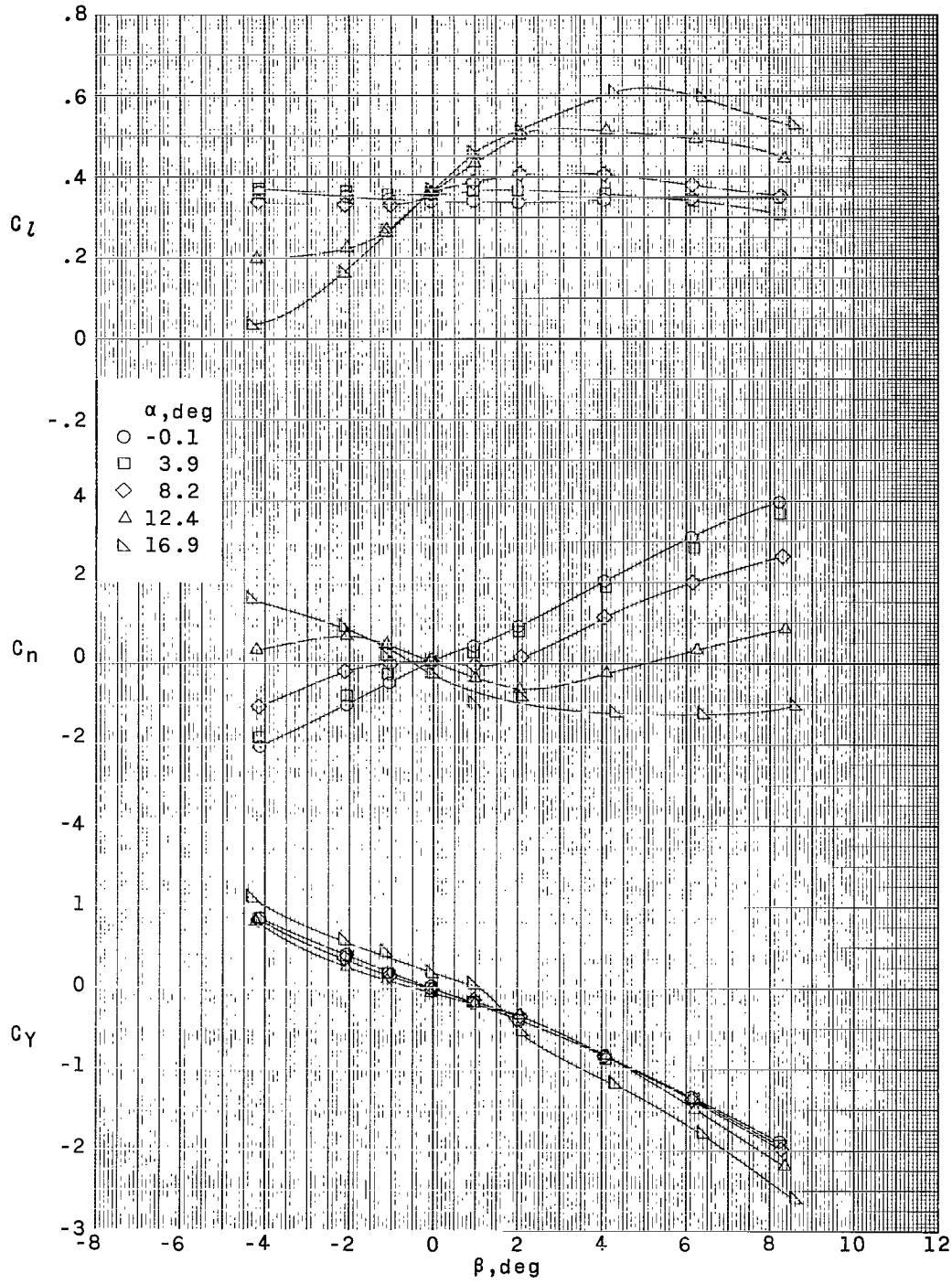

(b) M = 1.80.

Figure 9.- Continued.

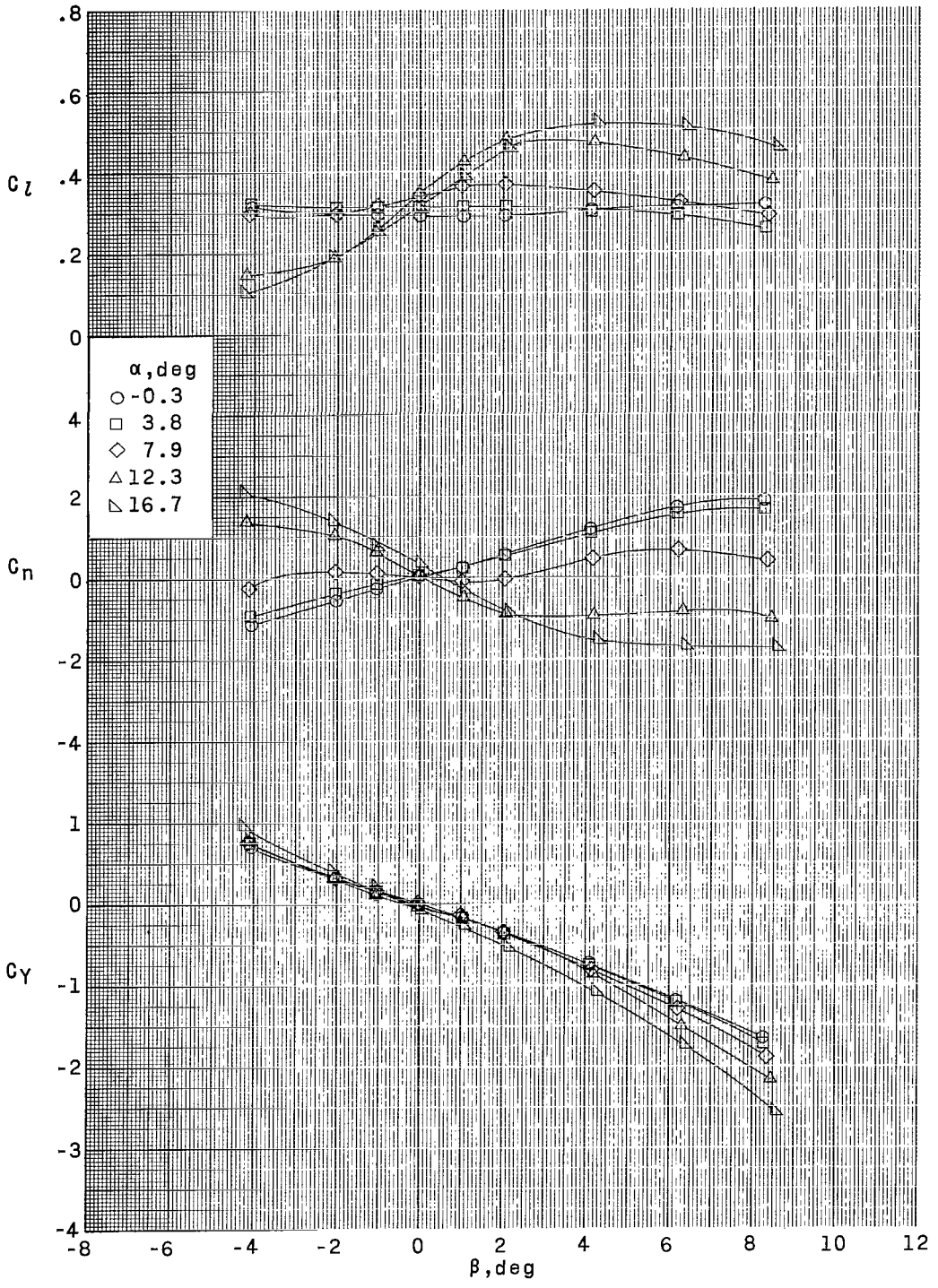

(c) M = 2.30.

Figure 9.- Continued.

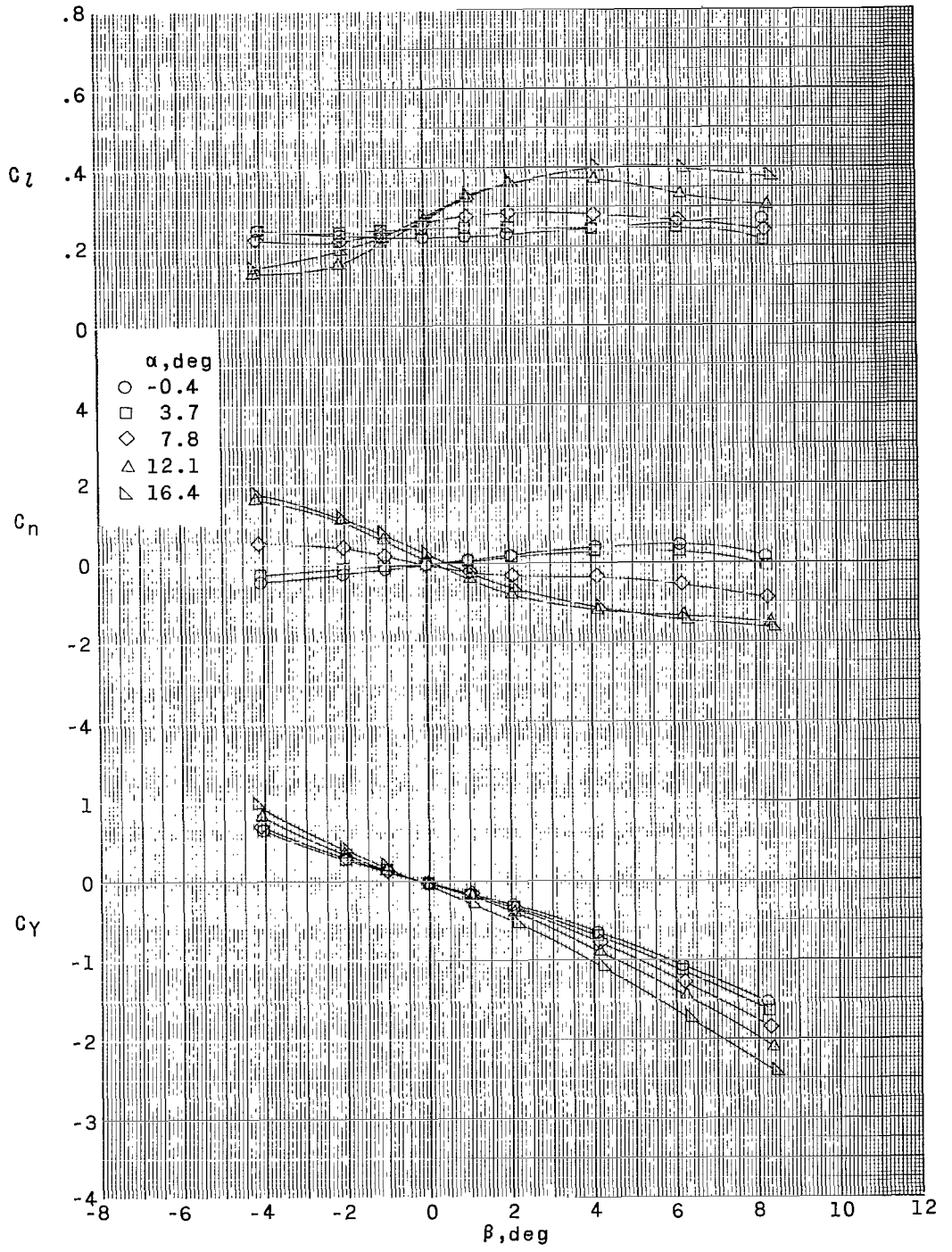

(d) M = 2.96.

Figure 9.- Continued.

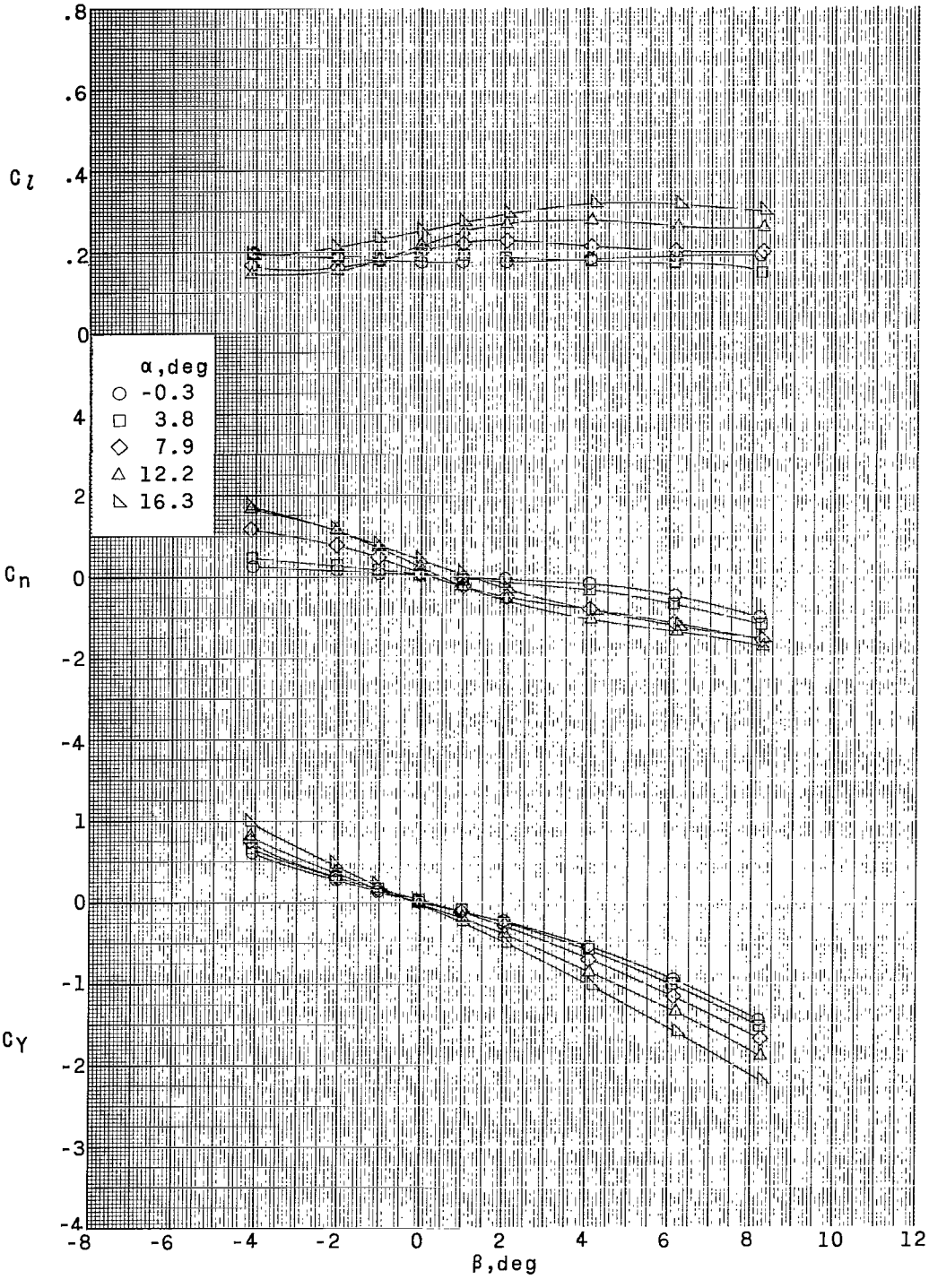

(e) M = 3.96.

Figure 9.- Continued.

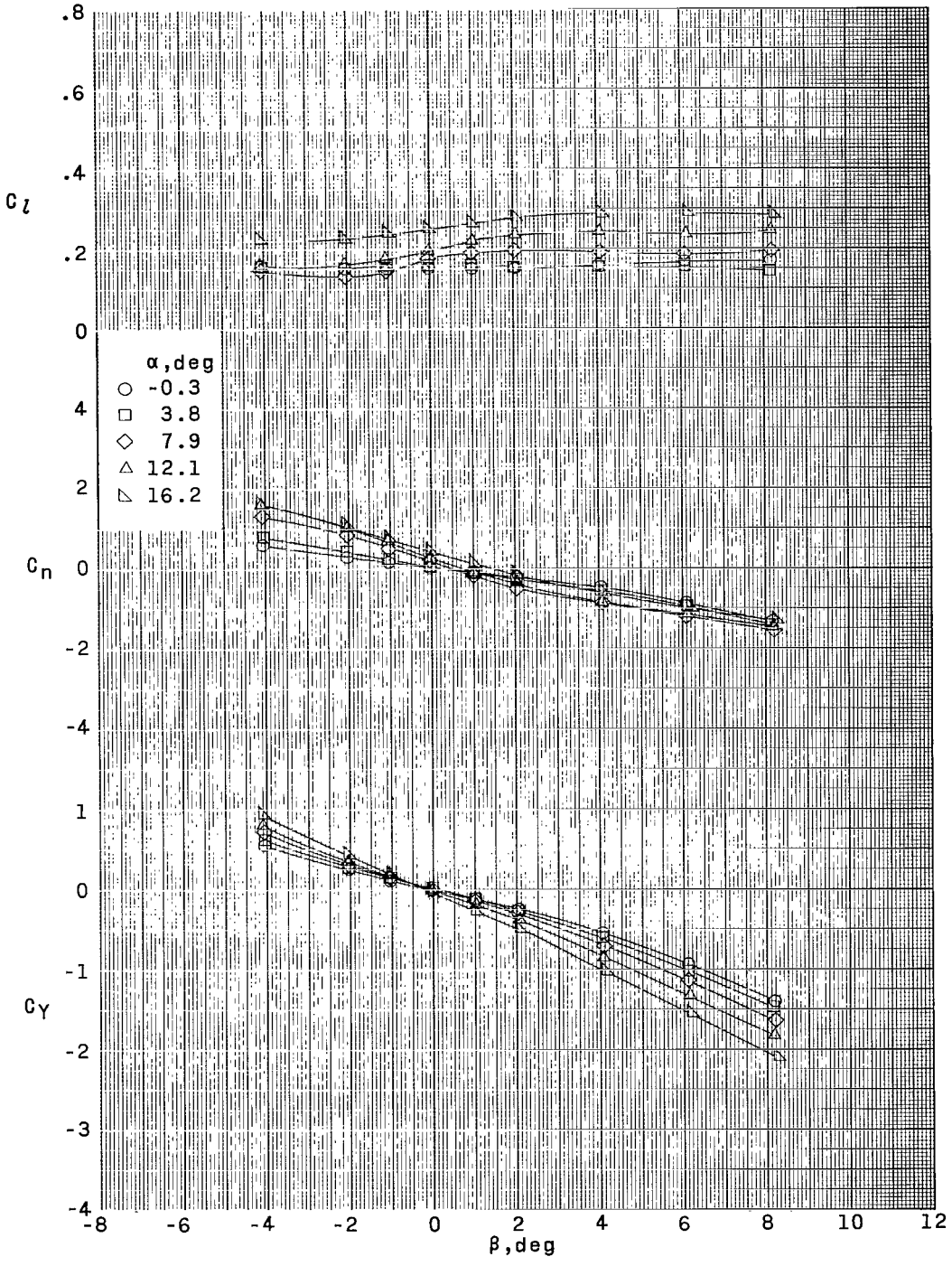

(f) M = 4.63.

Figure 9.- Concluded.

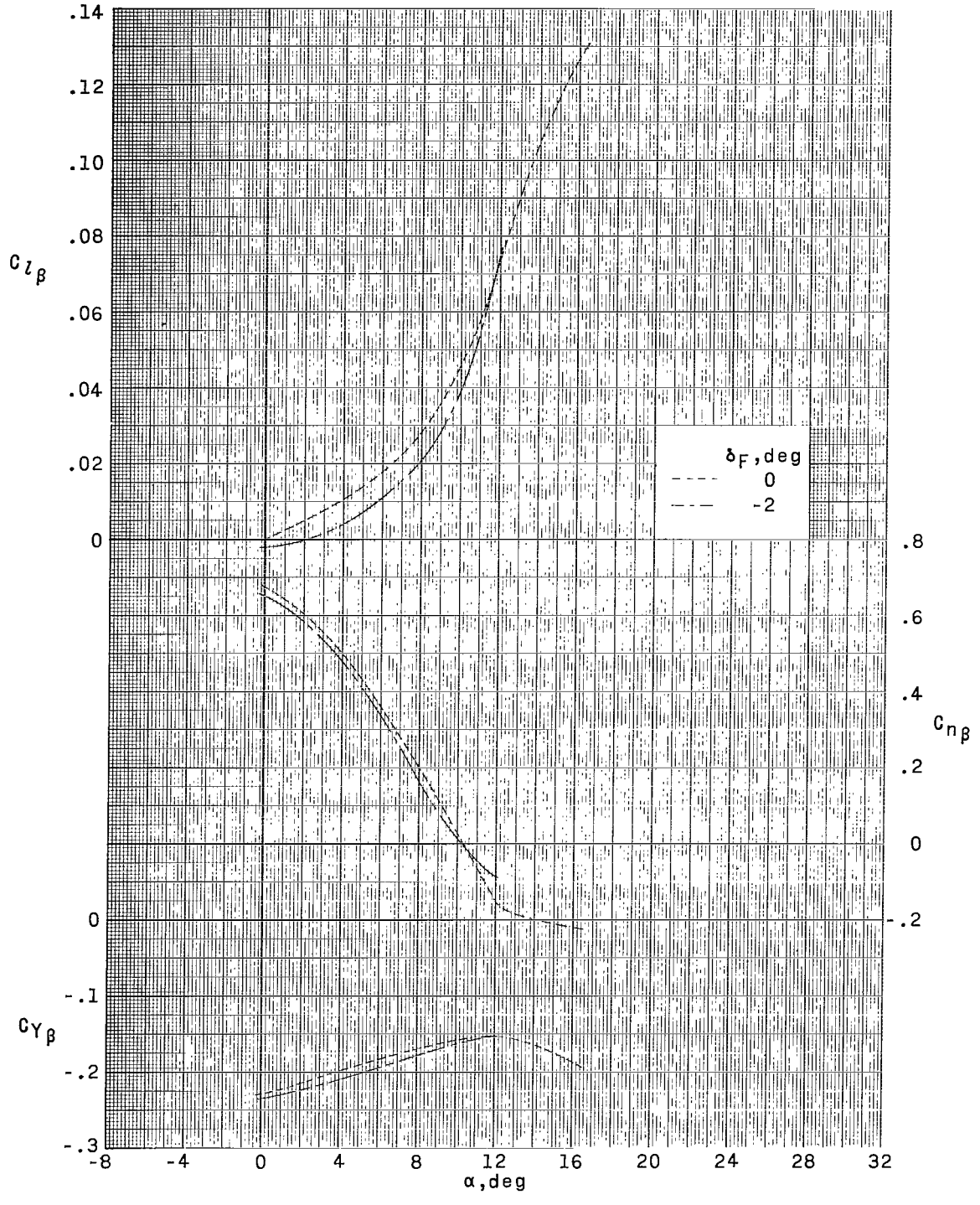

(a) M = 1.50.

Figure 10.- Sideslip parameters for configuration 1.

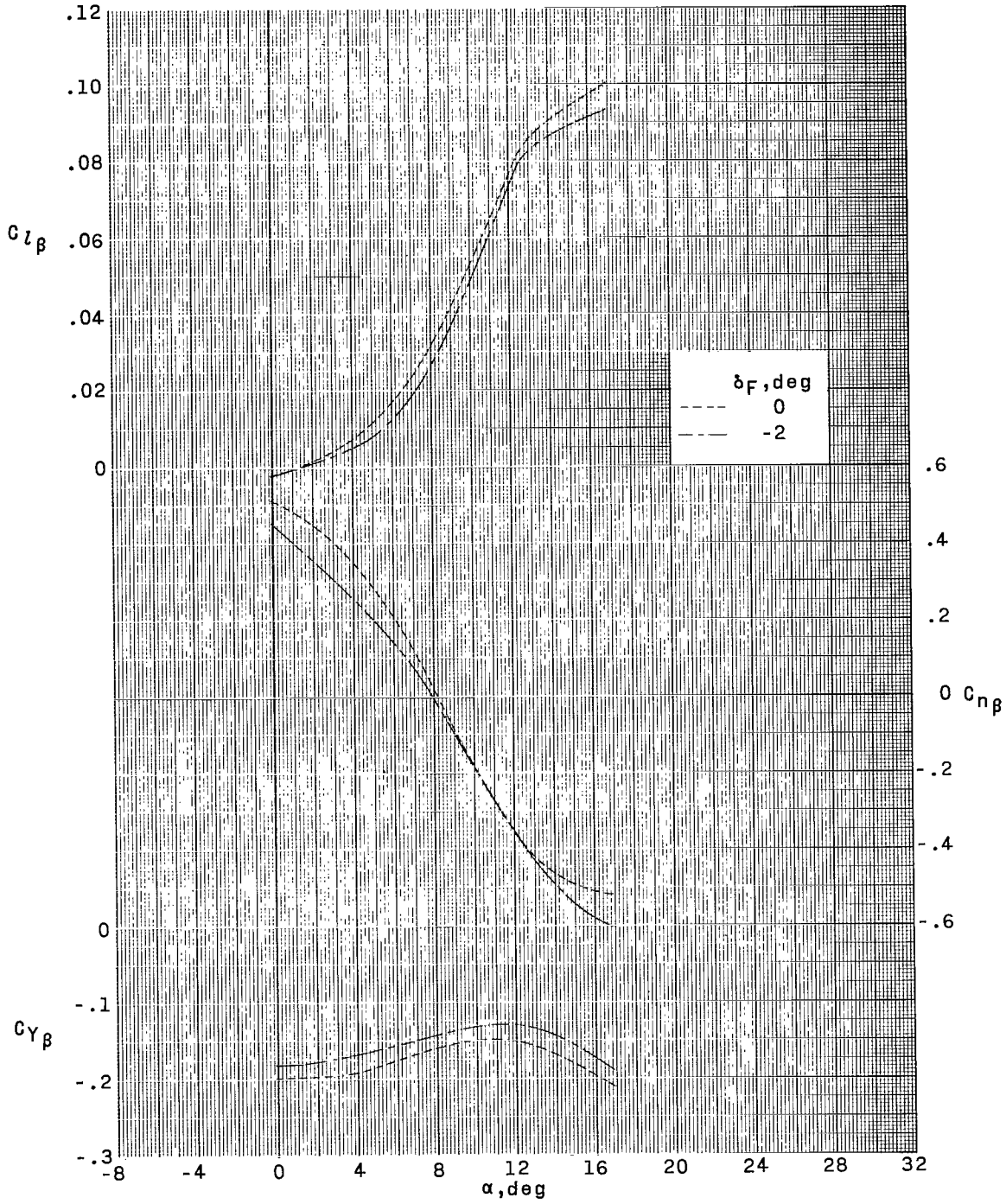

(b) M = 1.80.

Figure 10.- Continued.

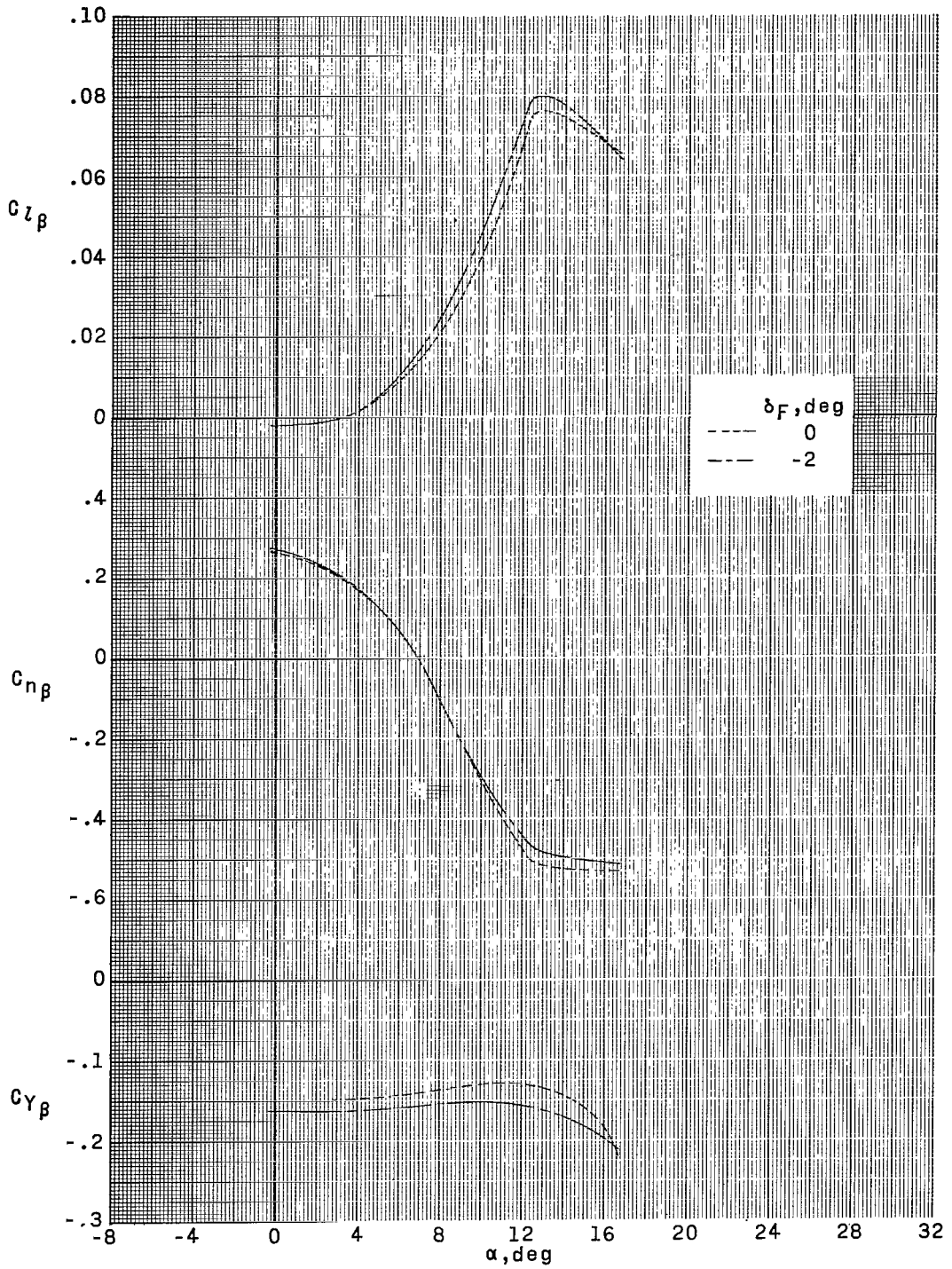

(c) M = 2.30.

Figure 10.- Continued.

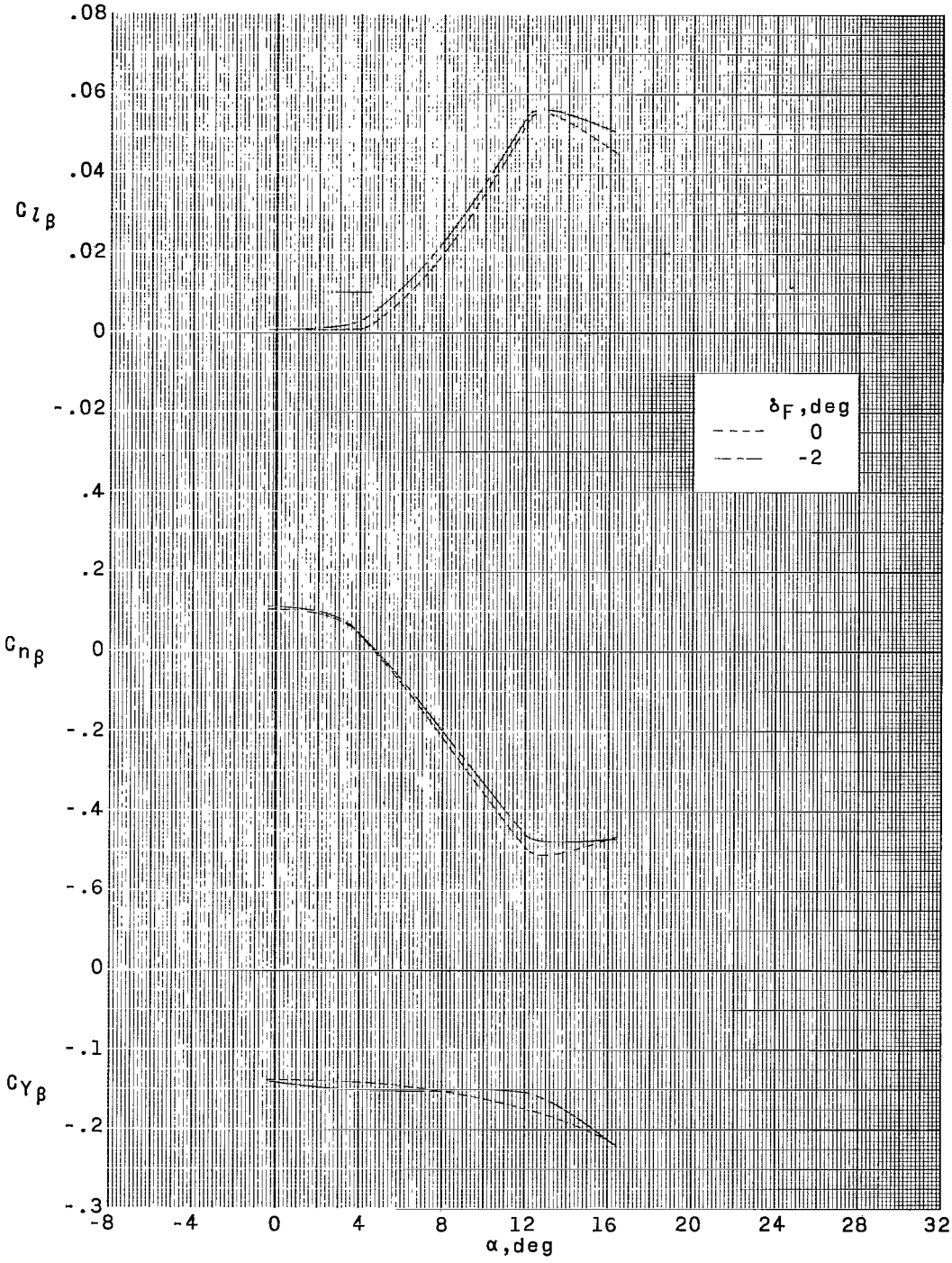

(d) M = 2.96.

Figure 10.- Continued.

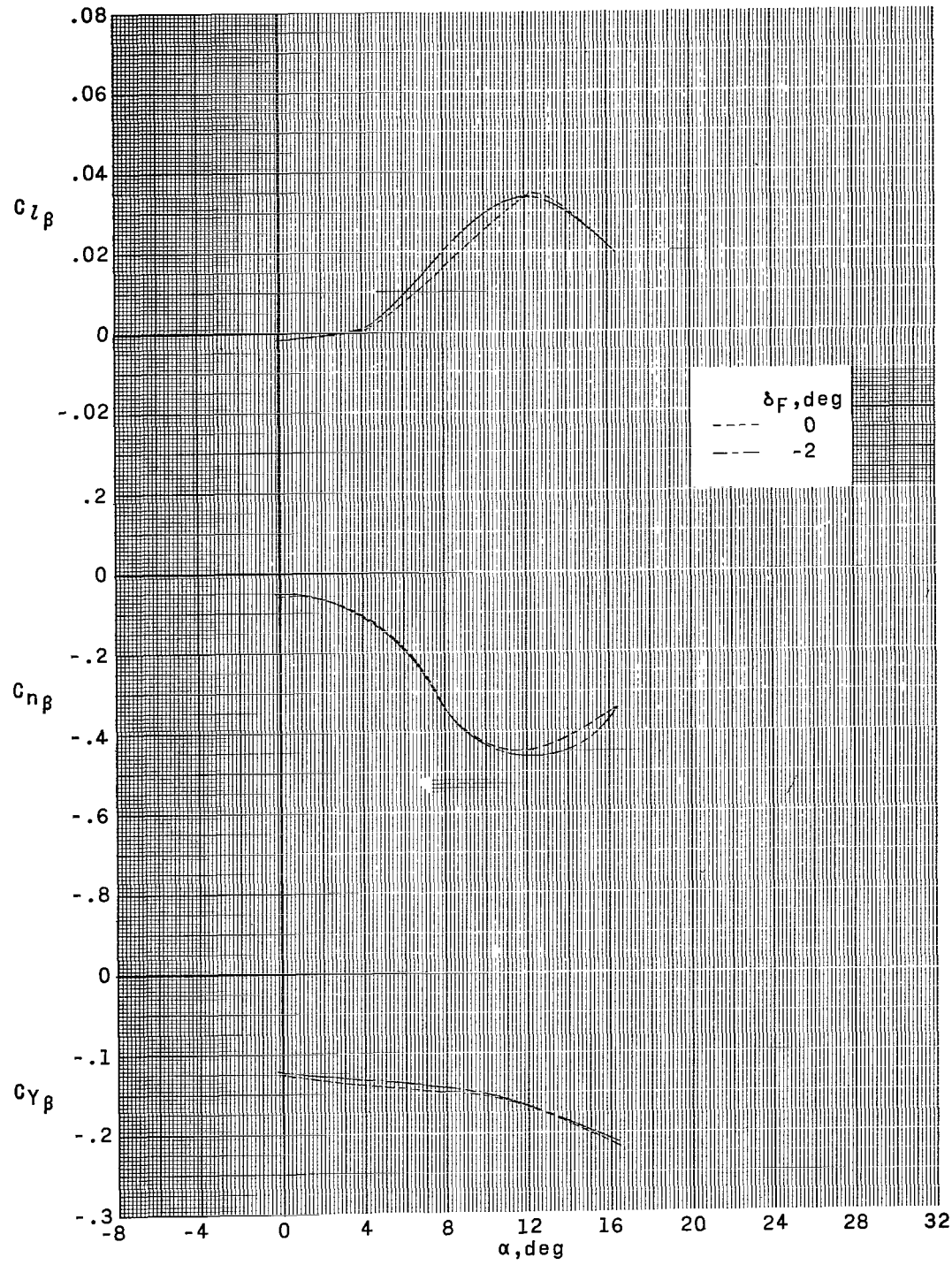

(e) M = 3.96.

Figure 10.- Continued.

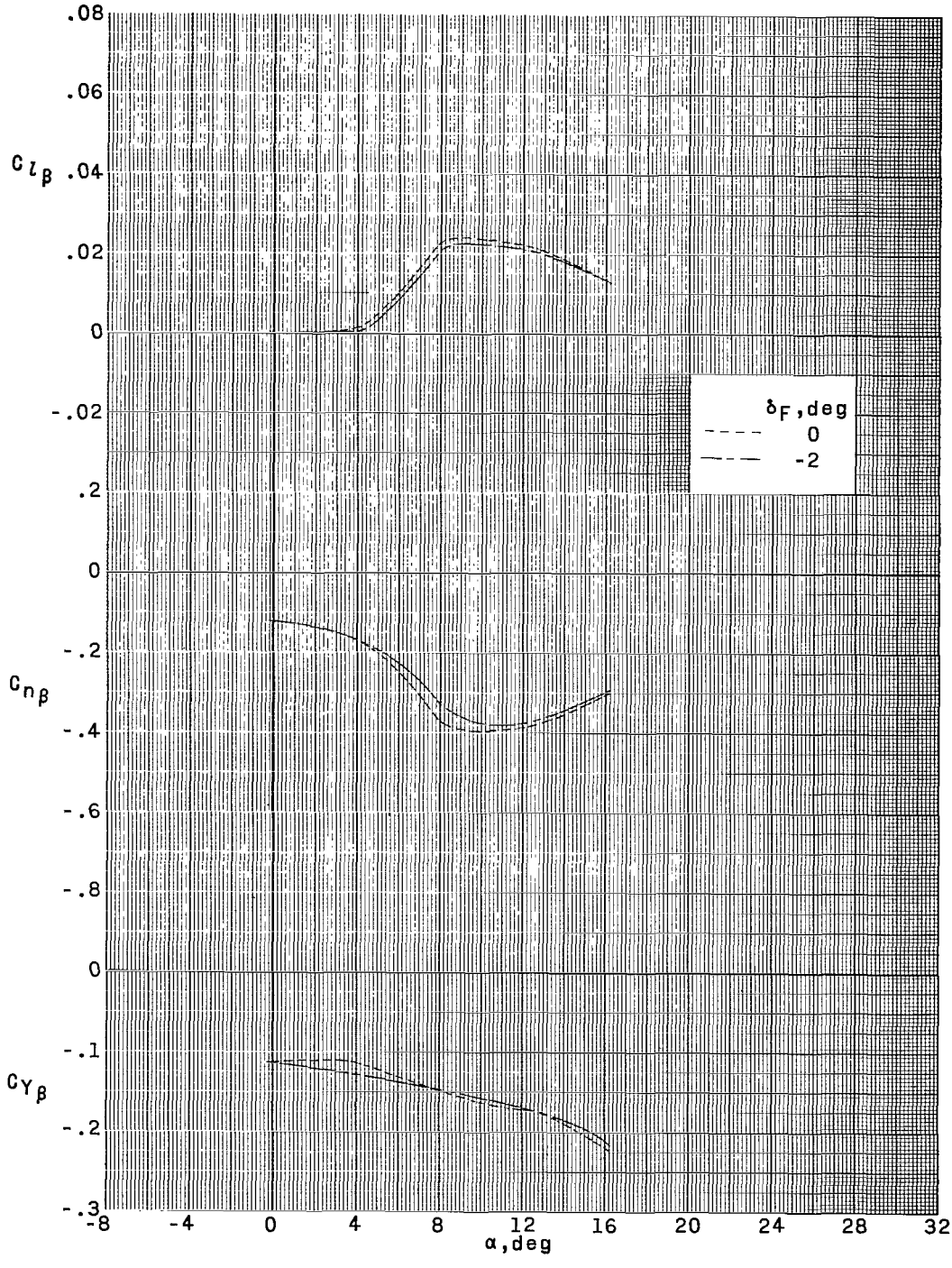

(f) M = 4.63.

Figure 10.- Concluded.

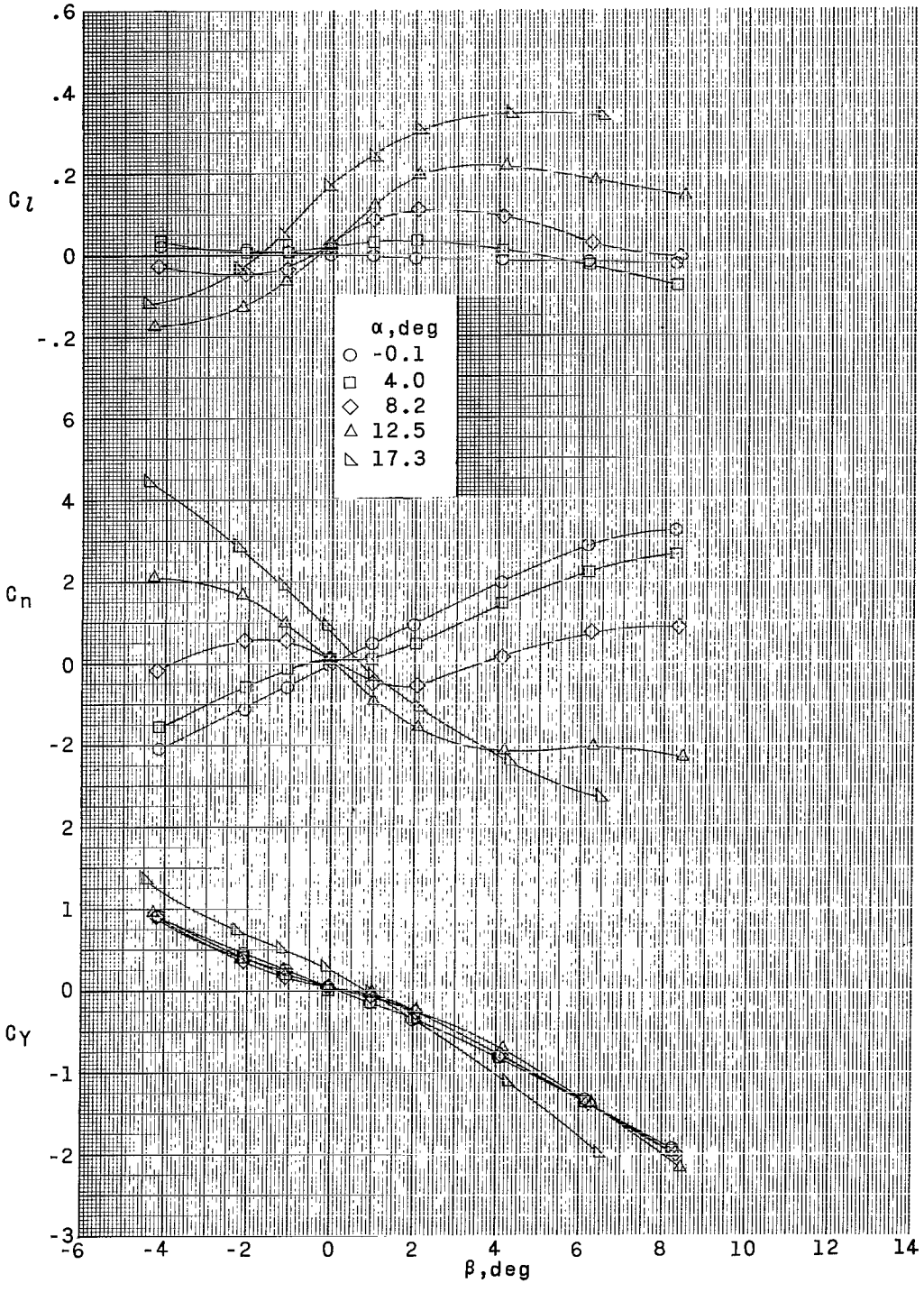

(a) M = 1.80.

Figure 11.- Aerodynamic characteristics in sideslip for configuration 2. $\delta_F = 0^0$.

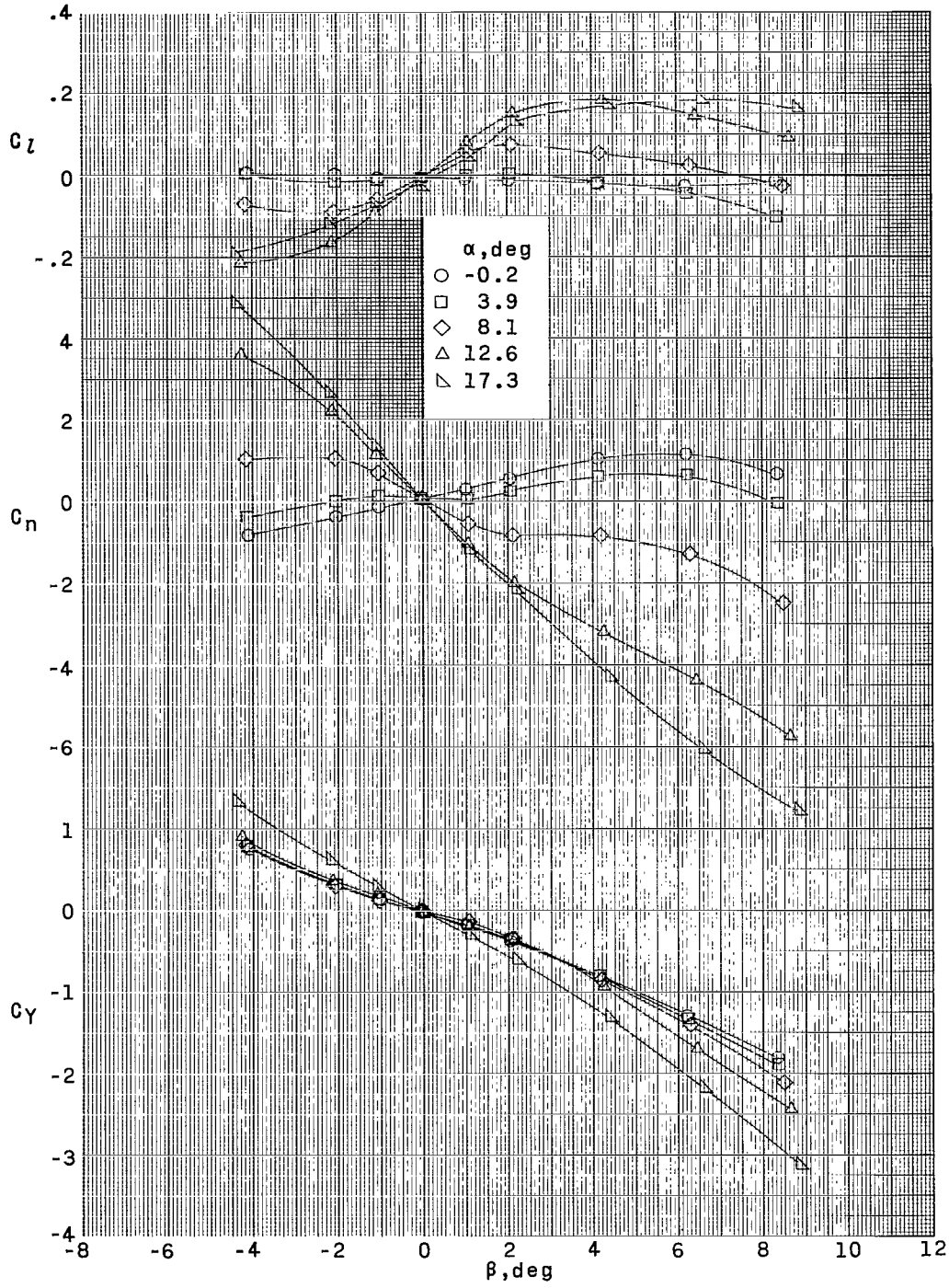

(b) M = 2.30.

Figure 11.- Continued.

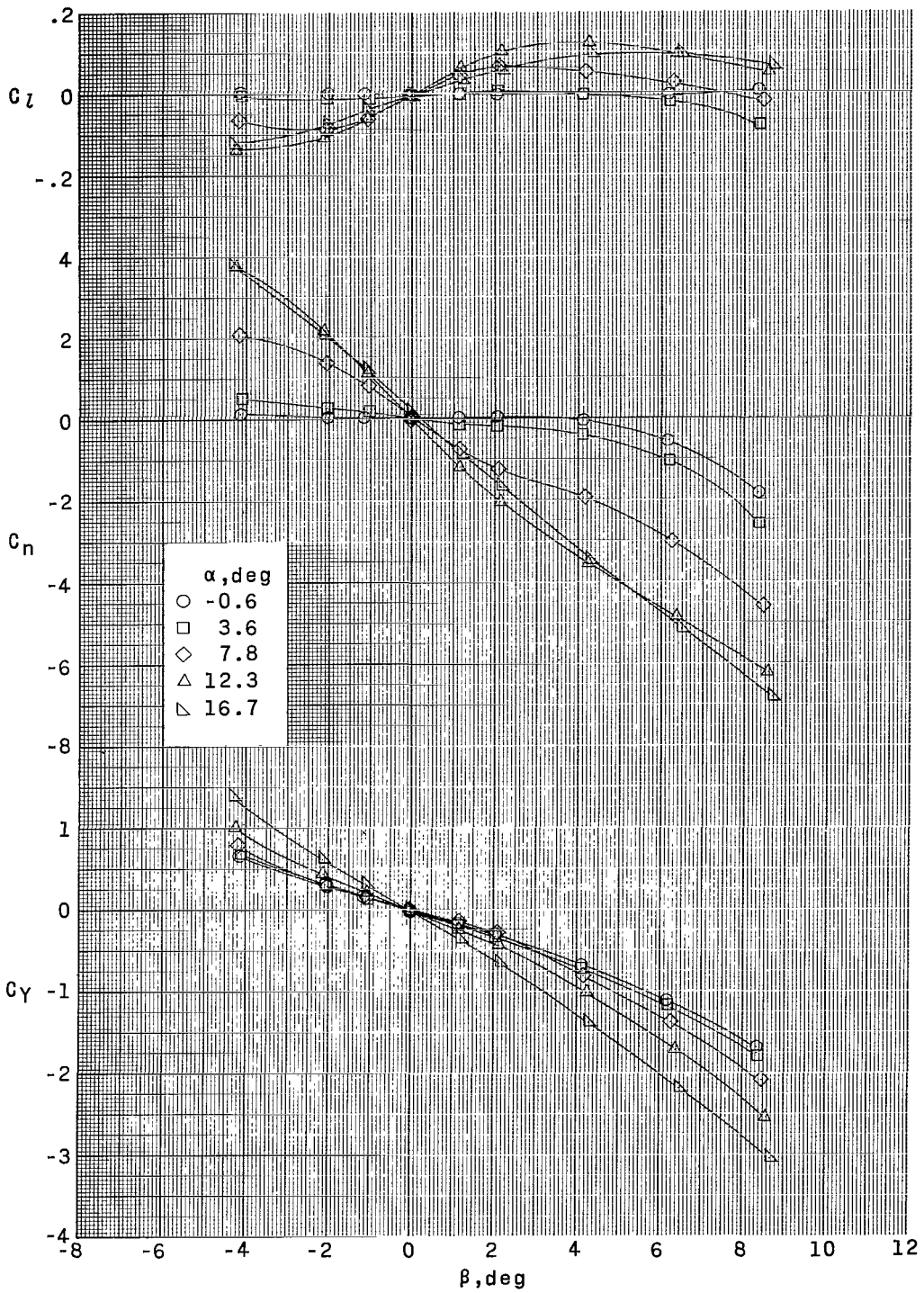

(c) M = 2.96.

Figure 11.- Continued.

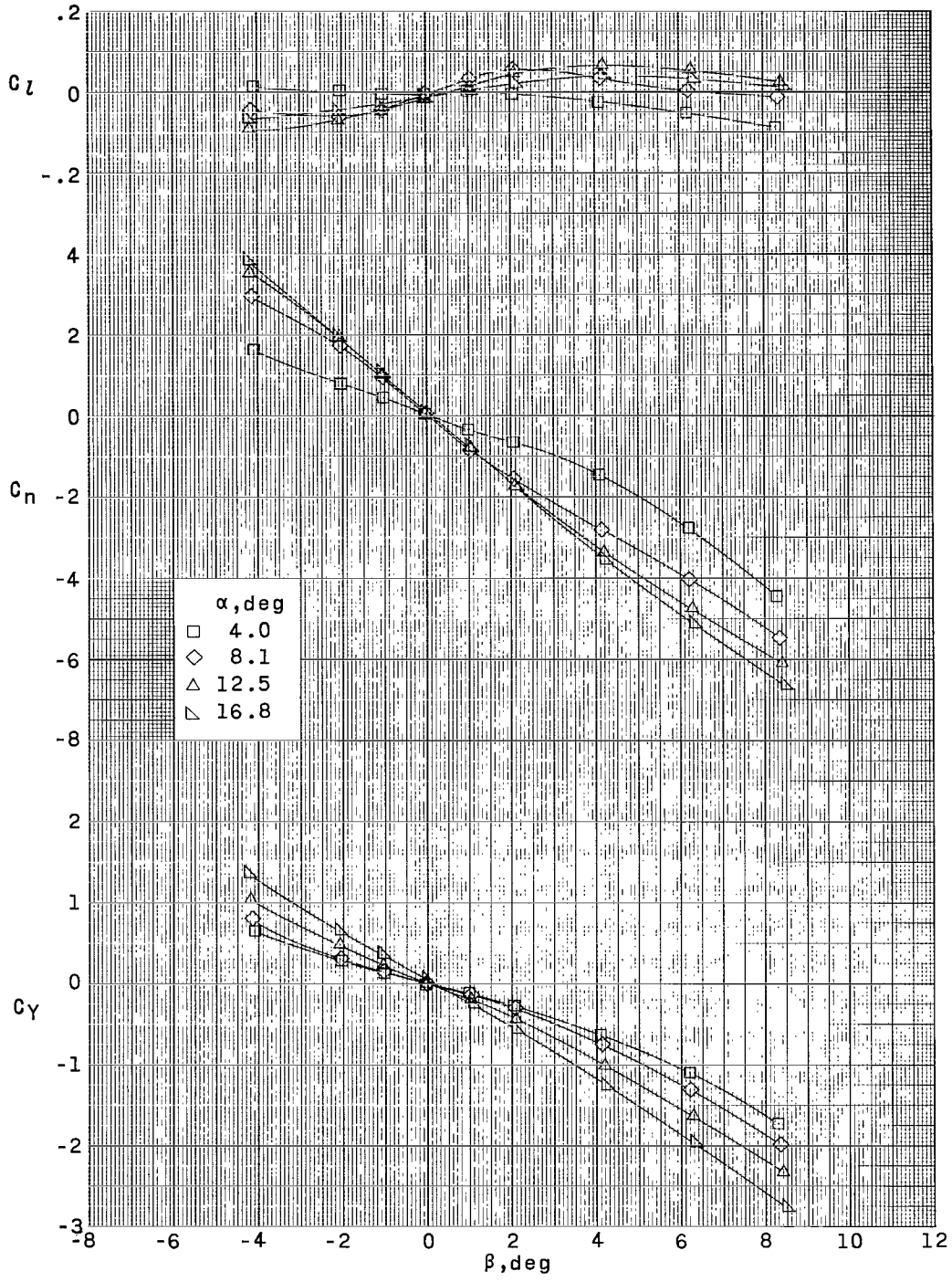

(d) M = 3.96.

Figure 11.- Continued.

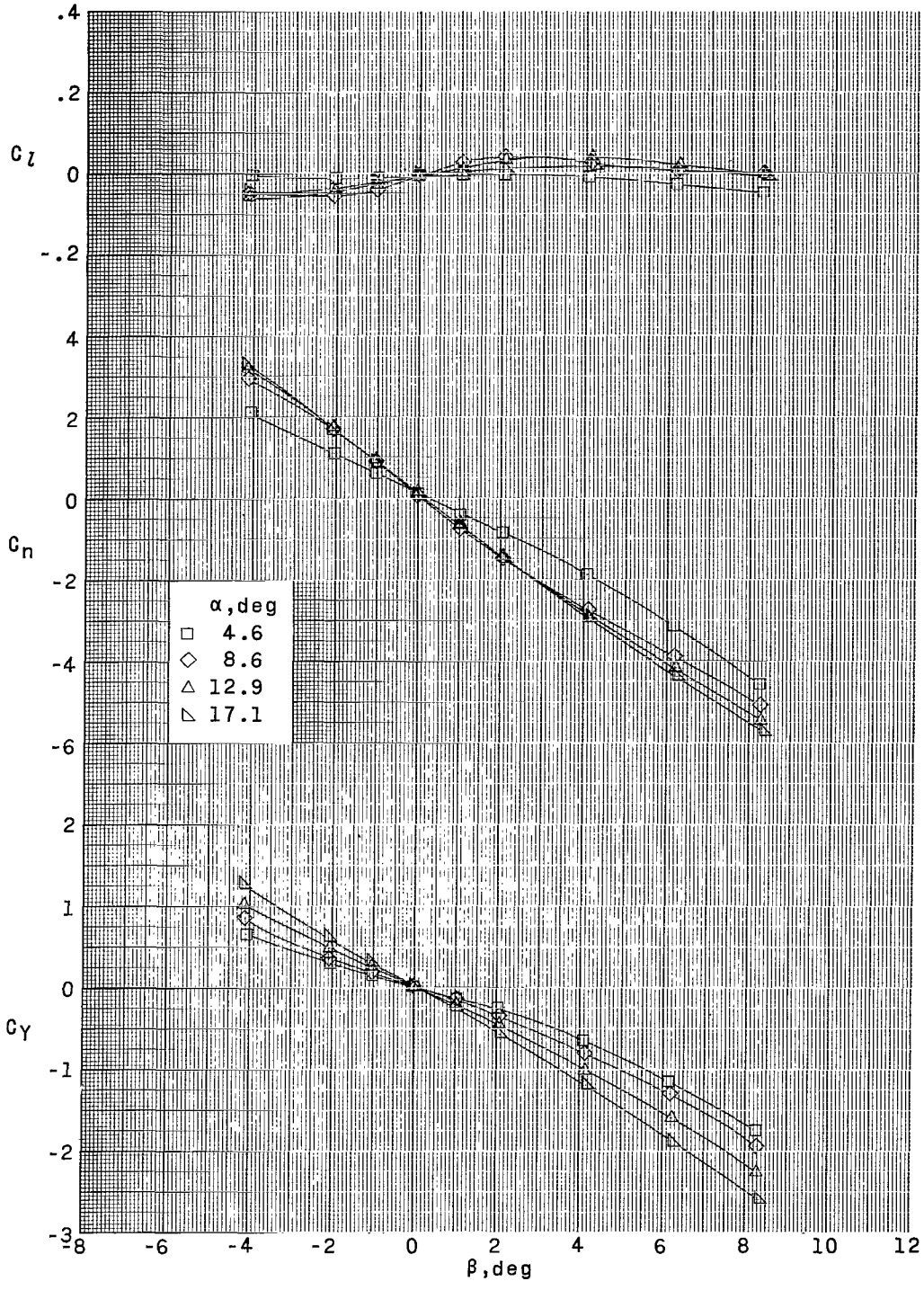

(e) M = 4.63.

Figure 11.- Concluded.

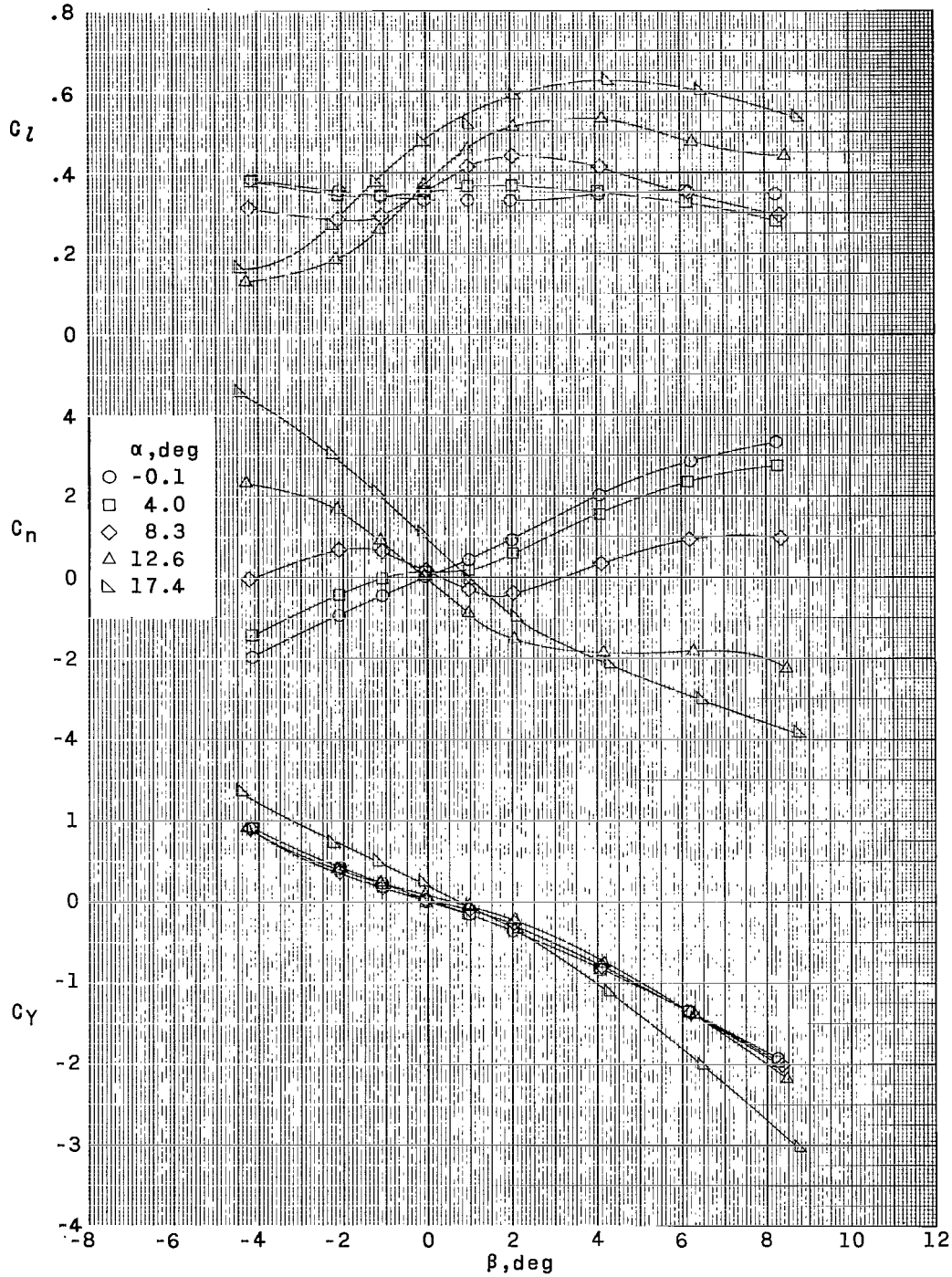

(a) M = 1.80.

Figure 12.- Aerodynamic characteristics in sideslip for configuration 2. $\delta_F = -2^o$.

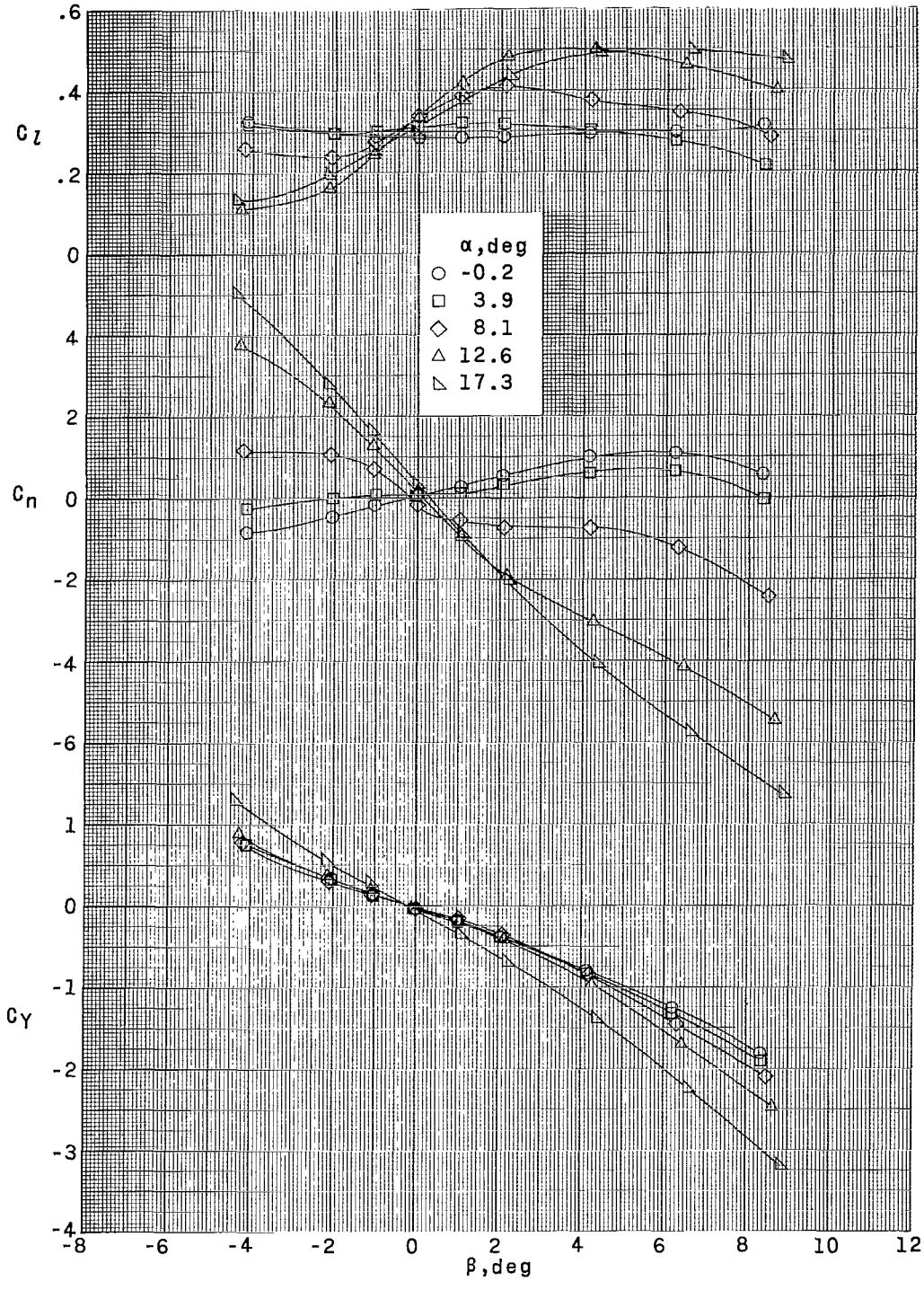

(b) M = 2.30.

Figure 12.- Continued.

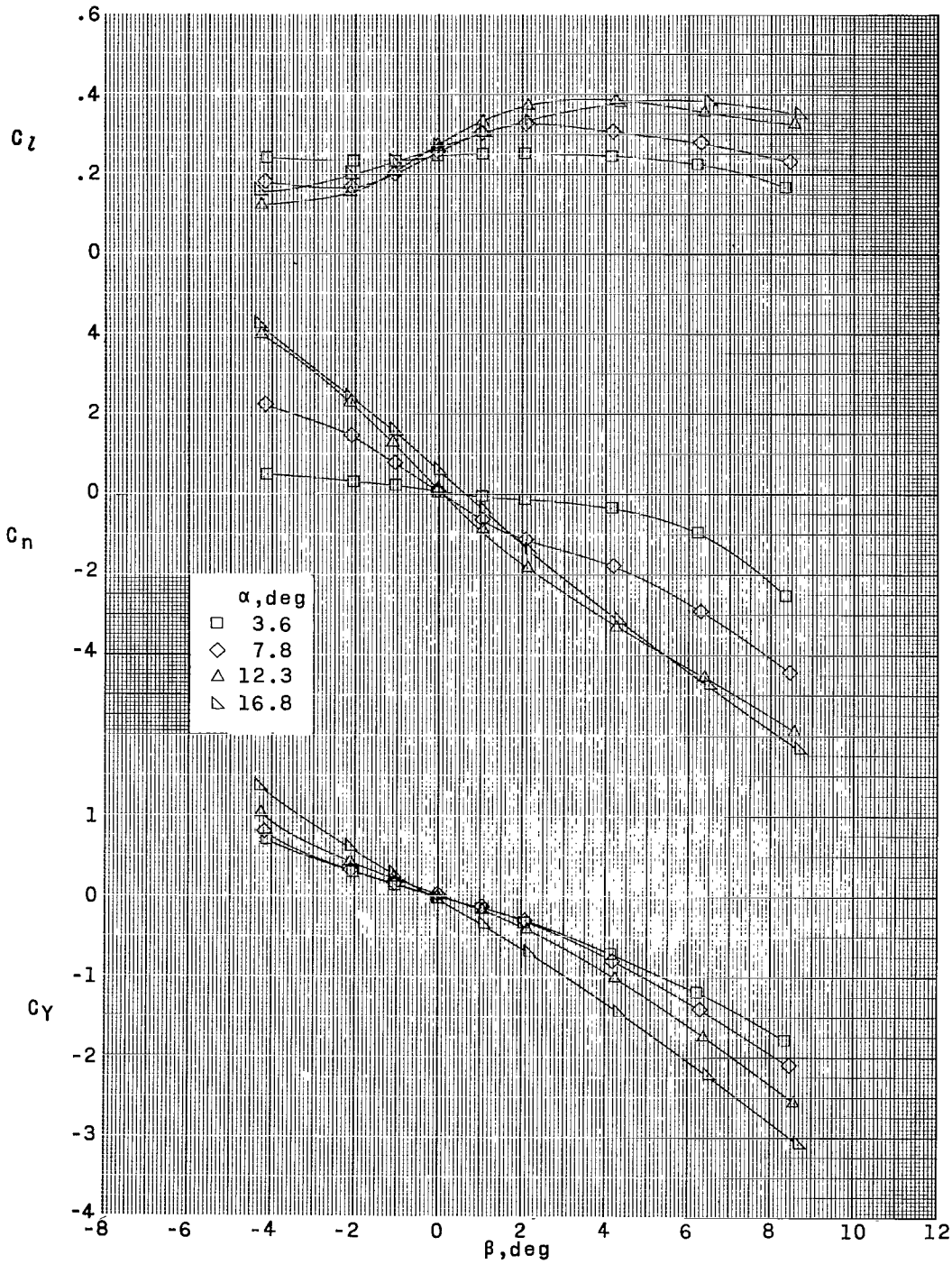

(c) M = 2.96.

Figure 12.- Continued.

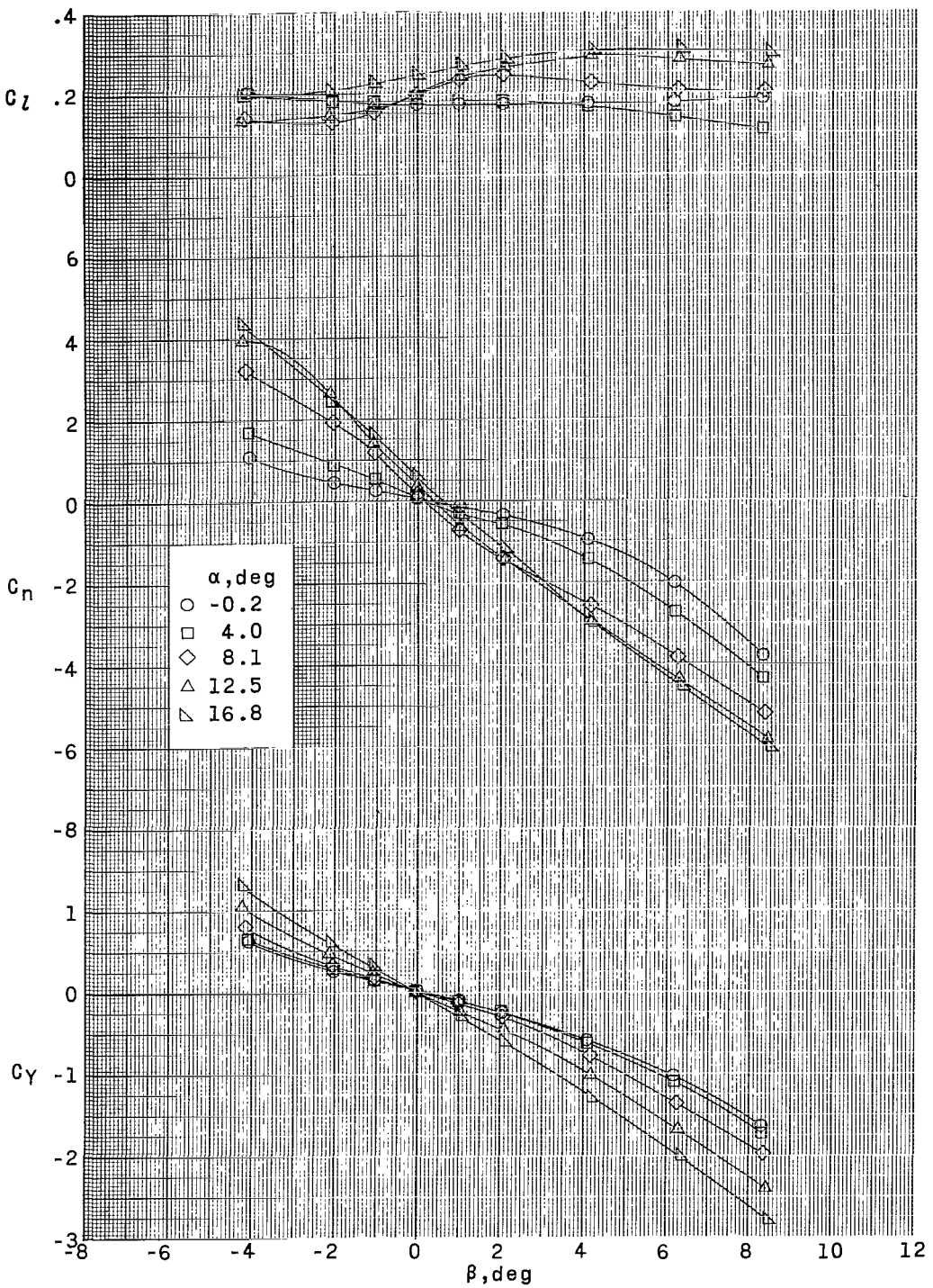

(d) M = 3.96.

Figure 12.- Continued.

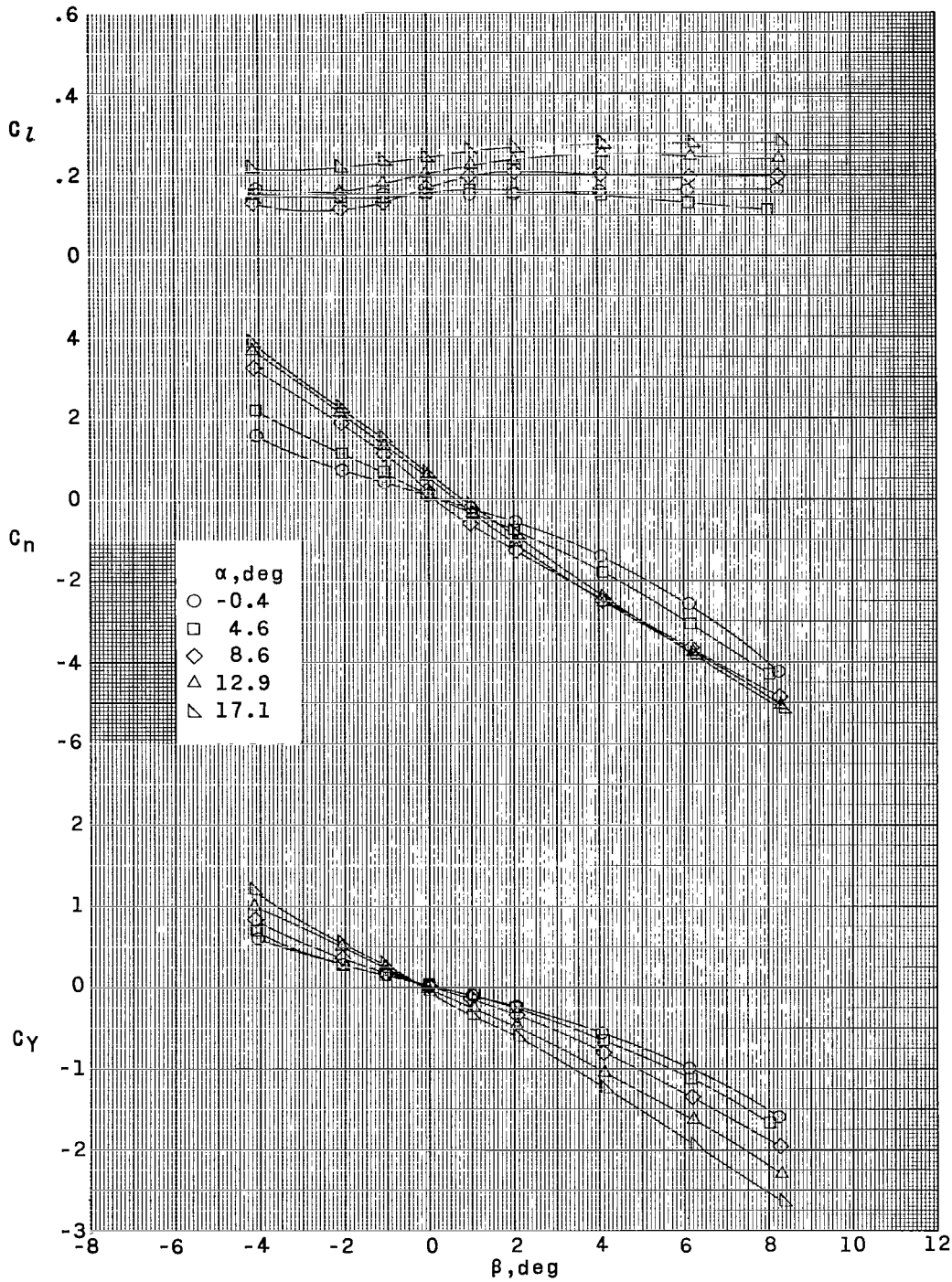

(e) M = 4.63.

Figure 12.- Concluded.

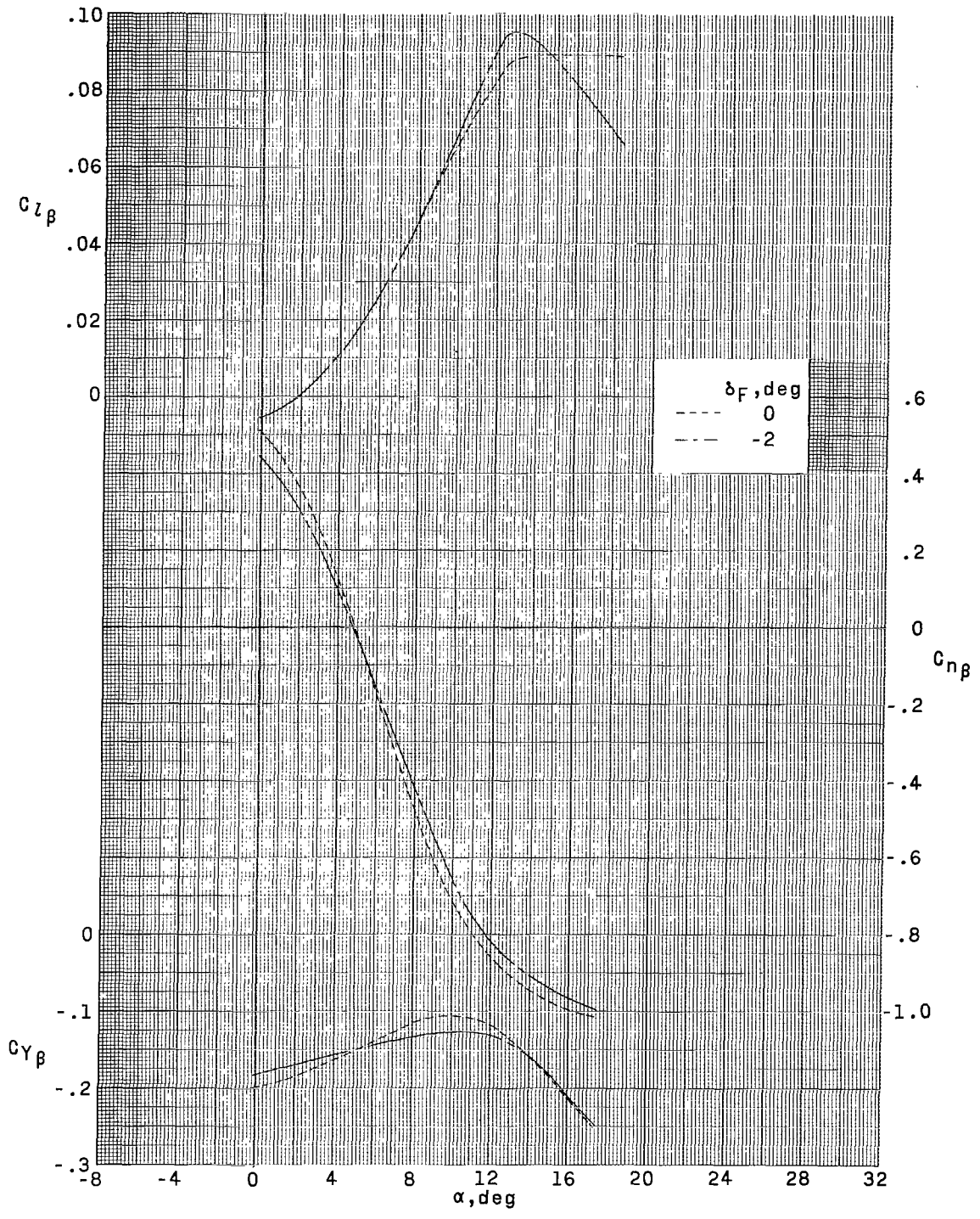

(a) M = 1.80.

Figure 13.- Sideslip parameters for configuration 2.

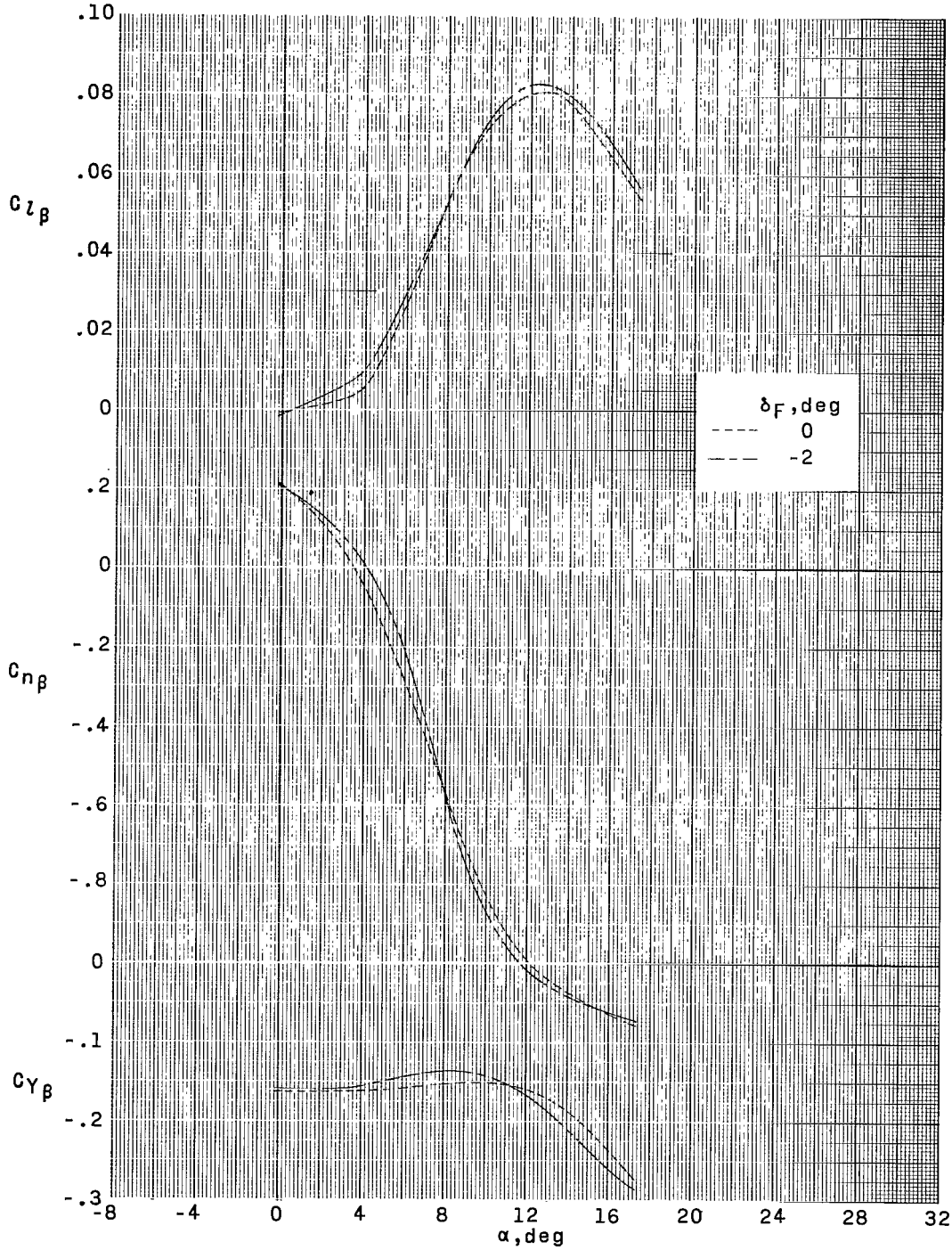

(b) M = 2.30.

Figure 13.- Continued.

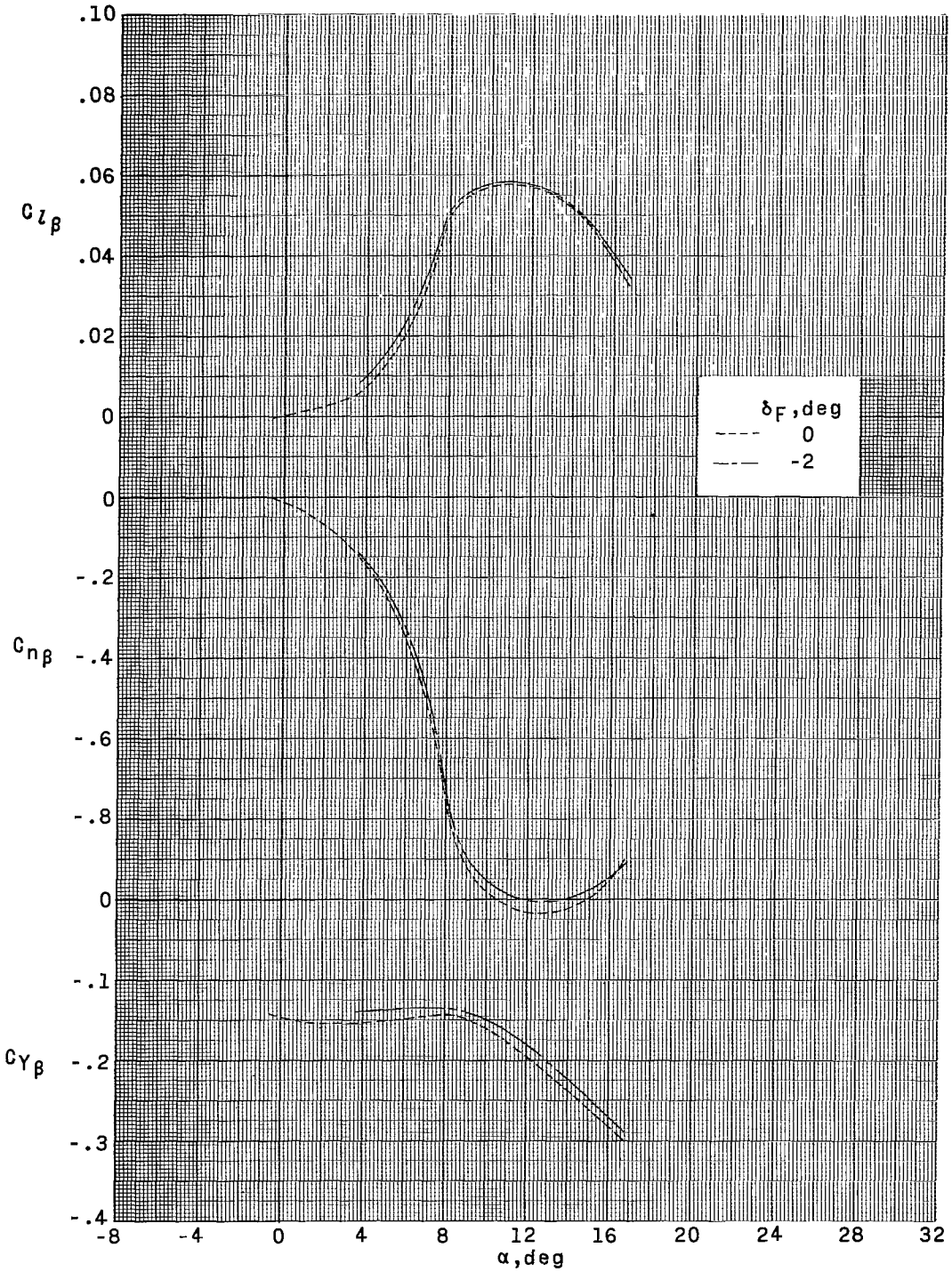

(c) M = 2.96.

Figure 13.- Continued.

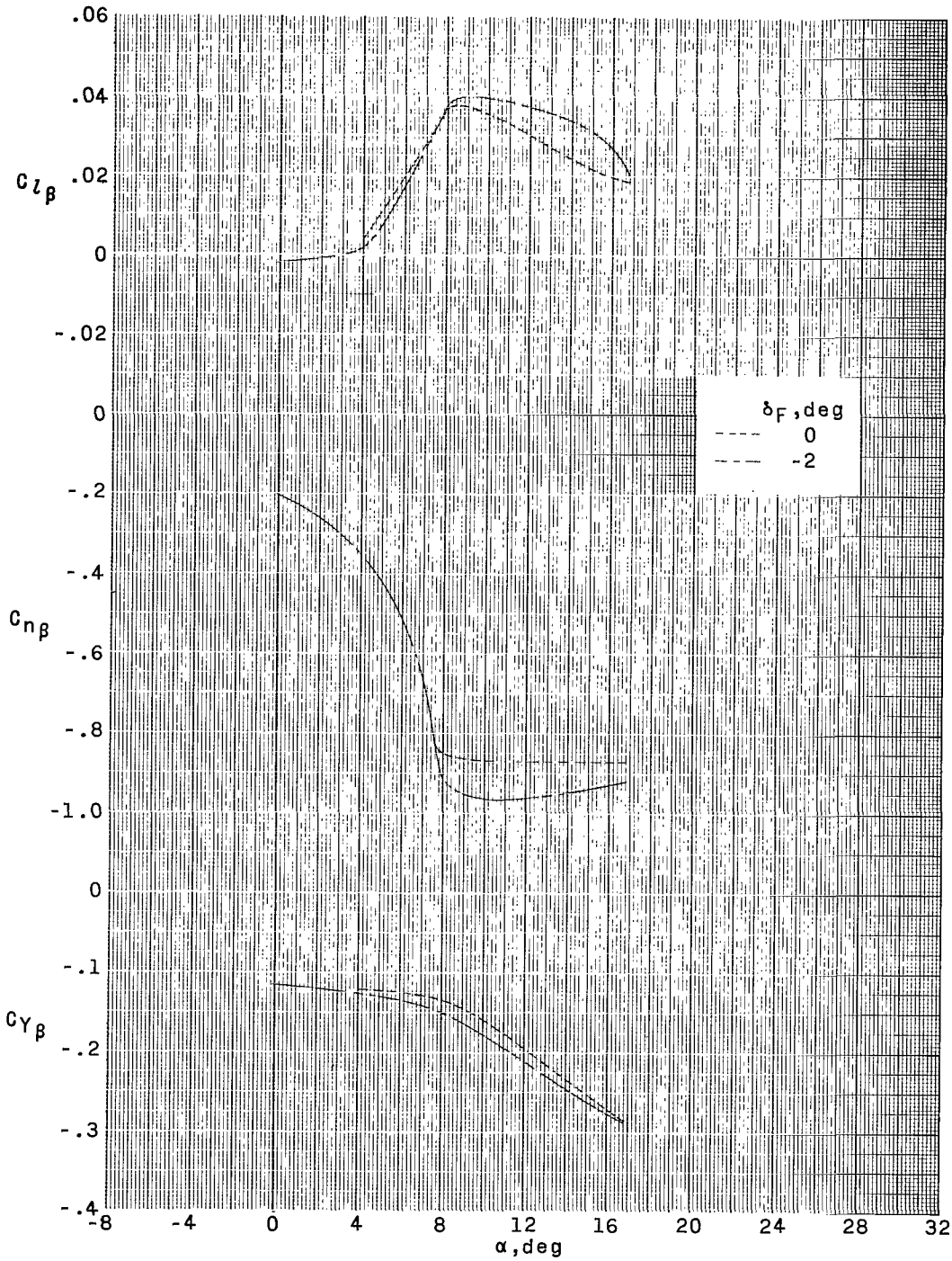

(d) M = 3.96.

Figure 13.- Continued.

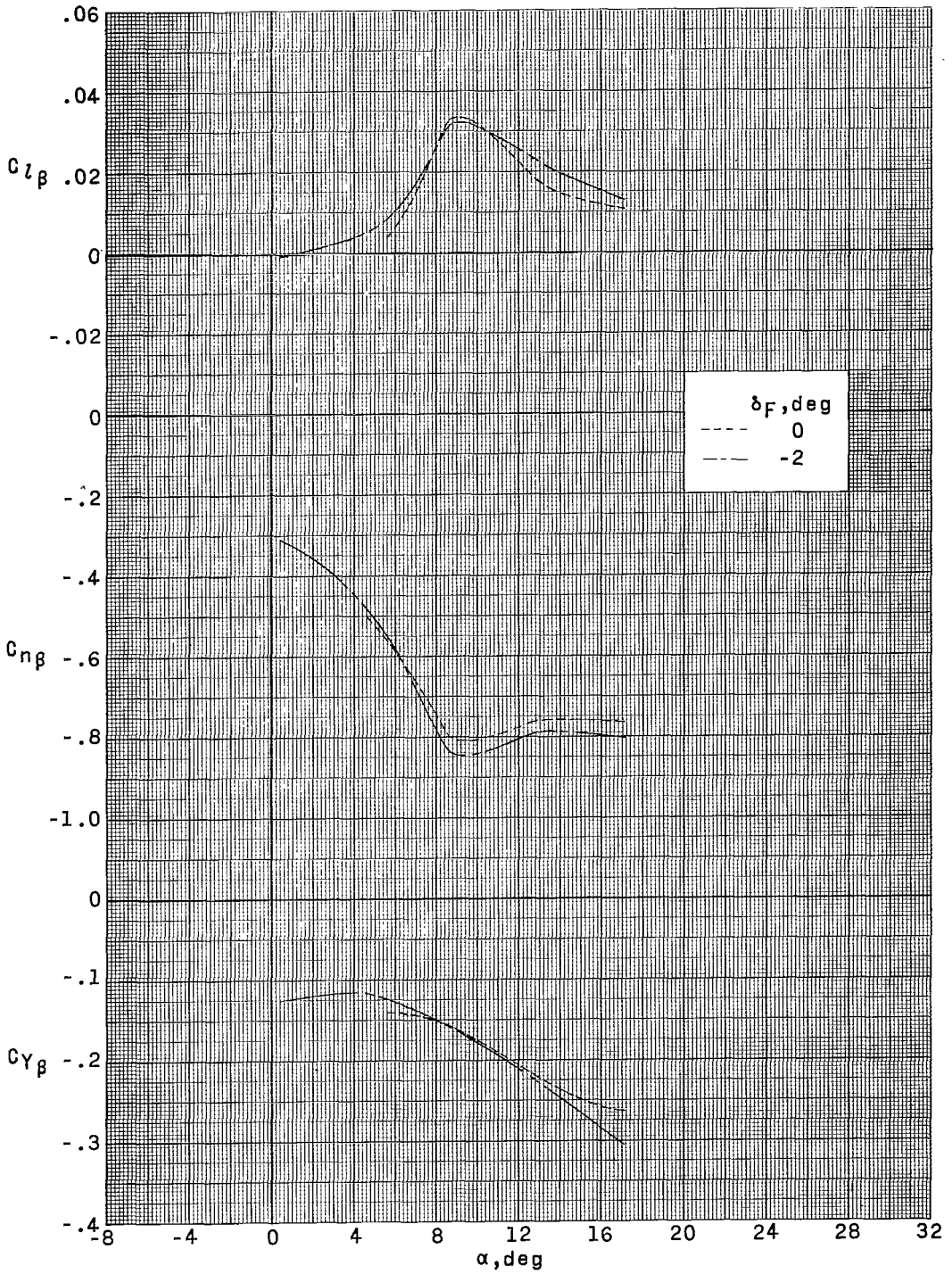

(e) M = 4.63.

Figure 13.- Concluded.

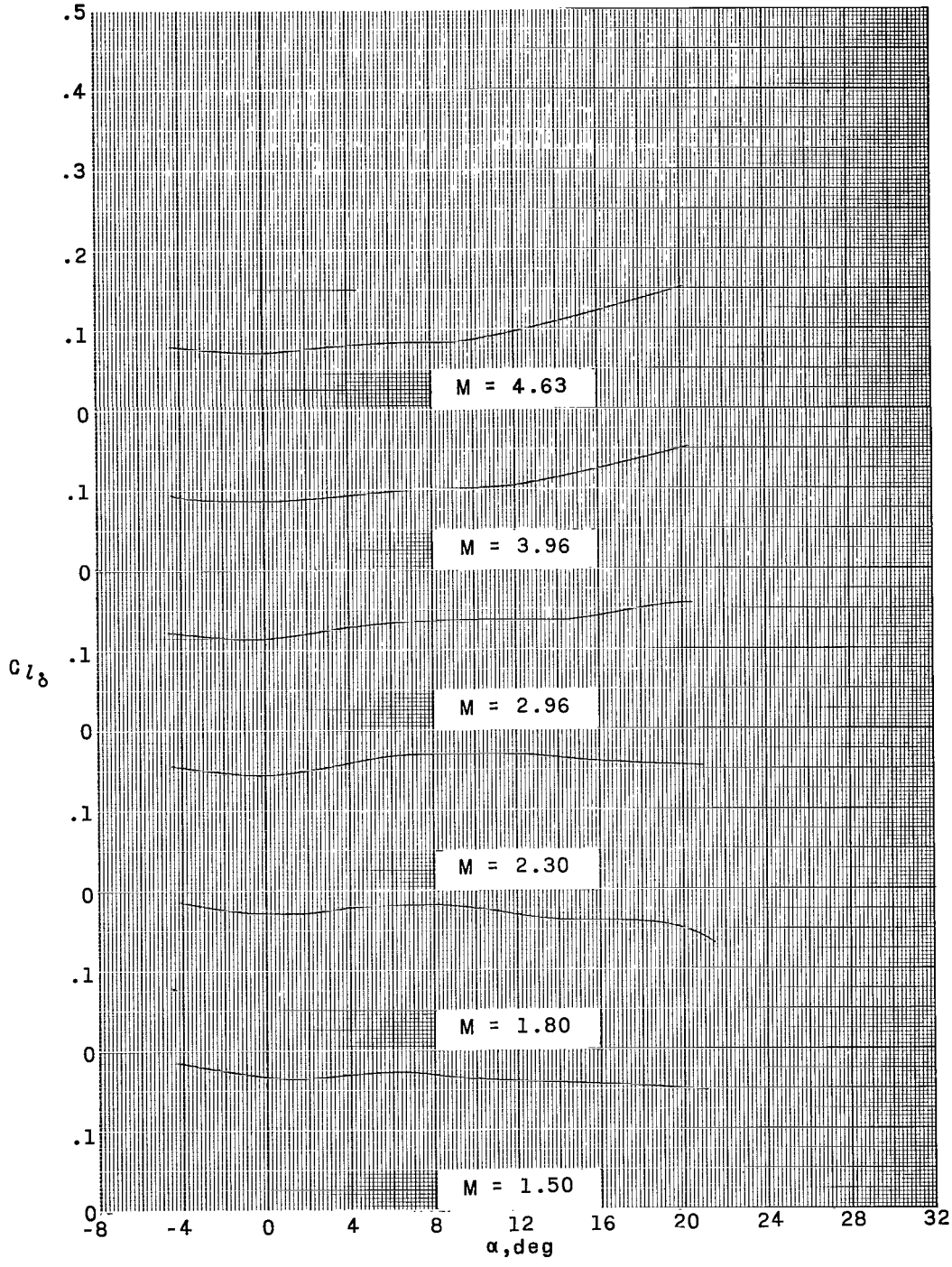

(a) Configuration 1.

Figure 14.- Roll effectiveness due to fin cant.

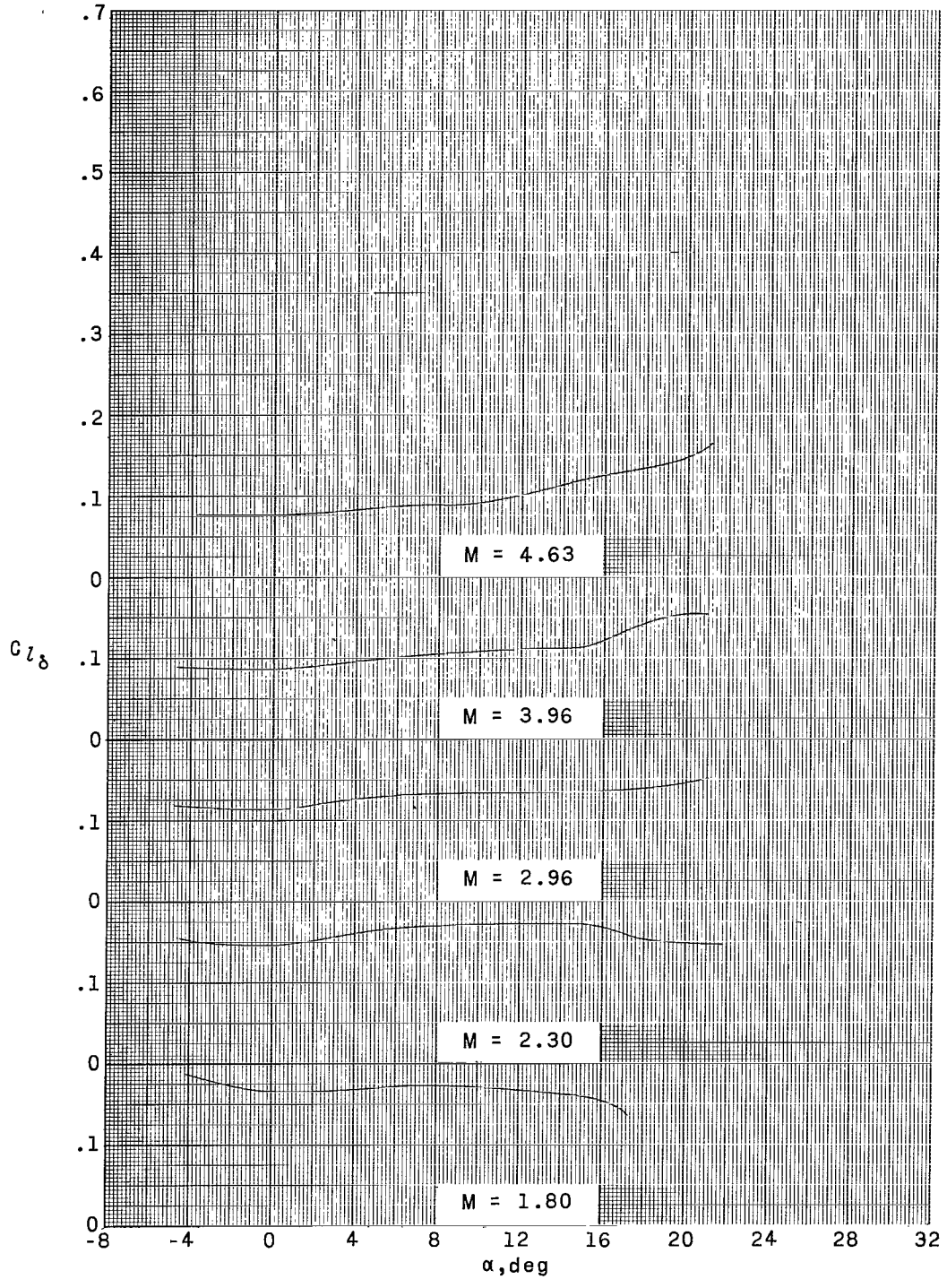

(b) Configuration 2.

Figure 14.- Concluded.

NASA-Langley, 1967 —— 31 L-4837

"The aeronautical and space activities of the United States shall be conducted so as to contribute . . . to the expansion of human knowledge of phenomena in the atmosphere and space. The Administration shall provide for the widest practicable and appropriate dissemination of information concerning its activities and the results thereof."

—NATIONAL AERONAUTICS AND SPACE ACT OF 1958

NASA SCIENTIFIC AND TECHNICAL PUBLICATIONS

TECHNICAL REPORTS: Scientific and technical information considered important, complete, and a lasting contribution to existing knowledge.

TECHNICAL NOTES: Information less broad in scope but nevertheless of importance as a contribution to existing knowledge.

TECHNICAL MEMORANDUMS: Information receiving limited distribution because of preliminary data, security classification, or other reasons.

CONTRACTOR REPORTS: Scientific and technical information generated under a NASA contract or grant and considered an important contribution to existing knowledge.

TECHNICAL TRANSLATIONS: Information published in a foreign language considered to merit NASA distribution in English.

SPECIAL PUBLICATIONS: Information derived from or of value to NASA activities. Publications include conference proceedings, monographs, data compilations, handbooks, sourcebooks, and special bibliographies.

TECHNOLOGY UTILIZATION PUBLICATIONS: Information on technology used by NASA that may be of particular interest in commercial and other non-aerospace applications. Publications include Tech Briefs, Technology Utilization Reports and Notes, and Technology Surveys.

Details on the availability of these publications may be obtained from:

SCIENTIFIC AND TECHNICAL INFORMATION DIVISION

NATIONAL AERONAUTICS AND SPACE ADMINISTRATION

Washington, D.C. 20546